AN INJECTABLE HYDROGEL OF PORCINE CHOLECYST EXTRACELLULAR MATRIX FOR ACCELERATED WOUND HEALING

Pratheesh K V

Ph.D. THESIS

2024

SREE CHITRA TIRUNAL INSTITUTE FOR MEDICAL SCIENCES AND TECHNOLOGY, TRIVANDRUM

An Institution of National Importance established by an Act of the Indian Parliament

(Act No.52 of 1980)

Ministry of Science and Technology, Government. of India

www.sctimst.ac.in

AN INJECTABLE HYDROGEL OF PORCINE CHOLECYST EXTRACELLULAR MATRIX FOR ACCELERATED WOUND HEALING

A THESIS SUBMITTED BY

Pratheesh KV

TO

SREE CHITRA TIRUNAL INSTITUTE FOR MEDICAL SCIENCES AND TECHNOLOGY, TRIVANDRUM

IN PARTIAL FULFILMENT OF THE REQUIREMENTS

FOR THE AWARD OF

DOCTOR OF PHILOSOPHY

2024

DECLARATION

I, **Pratheesh KV** hereby certify that I had personally carried out the work depicted in the thesis titled, **"An injectable hydrogel of porcine cholecyst extracellular matrix for accelerated wound healing"**, except where due acknowledgement has been made in the text. No part of this thesis has been submitted for the award of any other degree or diploma prior to this date.

Pratheesh KV

Reg. No: 2018/PhD/06

Thiruvananthapuram

Date: 30/11/2024

Department of Applied Biology
SREE CHITRA TIRUNAL INSTITUTE FOR MEDICAL SCIENCES AND TECHNOLOGY
(An institute of national importance under Government of India)

Biomedical Technology Wing, Satelmond Palace Campus
Poojappura, Thiruvananthapuram 695012, Kerala

Phone: +91-9447017506 **E-mail: tvanilkumar@sctimst.ac.in** **www.sctimst.ac.in**

Prof. T. V. Anilkumar, *PhD (London), FRCPath (England), CertLAM (Guelph), MVSc, BVSc&AH.*
Scientist-G (Experimental Pathology) and Head of the Department of Applied Biology
Visiting Professor, Indian Institute of Science Education and Reserach Thiruvananthapuram (IISER-TVM)
Fellow of the National Academy of Sciences (India)

CERTIFICATE

This is to certify that **Pratheesh KV,** in the Division of Experimental Pathology of this institute, has fulfilled the requirements prescribed for the Ph.D. degree of the Sree Chitra Tirunal Institute for Medical Sciences and Technology, Thiruvananthapuram.

The thesis entitled **"An injectable hydrogel of porcine cholecyst extracellular matrix for accelerated wound healing"** was carried out under my direct supervision. No part of the thesis was submitted for the award of any degree or diploma prior to this date.

Thiruvananthapuram
Date 30/11/2024

APPROVAL OF THE THESIS

The thesis entitled

AN INJECTABLE HYDROGEL OF PORCINE CHOLECYST EXTRACELLULAR MATRIX FOR ACCELERATED WOUND HEALING

Submitted by

Pratheesh KV

for the degree of

Doctor of Philosophy

of

SREE CHITRA TIRUNAL INSTITUTE FOR MEDICAL SCIENCES AND TECHNOLOGY, TRIVANDRUM

is evaluated and approved by

16/11/2024

(Name & Signature of the Guide)

Prof. T.V. Anilkumar, *PhD (London)*
BVSc&AH, CertLAM (Guelph), FRCPath (England), FNASc, FNAAS
Scientist-G (Experimental Pathology)
Head, Department of Applied Biology, Biomedical Technology Wing
Sree Chitra Tirunal Institute for Medical Sciences and Technology
Thiruvananthapuram 695012

Dr NAVEEN KUMAR

16/11/2024

(Name & Signature of Thesis Examiner)

ACKNOWLEDGEMENTS

I express my sincere gratitude and respect to my research supervisor ***Prof. T V Anilkumar****, for the valuable guidance, critical evaluation, and encouragement throughout my life. I am extremely thankful for the overall support and training Sir provided to explore Science.*

I am extremely grateful to the members of the Doctoral Advisory Committee, Dr. Prabha D. Nair, Dr. Rekha MR, and Dr. Praveen KS for their valuable support, suggestions, and comments

I am thankful to the Director, SCTIMST, and the Head, BMT Wing, SCTIMST for all the facilities provided during the course of my work

I convey thanks to the Registrar, the Dean, the Associate Dean (Ph. D.), and the staffs of the academic division for their administrative support

I thank the staff of accounts, library, computer division, stores, and purchase – BMT Wing for their help.

I am extremely thankful to the Council of Scientific and Industrial Research, Govt. of India for providing the research fellowship

I am grateful to Dr. Purnima C and Dr. Geetha C S from my host laboratory Division of Experimental Pathology, who performed the animal surgery with dedication and patience

I also thank Dr. V. S. Harikrishnan, Dr. Sachin J Shenoy, Mr. Sarath, Mr. Manoj, Mr. Sunil, and all members of the Division of Laboratory Animal Science for their help during animal experiments

I am thankful to Dr Prabha D Nair, Dr Lynda V Thomas, Dr. Merlin Rajesh Lal, Dr Amrita Natarajan, Dr. Jijo Wilson, Dr. Rahul, and all staff from the Division of Tissue Engineering and Regenerative Technology for spectrophotometry and Fourier transform infrared spectroscopy, and RT-PCR

I thank Dr PR Anilkumar, Dr. Praveen KS, Dr. Naresh Kasoju, Dr. Roopesh, Mr Vinod, Ms. Kripa, and Ms Anupama, and all staff from the Division of Tissue Culture for providing L929 fibroblast cells and the friendship

I thank Dr Anugya Bhatt, Dr. Renjith, Ms. Athira KR, Ms. Deepa, Ms. Mahima, and all staff from the Thrombosis research unit for fluorescence spectroscopy.

I extend my thanks to Dr. Sabareeswaran A, Mr. Joseph Sebastian, and Mrs Sandhya from the Division of Histopathology for reagent sharing

I thank Dr. Renjith, Mr. Willipaul, Mrs. Nimy, and Mrs. Priyanka from the Central Analytical Facility for the injectability studies

I thank Kerala University CLIFF for the SEM analysis

I am extremely thankful to Dr Rekha M R, Dr. Rajaleshmi G P, Dr. Caroline, Dr. Priya S, Ms. Linju MC, Ms. Divya Raghav, Mrs Annie, from the Division of Biosurface Technology for reagent sharing and friendship

I am grateful to ***Dr. Geetha C S, Dr. Reshma S, Dr. Purnima C, Dr. Reshmi Raj, Dr. Akhila, and Dr. Lakshmi,*** *from my host laboratory the* ***Division of Experimental Pathology*** *for their immense support, encouragement, and friendship*

I thank all my friends for their encouragement and for giving heartfelt support which helped me to overcome my hard times.

I extend my heartfelt regards to my ***Mother, Father, Brother, Sister-in-law and Devu*** *for their constant love, motivation and prayers.*

I bow before the ***Supreme Energy*** *for giving me strength and showering blessings throughout my life.*

I am grateful for having an extremely good PhD guide who helped me to modulate my life to a higher level.

Pratheesh KV

TABLE OF CONTENTS

LIST OF FIGURES

LIST OF TABLES

ABBREVIATIONS

CECM	Cholecyst extracellular matrix
CG	Collogel
CMC	Carboxymethyl cellulose
ColT1	Collagen type I
ColT3	Collagen type III
DMEM	Dulbecco‟s Modified Eagle‟s Media
ECM	Extracellular matrix
ETO	Ethylene oxide
FBS	Fetal bovine serum
FTIR	Fourier-transform infrared spectroscopy
H & E	Hematoxylin and eosin
HPF	High Power Field
IHC	Immunohistochemistry
IL-10	Interleukin 10
iNOS	Inducible Nitric Oxide Synthase
MMP	Matrix metalloproteinase
MTT	(3-(4,5-Dimethylthiazol-2-yl) -2,5-diphenyltetrazolium bromide
NBF	NBF Neutral buffered formalin
OW	Open wound
PBS	Phosphate buffered saline
PDGF	Platelet derived growth factor
PVC	Polyvinyl chloride
qPCR	Quantitative Real-Time Polymerase Chain Reaction
SEM	Scanning electron microscope
TGFβ	Transforming growth factor-beta
TNF	Tumor necrosis factor
UHMWPE	Ultra-high molecular weight polyethylene
UV	Ultraviolet
VEGF	Vascular endothelial growth factor

SYNOPSIS

AN INJECTABLE HYDROGEL OF PORCINE CHOLECYST EXTRACELLULAR MATRIX FOR ACCELERATED WOUND HEALING

BY

Pratheesh KV

for PhD Degree

of

SREE CHITRA TIRUNAL INSTITUTE FOR MEDICAL SCIENCES AND TECHNOLOGY, TRIVANDRUM

SYNOPSIS

Impaired wound healing is one of the major concerns in modern healthcare management system. In order to minimize wound healing complications and speed up the healing process, sophisticated wound care products have been proposed. There are a variety of therapeutic products of synthetic or biological origins are now available on market that can help speed up the healing process. The significance of advanced wound care products incorporating biomaterials obtained from animal organs or tissues is highly demanding in this setting. The advanced wound care products obtained from animals have been shown to function as signals to promote a pro-regenerative process of healing. Mammalian extracellular matrices (ECM) are reliable sources of raw materials for the production of cutting-edge wound care products, particularly those derived from various organs and tissues. Among these products, hydrogels have several advantages over conventional pharmaceutical preparation, particularly in terms of handling easiness and treatment efficacy for wounds with uneven edges and varying depths and sizes. Moreover, hydrogels have capacity to maintain a moist environment over the wound bed.

The development of wound care product using a porcine cholecyst extracellular matrix (CECM) scaffold is the main focus of this thesis. The healing potential of lyophilized sheet form CECM has been demonstrated in numerous animal models, such as the rabbit cutaneous burn wound model, the dog lacerated skin wound model, the streptozotocin-induced diabetic rat wound model, the rat abdominal hernia repair model, and the rat myocardial infarction model. In the year 2023, the host laboratory developed "*Cholederm*", the first indigenously made animal-derived "Class D" medical device, as per the Medical Device Rules 2017 (Government of India), which complied with all legal conditions set forth by the Central Drug Standards Control Organization. Unfortunately, the CECM is not appropriate for preparing a gel formulation, using the traditional pepsin digestion and pH neutralization method. This is likely because the scaffold preparation process involves a cross-linking process. Therefore, different gelling methods have been suggested. For instance, using a synthetic polymeric gelling agent called poly-ethylene glycol diacrylate and free radical polymerization mediated by the 1-ethyl-3-(3-dimethyl aminopropyl) carbodiimide and N-hydroxysuccinimide acrylate reaction, a gel formulation of CECM was developed. The hydrogel developed using this technique was suitable for surface coatings on implantable polymeric meshes for mitigating the nature of tissue response, but due to its hardness and weak viscosity, it was unsuitable for wound healing applications. In light of this, the thesis suggests the incorporation of sodium carboxymethyl cellulose (CMC) as the base by an ionic crosslinking reaction to generate a gel formulation of CECM.

This thesis is presented essentially in 6 chapters

Chapter 1 gives a brief introduction to the study topic, focusing on wound healing, complications of wound healing and the global burden of skin wounds. The importance of advanced wound care materials in the treatment of non-healing wounds is also described in this chapter. This chapter also introduces the relevance of ECM scaffolds in tissue engineering and the rationale for choosing CECM as an injectable hydrogel for wound healing. This chapter ends by stating the objectives of the study.

The specific objectives of the study were the following.

1. Preparation of an injectable hydrogel formulation of porcine cholecyst extracellular matrix (CECM)
2. Evaluation of the biomaterial properties of the hydrogel
3. Evaluation of wound healing properties of the hydrogel on experimental rat full-thickness skin wound model

Chapter 2 contains an extensive, literature review relevant to the study topic. It describes the complications of wounds, types of skin wounds as well as the components of wound healing especially the nature of cellular response during wound healing. This chapter describes the relevance of tissue engineering and advanced wound care products for the management of wound healing. Then the chapter explains extracellular matrix scaffolds and their use in wound healing. This chapter ends with describing the porcine CECM scaffold and its efficacy in wound healing applications.

Chapter 3 describes in detail the “materials and methods” performed to achieve the study objectives. These are presented in three sections.

The first section explains the preparation of CECM scaffolds by a nonenzymatic/detergent method. This section also explains the preparation of an injectable hydrogel formulation of porcine cholecyst extracellular matrix with CMC by an ionic crosslinking reaction. The study prepared five formulations of the hydrogel containing variable proportions of CECM and CMC which were identified as HG00, HG50, HG60, HG70 and HG80 based on the content of CECM in the final formulation

The second section describes the procedures adopted for the evaluation of the biomaterial properties of the CECM hydrogel focusing physicochemical characterization of the hydrogel such as gross appearance, procedure for Fourier transform infrared spectroscopy (FTIR) studies by rheology technique, results of studies on measurement of water contact angle evaluation of swelling rate, assessment of equilibrium water content, procedure for scanning electron microscopy, method adopted for evaluating *in vitro* degradation studies and finally the method for studying injectable properties.

Following this a description of the procedures for *in vitro* biological evaluation consisting of a direct contact test, neutral red staining, Live/Dead assay and MTT assay. This section then explains the rationale for the selection of a predicate device for the *in vivo* experiments. This section also contains the procedure for *invitro* scratch wound assay.

The last section of the third chapter describes procedures of *in vivo* studies on Sprague Dawly rats, which gives a detailed description of the creation of wounds and treatment HG60. In order to ascertain the extent of healing potential comparison with untreated group open wound wounds treated with a predicate device (Collogel), and the gel base was also conducted. This chapter also explains the procedure for tissue sampling, sectioning, and staining. The histology staining included hematoxylin and eosin staining, Masson’s trichrome staining, Herovici 's staining and immunohistochemistry for T lymphocytes CD4+ (Helper T cells), CD8+ (Cytotoxic T cells) and Macrophages CD80+ (M1 Macrophages), and CD163+ (M2 Macrophages). It also describes histomorphometry and stereology procedures used for evaluating the percentage re-epithelialization, quantification of collagen deposition, quantification of T-lymphocyte reaction, and quantification of macrophage reaction in the healing wounds.

Chapter 4 explains the “results” of the study in detail. These are presented in five sections. The first section explains the gross features of the CECM hydrogels. The second section explains the physicochemical characterization of the hydrogel detailing the percentage gel fraction, swelling rate as well as equilibrium water content of the hydrogel samples. This section explains the visco-elastic properties of the hydrogel samples by a rheology test. The other physicochemical properties including, the FTIR, SEM water contact angle, and enzymatic degradation explains in this section. This section also explained the injectability property of the hydrogels. The third section explains the *invitro* biological characterization of the hydrogel samples by *invitro* direct contact test, neutral red staining, Live/Dead assay, and MTT assay. The fourth section explains the selection of a best-suited hydrogel formulation for *in vivo* experiments based on the performed physicochemical and *invitro* biological characterization. This section also explains the noncytotoxic nature of the predicate device selected and also explains the cell migration rate by an *in vitro* scratch wound assay before going into *in vivo* experiments. The last section of this chapter describes results obtained from *in vivo* studies explaining the nature of wound healing reaction, as studied grossly and also by histomorphological evaluation by histomorphometry and stereology. This section also explains the fold change of mRNA levels of proinflammatory genes TNF-α, iNOS, and anti-inflammatory gene IL-10, as well as collagen Type I and Type III.

The fifth chapter is a “discussion” of all observations highlighting the significance of the study. The study gave an insight that CECM hydrogel can be prepared by ionic crosslinking reaction by incorporating CMC. The physicochemical and *in vitro* biological characterization of the hydrogel formulations showed the formulation can be used as a wound-healing hydrogel. Further the *in vivo* wound healing experiments showed the CECM hydrogels accelerated the wound healing process by modulating a pro-regenerative reaction predominated by M2 macrophages and also an effective collagen remodeling thereby minimizing scaring compared to the predicate device used.

The sixth chapter of the thesis is the “summary and conclusion” of the study. Briefly, the CECM injectable hydrogels prepared by ionic reaction with CMC have shown very good biocompatibility, and upon animal experimentation, there was accelerated wound healing with abundant M2 macrophage reaction and T helper lymphocytes. Furthermore, effective collagen remodeling was observed thereby minimizing scarring. Overall, the prepared formulation of CECM may be used as an advanced wound care product. This chapter also notes the significance of the study acknowledging the limitations and future perspectives of the study.

CHAPTER 1

1 INTRODUCTION

A wound refers to an injury or damage to the body that disrupts the integrity of the skin or underlying soft tissues (Kumar *et al.*, 2020). Wound healing is a pathophysiological response following the injury/damage (Rodrigues *et al.*, 2019). Generally, the healing response after damage to the soft tissue had overlapping stages including hemorrhage, blood coagulation, inflammation, angiogenesis, and collagen remodeling (Wilkinson and Hardman, 2020). Complications can cause delay in the wound-healing process (Guo and DiPietro, 2010). Impaired wound healing is considered one of the most serious problems in the healthcare system (Avishai, and Yeghiazaryan, 2017; Rodrigues *et al.*, 2019). Therefore, advanced wound care systems have been proposed to accelerate the healing responses by minimizing complications (Nguyen *et al.*, 2023). Indeed, to accelerate the healing progress, various advanced wound care products are now available in the market in the form of films, ointments, foams, and gels of biological or synthetic origin (Tavakoli and Klar, 2020; Gosai and Patel, 2021; Nguyen *et al.*, 2023; Tatarusanu *et al.*, 2023). In this context, wound care products containing animal-derived biomaterials have a lot of significance (Chattopadhyay and Raines, 2014; Murray *et al.*, 2019; Yu, Zhang, and Guo, 2022) because animal-derived products have been found to act as signals to stimulate pro-regenerative processes and promote wound heling (Diller and Tabor, 2022). Specifically, mammalian extracellular matrices (ECM) from different organs and tissues have been found as excellent raw materials for the fabricating advanced wound care products (Wolf *et al.*, 2012; Cramer and Badylak, 2020; Thomas *et al.*, 2023). Among these advanced wound care products, gels offer various benefits over other pharmaceutical preparations especially in terms of easiness of handling and efficacy in the treatment of wounds with variable depth/size and uneven edges (Pan, and Ye, 2021). Furthermore, the capability of gels to maintain a moist environment by holding a significant amount of water across the wound bed is an advantage.

This thesis is centered on the use of porcine cholecyst extracellular matrix scaffold (CECM) for fabricating advanced wound care products. The host laboratory fabricated *Cholederm*, the first indigenously developed animal-derived Class D Medical Device, as per the Medical Device Rules 2017 (Government of India), that satisfied all statutory requirements of the Central Drug Standards Control Organization in the year 2023. The laboratory demonstrated the wound healing ability of lyophilized sheet form of CECM prepared by controlled cross-linking of biomolecules (Anilkumar *et al.*, 2014; Mony and Anilkumar, 2020) in several animal models including full-thickness rabbit skin excision wound, rabbit skin burn wound (Revi *et al.*, 2016), lacerated skin wounds in dogs (Karthika *et al.*, 2018), streptozotocin-induced diabetic rat skin wound model (Mony *et al.*, 2021), rat abdominal hernia repair model (Raj *et al.*, 2021), and rat myocardial infarction model (Nair *et al.*, 2023). The scaffold is known to modulate collagen remodeling (Revi *et al.*, 2013) as well as promoting a pro-regenerative reaction through M2 macrophages/Th2 lymphocytes (Muhamed *et al.*, 2015) and regulating angiogenesis (Mony *et al.*, 2021).

Unfortunately, unlike the conventional pepsin digestion and pH neutralization method commonly employed for making gel preparations (Freytes *et al.*, 2008), ECM is not suitable for preparing CECM gel probably due to a cross-linking process involved in the preparation of the scaffold (Mony and Anilkumar, 2020). Hence alternate gelling techniques have been proposed. For example, a gel formulation of CECM was prepared through free radical polymerization with a synthetic polymeric gelling agent poly-ethylene glycol diacrylate, mediated by 1-ethyl-3-(3-dimethyl aminopropyl) carbodiimide and N-hydroxysuccinimide acrylate reaction (Raj *et al.*, 2020). The gel prepared by this method was suitable as a biomedical device for surface coatings on polymeric meshes for mitigating host tissue response (Raj *et al.*, 2021) but it was largely unsuitable for wound healing applications because of its hardness and poor viscosity.

Against this background, this thesis proposes the preparation of a gel formulation of CECM by ionic crosslinking reaction with Sodium Carboxymethyl Cellulose (CMC) as the base. The specific objectives of this study were the following

1. Preparation of an injectable hydrogel formulation of porcine cholecyst extracellular matrix (CECM)
2. Evaluation of the biomaterial properties of the hydrogel
3. Evaluation of wound healing properties of the hydrogel on experimental rat full-thickness skin excision wound model

CHAPTER 2

2 REVIEW OF LITERATURE

2.1 Skin wounds

A wound is classically defined as a breach in the continuity of soft tissues, such as skin or mucus membrane, as a result of mechanical, thermal, chemical, and radiogenic trauma (Kujath 2008). Although deep tissue wounds may involve underlying skeletal muscle, bone or even visceral organs (Smart, 2013) but skin wounds are essentially superficial wounds restricted to different layers of skin epidermis, dermis or hypodermis (Natsui, 2003).

There are different ways of classifying skin wounds (Sen, 2021). Skin wounds can be caused by superficial friction or minor injuries. Lacerations involves irregular deep cuts with jagged edges which are usually caused by being in contact with sharp objects (Newman and Mahdy, 2022). On the other hand, puncture wounds are due to pointed materials piercing the skin which may introduce bacteria deep into tissues (Baldwin and Colbourne, 1999).

Incision wounds (Herman and Bordoni, 2023) are clean knife cuts happening spontaneously but mostly made intentionally during surgical procedures with blades dedicated for the purpose (Jelinek and Jones, 2023). At the other end, we have contusions that are caused by blunt force trauma that damages blood vessels and other structures beneath the skin typically observed as some indicative discoloration depending on the age of the wound and the structures involved (Buttaravoli, 2007).

Burn wounds were caused by thermal factors, which include both heat (Schaefer and Tannan, 2023) and cold shocks (Jeschke *et al.*, 2020). Chemical injuries happen following exposure to corrosive chemical substances.

Irrespective of the different types of skin wounds described above, the favorite classification is to differentiate words into acute and chronic wounds (Raziyeva *et al.*, 2021), and these are described below. Chronic wounds such as ulcers were sustained over an extended period and were often associated with underlying health problems like diabetes or complications related to ageing.

Acute injuries result from sudden trauma or a specific event ranging from abrasions to punctures to cuts (Tejiram *et al.*, 2016). They typically heal quickly by themselves with minimal care in cleaning and putting on the right kind of dressing after disinfecting them so as not to leave any chance for infections but supporting the natural healing process (Moy 1993; Ramasastry 2005).

Chronic wounds unlike acute wounds, are generally stuck in early phases of the healing process (described later) without progression to further stages, leading to extended healing time or lack of advancement in normal wound repair processes. It is comprised of many healing reactions that remove aetiology simultaneous with the progression of the healing. Diabetic foot ulcers, pressure sores, and varicose ulcers are among the examples of chronic wounds (García *et al.*, 2016). Needless to say, these are associated with an underlying disease problem (Sen, 2021).

2.2 Social significance of wounds

The prevalence of acute and chronic wounds affected millions of people globally and overburdened healthcare systems (Sen, 2021). Lifestyle changes and aging were among the contributory factors to the increase in chronic wounds often associated with conditions like diabetes and vascular diseases (Järbrink *et al.*, 2017), obviously making it an economic, social, and healthcare problem worldwide (Sen *et al*., 2009). In fact, skin wounds ranked fourth among non-fatal disease burdens worldwide (Hollestein and Nijsten 2014).

Therefore, different advanced health care systems have been proposed to address the issue (Farahani and Shafiee, 2021). Actually, there were great disparities in terms of quality wound care provision across regions while low-resource areas suffered most due to lack of healthcare facilities. The financial effect was significant as direct costs of healthcare, loss of productivity, and enduring results from untreated or badly managed sores were taken into account (Fayne *et al*., 2020).

Needless to say, India needs advanced wound care products at affordable cost (Shivani Gupta, 2021).

2.3 Wound healing

Wound healing is a complicated but well-organized process that takes place to restore tissue integrity following an injury (Gonzalez *et al.*, 2016). It takes place *via* a sequence of well-ordered events which can be categorized into two major types: regeneration and repair. The entire restoration of the damaged tissue happens during regeneration. Usually this is restricted to superficial wounds involving epidermis or minor injuries to underlaying basement membrane and minimally injured hypodermis (Eming, and Martin, 2014). However, in the repair process, only parts of the destroyed tissue will be restored If at all any restoration happens, some deformities can be expected. These deformities need not be life threatening (Velnar, and Bailey, 2009).

In short, if only the outermost layer of the skin gets injured then it is said that there is limited damage and it will regenerate itself. But if what is beneath this surface such as the dermis or subcutaneous layers are affected then healing will take place through the repair process (Kumar *et al*., 2020).

2.4 Components of wound healing

At least four separate components have been identified in the wound healing process namely hemostasis, inflammation, angiogenesis, collagen deposition and remodeling (Almadani *et al.*, 2021).

2.4.1 Hemorrhage and hemostasis

After an injury, hemorrhage starts which is soon encountered to maintain hemostasis in the body (LaPelusa and Dave, 2023). Here in this, the blood vessel breakage would trigger certain mechanisms to stop blood flow. The adhesion of platelets to the walls of vessels could initiate clot formation. On the other hand, affected vessels may narrow down to decrease the quantity of blood going into the area. Platelets and thrombin then create a clot which can act as a temporary sealant while further bleeding gets prevented (T Chan *et al.*, 2020). All subsequent wound-healing processes were directed by this common scheme among higher animals (Cigna, 2008; Kumar, 2020).

2.4.2 Inflammation

Vasodilation occurs in blood vessels during the inflammatory phase to increase blood flow thus aiding in the transportation of immune cells which mostly are neutrophils and mononuclear blood cells. Removal of foreign substances and debris by the neutrophils by phagocytosis is a major objective of inflammation (Velnar, 2009). After this, subset of monocytes leads to the formation of M1 and M2 types of macrophages. Further phagocytosis occurs through M1 macrophages, which are also referred to as classically 'activated macrophages' apart from secreting various proinflammatory cytokines such as interleukins 1 and 6, tumor necrosis factor alpha among others including reactive oxygen species plus nitric oxide. On the contrary the M2 macrophages are mainly involved in the regenerative aspects of wound healing. The M2 macrophages releases growth factors like platelet-derived growth factor, vascular endothelial growth factor, and transforming growth factor beta, as well as anti-inflammatory cytokines like interleukin 10. As a result of this, many other cells types will be recruited or native cell types will be stimulated. The major cell types are fibroblast, T lymphocytes, macrophages etc. (Brown *et al.*, 2012).

2.4.3 Angiogenesis

Angiogenesis is an essential process involved in wound healing, essentially formation of new blood vessels. Tight series of molecular and cellular events regulate this process (Eming, Martin and Tomic-Canic, 2014). Different growth factors released at the wound site by immune cells, platelets, and other resident cells including VEGF can tailor angiogenesis (Tonnesen, and Feng, 2000). These factors encourage endothelial cells in the existing blood vessels to migrate and proliferate toward the injured area. The endothelial cells form capillary-like structures as they accumulate thereby creating a network of new capillaries for oxygen, nutrients, and immune cells delivery to the healing tissue (Carmeliet, 2005). Angiogenesis is essential to support the increased metabolic activities of proliferating cells participating in of the wound healing, like matrix deposition and remodeling (Carmeliet, 2005).

2.4.4 Collagen remodeling

Collagen synthesis and deposition are primarily carried out by fibroblasts (Zhou *et al.*, 2013). The tensile strength of the healing wound is largely contributed by collagen which also provide a foundation for cell growth and tissue regeneration (Mathew-steiner, and Roy, 1969). In fact, tightly regulated collagen deposition to create a well-functioning extracellular matrix has been recognized at least over half a century (Widgerow *et al.*, 2000).

Collagen remodeling is a critical phase in wound healing and largely regulated by two types of collagen namely type I collagen and type III collagen. Initially, fibroblasts lay down a provisional matrix wherein they deposit type III collagen during proliferation (Singh, Rai and Agrawal, 2023), however this structure has much low mechanical strength especially easily degraded by collagenases and matrix metalloproteinases (MMPs) (Toriseva *et al.*, 2007). These enzymes work by breaking off excessive or misaligned fibers of type III collagen bundles with better tensile strength made up mainly of fibroblasts from type 1 collagen. The process ensures the changeover thus promoting from immature provisional scar to mature resilient tissue. Overall, the balance between collagen synthesis and degradation gives the optimal strength and flexibility of the tissue (Singh, and Rai, 2023).

2.5 Cellular response in wound healing

The wound healing process involves multiple specialized cells with each serving different purposes in various stages of regeneration and repair (Rodrigues *et al.*, 2019). Initially, platelets respond to injury by helping the blood to clot thus minimizing blood loss (Richter *et al.*, 2023). Neutrophils which are also early responders clears debris and potential pathogens in the inflammatory phase (Wilgus, and Roy, 2013).

Throughout the healing process, macrophages play a pivotal role (Koh and DiPietro, 2011). The M1 macrophages (Uygun *et al.*, 2018) engulf dead or dying cells. On the other hand, there are growth factors released by M2 macrophages (Krzyszczyk *et al.*, 2018) which promote tissue regeneration in the proliferative phase. Fibroblasts (Tracy, and Minasian, 2016) are responsible for the synthesis of collagen among other components needed for the strength and structure of tissues. During angiogenesis, new blood vessels formed by endothelial cells (Tonnesen, and Feng, 2000) supply oxygen as well as nutrients that are required for the healing tissues. The keratinocytes contribute to re-epithelialization by multiplying and then moving towards covering up the wound surface (Julier *et al*., 2017).

2.5.1 Role of T cells in wound healing

Recognized for their part in adaptive immunity, T cells were found to be essential for healing wounds. The participation of T cells is essential during the phase of inflammation (Boyce *et al.*, 2000). Cytokines released by CD4+ T cells, also known as helper T cells, to control the actions of other immune cells and improve the clearance of debris and potential pathogens. On the other hand, CD8+ cytotoxic T cells get rid of damaged or infected cells. The shift from the inflammatory phase to the proliferative phase is controlled by T helper cells which secrete growth factors that stimulated fibroblast activity as well as collagen deposition (Adusei, and Ngo, 2021). Studies have revealed that an appropriate balance of T cell reactions is vital for effective wound healing since both overexpression and under-expression of T cell functions could impair it (Boyce *et al*., 2000; Toulon *et al*., 2008).

2.5.2 Role of macrophages in wound healing

Macrophages play a critical role in wound healing, involving themselves in essential activities throughout the inflammatory and proliferative phases (Koh and DiPietro, 2011). After an injury, monocytes are initially attracted to the site which differentiate into macrophages during the inflammatory phase (Kotwal and Chien, 2017). Macrophage polarization occurs through either classical or alternate activation (Krzyszczyk *et al.*, 2018). Certain molecules like interferon gamma, interferon gamma with lipo-polysaccharides, or tumour necrosis factor alpha will activate M1 pro-inflammatory macrophages. These phagocytic cells act as the first line of defense when they ingest and digest debris, dead cells, and pathogens thereby enhancing inflammation resolution. (Brown *et al*., 2012)

During the healing process, the transition to the reparatory phase led by M2 macrophages takes place (Kotwal and Chien, 2017). Different signals induce the activation, including cytokines such as interleukin-4, interleukin-10, and interleukin-13 immune complexes, glucocorticoid, or secosteroid hormones (vitamin D3). Moreover, these cells secreted growth factors like TGF-β and PDGF which in turn lead to fibroblast proliferation and migration as well as that of endothelial cells and keratinocytes (Brown *et al*., 2012).

Within the sphere of constructing extracellular matrices, fibroblasts were made to produce collagen, elastin, and other supportive proteins necessary for restoring tissue integrity by M2 macrophages (Murray and Wynn, 2011). This collagen framework offers mechanical support and also acts as a scaffold for cellular migration. The synthesis and breakdown of ECM components were influenced by fibroblasts and macrophages so that the scar formation could be regulated appropriately to ensure proper tissue remodeling (Rodrigues *et al*., 2019; Hassanshahi *et al*., 2022).

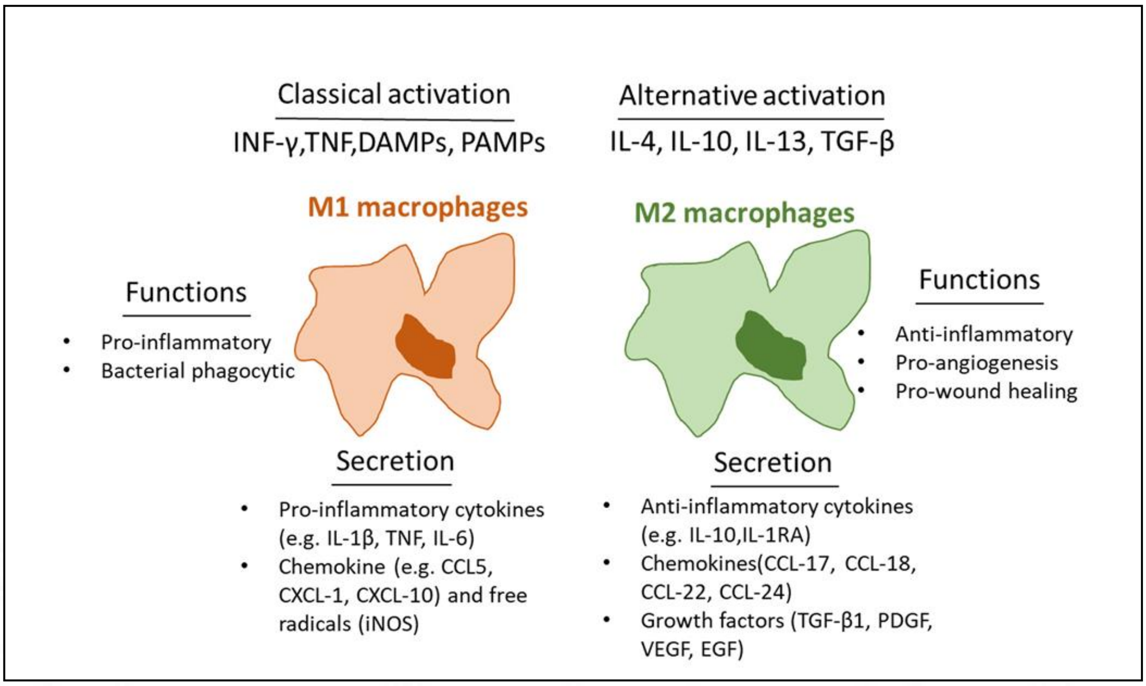

Fig. 1. Classical activation and alternate activation of macrophages (doi.org/10.3390/cells11192953)

2.5.3 Collagen deposition in wound healing

Collagen production plays a major part in healing of damaged tissues (Mathew-Steiner, and Roy, 1969). After the initial inflammatory phase, fibroblasts start releasing collagen through synergistic signals. Most of the extracellular matrix proteins are composed of collagen protein providing structural support necessary for cellular migration (Madden and Peacock, 1971; Singh, and Rai, 2023).

2.5.4 Collagen remodeling in wound healing

During the first stage of wound healing, fibroblasts produce collagen type III, which is the soluble form with low mechanical stability. This is later removed and replaced with type I collagen, a stronger and more organized protein that enhances the tensile strength of the repairing tissue. The fibers of this particular protein were aligned in a woven manner to add elasticity and firmness to the newly formed tissue. Synthesis of these proteins had to be equal to their breakdown for effective remodeling (Kim *et al.*, 2023).

Following the induction of collagen in the proliferative phase, there is a dynamic and highly regulated process of manipulation and modification that take place within the ECM. This remodeling is carried out by different types of cells such as fibroblasts, macrophages, and enzymes like MMPs (Lauer-Fields and Juska, 2002).

As the healing process continue, fibroblasts and myofibroblasts remain active synthesizing more collagen and other components of ECM (Madden and Peacock, 1971). At the same time, MMPs degrades surplus improperly arranged collagen fibers keeping actual levels within check for an orderly mature scar tissue to formation (Toriseva *et al.*, 2007). It also implied that inter-fiber bonding increases tensile strength in wound closure sites where cross-linked binding occur. This phase could last for a long time and in some cases continue for months to years as the scar goes through further refinement (Sung *et al.*, 2005; Toriseva *et al.*, 2007).

2.6 Complications in wound healing

The wound healing is complicated by many things (Avishai, and Yeghiazaryan, 2017). Infections are a big problem, especially in wounds with weak immune systems or ones that haven't been cleaned well enough, can grow bacteria quickly and stop them from healing (Rosique, and Rosique, 2015). Medical conditions like diabetes and heart disease can also slow down defense mechanisms, which takes longer for wounds to heal or they don’t heal at all (Anderson and Hamm, 2012). When inflammation lasts too long, it can damage nearby tissues as well, so they cannot move into the next stage of healing. If abnormal amounts of collagen are laid down and not enough of it is broken up again afterward, then thick scars called hypertrophic scars or lumpy ones known as keloids may form (Ekstein *et al.*, 2022). Further contractures can happen when burns or deep cuts which make skin tighten up over them stopping people from being able to move those parts of their body easily (Rodrigues *et al*., 2019).

Factors affecting wound healing are classified into systemic factors and local factors (Guo and DiPietro, 2010b). Chronic medical conditions like diabetes, vascular diseases, and immune disorders might slow down the ordinary process of healing (Guo and DiPietro, 2010a). Lifestyle changes including smoking as well as poor nutrition could also affect wound healing. These would reduce blood flow and the availability of necessary nutrients in the wound (Guo and DiPietro, 2010b).

Infections could also lengthen the period taken for inflammation to subside (Efron and Barbul, 2001). Moreover, sizes or depths of wounds matters a lot in terms of their healing. Bigger ones need more complex repair mechanisms than smaller ones do, while those that are deeper require even more attention than shallow ones do. Additionally, certain drugs especially those that affect the immune system or blood coagulation could either quicken or delay the wound healing process but this depends on how they are used (Raziyeva *et al*., 2021).

According to local conditions, which change the environment where the injury occurred, the healing process has many levels of involvement. The inflammatory response to contamination is a part of it (Theoret and Stashak, 2014). Microorganisms would certainly slow down healing, while the repair process leading to more complications. In addition, mechanical tension from movements or stretching can be affected all cell proliferation processes (Anderson and Hamm 2012).

2.7 Management of wound

A suitable method for managing skin injuries is used to speed up the process of healing with as little discomfort to the patient as possible (Moon, 2021). The first thing one needs to do when managing wounds is assess them thoroughly, taking into account the type, size, depth, etc., of the wound but also whether they may contain foreign objects that could lead to infection if not removed or treated properly (Thomas *et al.*, 2021).

The right dressings are a key in caring for wounds. They serve different purposes such as creating wet conditions which aid in healing thus preventing infections from taking place or absorbing extra fluids produced (Moon, 2021).

2.7.1 Advanced wound care products

Advanced wound care products are a complex and evolving group of medical products that are designed to help healing of complex or chronic wounds. These go beyond normal dressings and are made to create the perfect conditions for healing a wound (Murphy and Evans, 2012). An example of this is gel dressings which keep the wound moist for supporting cell migration, proliferation, and angiogenesis. Hydrocolloids and foams may be used as types of advanced wound care products that act as barriers against infection while absorbing extra wound exudate (Nuutila and Eriksson, 2021). To manage or prevent infections, some antimicrobial dressings with silver or iodine have been over time (Tian *et al.*, 2007).

To encourage tissue regeneration and speed up healing, growth factors and cytokines can be added to certain types of dressings (Deng, and Gould, 2022). For severe wounds, bioengineered skin substitutes which consist of living cells or tissue matrices have been used as alternatives. Indeed, such products denoted a paradigm shift in the management of wounds as they provided ideal solutions that promote faster healing while minimizing complications (Deng and Gould, 2022; Nguyen *et al.*, 2023).

2.7.2 Hydrogels for wound healing

Hydrogels for wound healing are advanced wound care products (Aswathy, and Narendrakumar, 2020). Normally, these semi-solid or transparent materials would stick on the wound surface creating a safe place that would aid in the healing process (Cao *et al.*, 2023). The fundamental goal of such gels is to ensure moisture balance at the site of injury vitally required for cellular activities in tissue repair. The wound healing gels are not only effective and convenient for acute wound care but also valuable for treating chronic wounds, burns, and abrasions as they may provide pain relief, lowered the risk of infection which contribute to better outcomes and patient comfort during recovery (Yates *et al*., 2007, Gupta, and Agarwal, 2011).

2.7.3 Injectable hydrogels for wound healing

All of the injectable hydrogels are created using several different biomaterials. In addition to natural polymers like alginate, collagen, hyaluronic acid, gelatin, carboxymethylcellulose, and synthetic polymers such as polyethylene glycol (Zhu *et al*., 2021). Hydrogels offer structural support to cells for growing into tissues and aid tissue regeneration. Injectable hydrogels had an upper hand over other types because they could take the shape of any wound including irregular ones and fill up cavities at wound sites (Wang *et al*., 2023).

Injectable hydrogels prepared using mammalian ECM have become very popular in a lot of medical areas where they can copy natural tissue environment (Aswathy, and Narendrakumar, 2020). These gels are usually made from decellularized tissues. This means taking out all cells but leaving behind the noncellular parts. This matrix could still provide a structural framework for the attachment of cells and other essential components needed by living tissues (Karmakar *et al.*, 2023). Moreover, it also has biomolecules for signals necessary for cell orientation and migration (Hunter *et al.*, 2022). Indeed, these biomolecules accelerate the wound-healing process through modulation of immune response while promoting adhesion, proliferation, and differentiation of cells (Xia *et al*. 2023; Cai and Weng, 2023).

2.7.4 Biomaterials for wound healing

The field of tissue engineering brings together the principles from both engineering and life sciences to create biological replacements that can be used to repair, sustain, or enhance tissue function in an organ or as a whole (Han *et al.*, 2020).

The use of ECM scaffolds in wound healing has been considered an advanced and promising strategy (Yi *et al.*, 2017). These scaffolds could imitate natural ECM, which is a complex network of supportive proteins for cell adhesion and proliferation. Biomaterials created from decellularized tissues mammals that mimic the properties of ECM (Howard *et al.*, 2008) and provide biological information for wound healing responses (Morwood *et al.*, 2023). Some of the benefits associated with these types of scaffolds included being biocompatible, and biodegradable as well as having the potential to augment the recruitment, proliferation, and differentiation of cells taking place in the wound regeneration/repair process. They acted as repositories for growth factors plus cytokines ideal for controlled, sustained discharge that influenced inflammation, angiogenesis, and collagen remodeling (Tabor, 2022).

2.7.5 ECM-based hydrogels for wound healing

Wound healing gels that were based on the ECM represents sophisticated formulations that exploited the regenerative capabilities ECM to quicken recovery (Xiao *et al.*, 2023). Often these gels are made from ECM components sourced from decellularized tissues or proteins of ECM such as collagen, fibrin, or even hyaluronic acid (Vriend *et al.*, 2022). The idea is to create an environment at the micro level resembling closely native ECM hence providing supporting structures for adhesion, migration, and proliferation of cells. In wound care, many advantages were associated with these types of gels because of desirable biocompatibility, ability to regulate inflammation, and promoting tissue regeneration (Sivaraj *et al.*, 2021). It is known that, many of these biomolecules could stimulate the activities of fibroblasts and many other cells that take part in the healing process of wounds (Gonzalez *et al.*, 2016; Rodrigues *et al.*, 2019). Moreover, gels based on ECM exhibits high moisture preservation abilities by creating an ideal condition for healing wounds. Such gels could be used topically on wounds to act as a barrier that would protect them while at the same time supplying essential components of ECM directly into injured sites (Ribeiro *et al.*, 2024). These gels are known to promote angiogenesis (Giraudo *et al.*, 2020), collagen formation and tissue remodeling (Diller and Tabor, 2022) and facilitate a more organized and functional repair process. Additionally, biomolecules present in them could accelerate the rate of healing (Cao *et al.*, 2023). The potentiality of ECM-based gel in advanced wound care is vast, because of its flexibility and biological relevance which made them suitable for treating chronic wounds where traditional methods have failed (Vriend *et al*., 2021).

2.8 Porcine cholecyst extracellular matrix scaffold

The host laboratory has developed a non-detergent/enzymatic process for the production of cholecyst-derived scaffolds from porcine gall bladders (Anilkumar *et al*., 2014) through a controlled crosslinking process that helped in maintaining important biomolecules within the final scaffold (Mony and Anilkumar, 2020). The scaffold had several potential medical applications focusing faster wound closure without much scarring in based on animal studies. An observation made was that it activated M2 macrophage and T helper 2 lymphocyte-dominated tissue remodeling response (Muhamed *et al*., 2015). In a burn wound model of rabbit skin, the fibroblast-loaded CECM perfectly healed the wound (Revi *et al*., 2016). Various proteins and biomolecules present in the CECM scaffold were identified, which were considered essential for the wound healing (Muhamed *et al*., 2017). Meanwhile, the effectiveness of CECM was tested on dogs with lacerated skin wounds (Karthika *et al*., 2018) and rats for skeletal muscle repair (Balakrishnan Nair *et al*., 2018). In addition, a hydrogel formulation for surface coating of polypropylene meshes for the mitigation of immune response in rat abdominal skeletal muscle repair was successfully demonstrated (Raj *et al*., 2021). Moreover, a gelatin modified scaffold of CECM showed faster rate of wound healing in diabetic rats with enhanced angiogenesis (Manjula *et al*., 2021). Recently modification of CECM with gold nanoparticles to form a cardiac patch for the mitigation of fibrosis after myocardial infarction in rats (Nair *et al*., 2023).

CHAPTER 3

3 MATERIALS AND METHODS

3.1 Formulation of porcine cholecyst extracellular matrix powder

3.1.1 Materials

Porcine gallbladder/cholecyst (Meat Products of India Ltd Edayar, Kerala, India). Formaldehyde solution 37-41% (Molychem, India), Ductless Fume Cabinet (ESCO, Singapore), Ultra-low $^{-}$80 deep freezer (Sanyo, Japan), Freeze dryer (Christ alpha 2-4 LD plus^{TM}, Germany), Tyvek® packaging material. Surgical scissors, Forceps, Freezer mill (Spex SamplePrep, 6770, USA), Liquid Nitrogen (Meera Traders, India), Desiccator

3.1.2 Methods

3.1.2.1 Preparation of CECM lyophilized sheet scaffolds

Gall bladder of pigs free from zoonotic disease slaughtered under veterinary supervision were purchased from Meat Products of India. The thin lyophilized sheets CECM was first prepared by a non-detergent/enzymatic method reported previously (Anilkumar *et al.*, 2014). Briefly, the specimens having no gross lesions collected at slaughter were transferred to a glass bottle containing 10% neutral buffered formalin (NBF) and brought to the laboratory and the extracellular matrix isolation from the cholecyst was performed within 48 hours in a fume hood (ESCO). The cholecyst was washed with tap water for 1 hour to remove the excess NBF. The apex and the fundus of the gallbladders were cut and removed with a scissor and a longitudinal cut was made to open the gall bladder. Then the thin layer of the extracellular matrix in the fibro-muscular layer was mechanically delaminated by removing mucosa, muscularis and serosa with forceps. The isolated wet sheets of extracellular matrix were then pre-frozen at $^{-}80$°C deep freezer (SANYO, Japan) and lyophilized in a freeze dryer (Christ–alpha 2-4LD plus^{TM}, Germany) for 16 hours. The freeze-dried sheets were sterilized with ethylene oxide (ETO) at 37^{0}C for six hours, and stored in a desiccator until further use.

3.1.2.2 Preparation of CECM powder

The lyophilized sheets of CECM prepared as described in section 3.1.2 were powdered in a freezer mill (Spex SamplePrep, 6770) with liquid nitrogen (Figure 2). Five repeated cycles were performed to obtain the fine powder. The CECM powder was then ETO sterilized and stored in a desiccator until used.

Figure 2. Preparation of CECM powder using a freezer mill

3.2 Preparation of porcine cholecyst extracellular matrix hydrogel by ionic crosslinking reaction with CMC

3.2.1 Materials

Powdered CECM resulted from the procedure described in section 3.1.3. Carboxymethylcellulose Sodium salt-high viscosity 500 - 600 cps (Molychem, India), Potassium Aluminium Sulphate (Sigma, USA).

3.2.2 Methods

3.2.2.1 Preparation of CECM-CMC hydrogel

The CECM-powder prepared as described in section 3.1.3 was made into a suspension of 5% wt/v in distilled water. Parallelly, the CMC powder was also made into a suspension of 3% wt/v in distilled water. Both these suspensions were kept separately on a magnetic stirrer for four hours to get a respective suspension. The two suspensions were then blended to form a pregel, according to four different blending ratios (Table 1). Gelation of the blended solution by crosslinking was achieved by adding the blended suspension to an equal quantity of 8mM Potassium Aluminium Sulphate (Figure 3). The four hydrogel formulations were designated as HG50, HG60, HG70, and HG80 according to the concentration of CECM in the hydrogel. After 2 minutes of crosslinking, the formed hydrogels were collected and washed with sterile distilled water to remove any unreacted crosslinker. The hydrogels were then collected in sterile vials sealed with parafilm and stored at 4^0 C until further use.

Table 1. List of CECM-CMC hydrogel formulations

Sl. No.	Hydrogel formulations	Proportion of the CECM suspension (Percentage)	The proportion of CMC solution (Percentage)
1	HG00*	0	100
2	HG50	50	50
3	HG60	60	40
4	HG70	70	30
5	HG80	80	20

**Note: HG00 and CMC gel are the same*

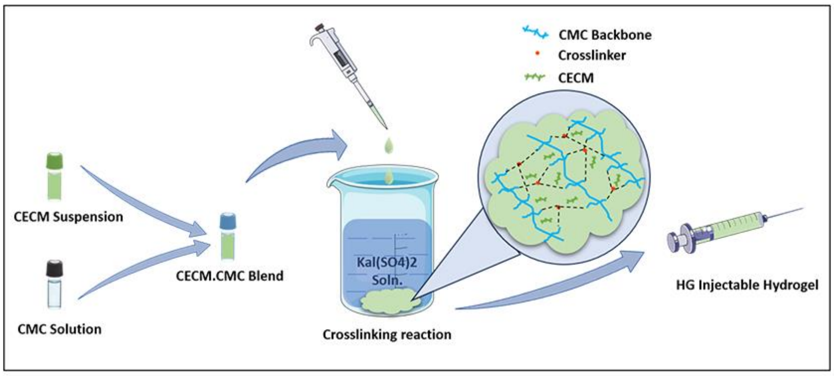

Figure 3. Schematic representation of the preparation of HG00, HG50, HG60, HG70, and HG80 formulations

3.2.3 Characterization of CECM-CMC hydrogels

3.2.3.1 Physicochemical characterization

3.2.3.1.1 Materials

Fourier Transform Infrared Spectrophotometer (Bruker alpha, USA), Ethanol (Himedia, India), Rheometer (Anton Paar MCR 102, Germany), Water contact angle Image analyzer (Optical Contact Angle System, OCA15 plus, Germany), Phosphate Buffered Saline (PBS), Scanning Electron Microscope (Carl Zeiss EVO 18, Germany), ImageJ (National Institutes of Health, USA), Collagenase enzyme (Sigma, USA), Ninhydrin (Sigma, USA), Acetone (Sigma, USA), Water bath (Julabo® TW20, USA), 96 well microplates Thermofisher, USA), Microplate reader (Biochrome Asys UVM 340, USA), Texture analyzer (Stable Micro Systems, TA XT Plus, UK)

3.2.3.1.2 Methods

3.2.3.1.2.1 Fourier transform infrared spectroscopy

The FTIR evaluation of the hydrogels was performed (Bruker alpha) by the Attenuated Total Reflection method with background subtraction. The infrared spectra of the hydrogels were recorded in the range of 500-3000 cm^{-1}. The FTIR spectra of hydrogels were then compared with the FTIR spectrum of lyophilized sheet of CECM originally reported by Anilkumar *et al*., 2014.

3.2.3.1.2.2 Gel fraction

The percentage gel fraction was calculated on the freeze-dried hydrogels by determining the weight loss of the gels before and after swelling in water for 16 hours. Briefly, the freeze-dried hydrogel samples were weighed and soaked in water for 16 hours. The hydrogel samples were then freeze dried and the final weight of the hydrogel samples were recorded. The percentage gel fraction was then calculated using the following formula.

Percentage gel fraction= = (Wd/Wi)×100 where, Wi and Wd were the initial weight and final weight of the dried insoluble part of the samples after freeze drying.

3.2.3.1.2.3 Rheology

The hydrogel's viscoelastic property was analyzed using a rheometer (Anton Paar, MCR 302, Austria). An amplitude sweep was performed to find the Linear Viscoelastic Region (LVER), making sure that the strain range was appropriately selected for the following measurements uniformly in all the samples. The frequency sweep was then performed and the mechanical properties of the hydrogel were examined. This was done to give insight into the storage modulus (G') which represented the elastic behavior, and the loss modulus (G") which indicated the viscous behavior of the hydrogel at increasing frequencies. Being injectable hydrogels, the viscosity was also measured against the shear rate which determined the shear thinning property of the hydrogel formulations.

3.2.3.1.2.4 Water contact angle

The water contact angle was measured to check the surface wettability of the hydrogel samples by sessile drop method (Djebbar Tiab, Erle C. Donaldson, 2012). Briefly, the water droplets were placed on hydrogels coated as thin films on glass slides. The images were visualized and analyzed through the image analyzer of the machine (Optical Contact Angle System, OCA15 plus).

3.2.3.1.2.5 Swelling rate

The swelling rate was calculated using the conventional gravimetric method (McBath and Shipp, 2010). Briefly, the freeze-dried hydrogel samples were pre-weighed and immersed in PBS at 37^0C and the weight of the swollen gels was measured at predetermined time points after removing the adsorbed PBS by gentle touch with a filter paper. The percentage swelling rate of hydrogels was calculated using the following formula.

Percentage swelling rate= (Mt-M0/M0) x100

Where M_t is the mass of the swollen gel at time T, and M_0 is the mass of the dry gel at time T.

3.2.3.1.2.6 Equilibrium water content

The equilibrium water content was studied by immersing the lyophilized hydrogel samples in PBS at room temperature for 48 hours to attain the maximum absorption and the final weight was measured (Mandal, Kapoor and Kundu, 2009). From this, the equilibrium water content was calculated using the following formula.

Equilibrium water content, EWC = $(M_e-M_0 X)/M_e$

Where M_e is the weight of the gel after attaining equilibrium, and M_0 is the initial weight of the dry gel

3.2.3.1.2.7 Scanning electron microscopy

The surface topography of the hydrogels was studied on the cut surfaces of lyophilized hydrogel samples images of the cut surface were acquired after sputter coating with gold (Carl Zeiss EVO 18). The Scanning Electron Microscopy (SEM) images of HG samples and HG00 were evaluated using ImageJ (National Institutes of Health), software to estimate the pore size of the hydrogels.

3.2.3.1.2.8 *In vitro* degradation studies

A nonenzymatic degradation study was performed with lyophilized samples in water as reported previously (Capanema *et al*., 2018). The weight loss at the time points 1, 3, 5, 7, 18 and 24 hours were recorded, and the percentage degradation was calculated based on the formula (Wi-Wd/Wi)100. Where Wi was the initial weight and Wd was the final dried weight of the samples at each time points.

In addition, the extent of enzymatic degradation was performed with collagenase enzyme (Grover and Rao 2015) since the major component (38.5mg/100mg) of CECM was collagen (Anilkumar *et al*., 2014). Briefly, 1mg of lyophilized samples of the hydrogels were incubated with 200 µl collagenase enzyme (500 U/ml) at 37^0C for 48 hours with constant shaking. 100 µl supernatant was pipetted out. To this 100 µl, 2% Ninhydrin reagent in acetone was added and boiled in a water bath (Julabo® TW20,) at 95^0C for 15 minutes. From this, 20µl solution was transferred to 96 well microplates (Thermofisher) and made up to 200 µl with distilled water. Then, optical density was measured at 570 nm in a microplate reader (Biochrome Asys UVM 340). For these measurements, the original CECM scaffold described in section 3.1.2 was used as the reference material. The HG00 was not included in the study, since it did not contain collagen.

3.2.3.1.2.9 Injectability

The injectable property of CECM-CMC hydrogels was tested in a Texture Analyzer (Stable Micro Systems, TA XT Plus, UK) (Zhang, Fassihi and Fassihi, 2018) with needles of five different gauges *via* 18G, 19G, 22G, 23G, and 26G (Figure 4). The cylinder probe (Syringe plunger SMS P/25,25mm diameter) was attached to the load cell of the texture analyzer and the height was positioned at 125mm using height calibration. Then 5ml syringe prefilled with the hydrogel samples was fixed onto the syringe extraction rig above the heavy-duty platform. A compression mode of the test was carried out by lowering the probe towards the syringe from its pre-calibrated height with a test speed of 1 mm/s. The force-distance curve was recorded until the pre-filled sample was emptied (45mm). Three parameters including the stiction force (the force required to enable the relative motion of the stationary syringe insert), dynamic glide force (the constant force required during the injection), and the end constraint force (the force between the plunger and the end of the syringe) were recorded.

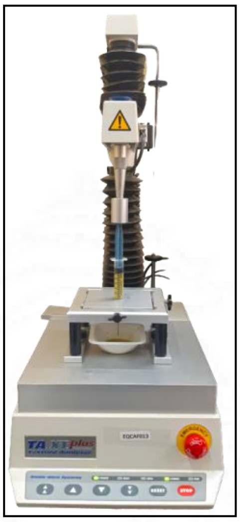

Figure 4. Injectability evaluation of hydrogel samples conducted in a Texture analyzer

3.2.3.2 *In vitro* biological characterization

3.2.3.2.1 Materials

Dulbecco’s Modified Eagle's Media (DMEM, Himedia, India), fetal bovine serum (FBS, Himedia, India). Penicillin and streptomycin (Gibco, USA). TrypLE (Thermofisher, USA), Laminar airflow hood (Kleanzone Devices India Pvt. Ltd). Calcein AM, and Ethidium homodimer-1 (Thermofisher, USA) and (3-(4,5-Dimethylthiazol-2-yl) -2,5-diphenyltetrazolium bromide- MTT (Sigma, USA).

3.2.3.2.2 Methods

3.2.3.2.2.1 Maintenance of L929 fibroblast cells

The L929 cells (obtained from the Division of Tissue Culture, an ISO 17025-certified laboratory of the host institute) were cultured and maintained in DMEM supplemented by 10 % FBS, 1% Penicillin and 1% Streptomycin. Cells were maintained in a T-25 tissue culture flask (Thermoscientific, USA) in a CO_2 incubator (Thermo Electron Corporation, Forma series II) with 5% CO_2 to get 70-80% of confluent cells. The cells were then detached with TrypLE and sub cultured by replacing DMEM every three days.

3.2.3.2.2.2 *In vitro* direct contact test

In vitro, direct contact cytotoxicity assay was performed based on the requirements of ISO 10993 Part 5. Hydrogel samples were sterilized by ultraviolet sterilized for 20 minutes inside a laminar airflow hood (Kleanzone Devices India Pvt. Ltd). Samples having dimensions of about 1/4th size of 24 well cell culture plates were used for the direct contact test. The samples were carefully placed in a monolayer of L929 mouse fibroblast cells and supplemented with 10% DMEM media for 24 and 48 hours at 37^0C in the CO_2 incubator (Thermo Electron Corporation, Forma series II). The positive control was polyvinyl chloride (PVC) and the negative control was ultra-high molecular weight polyethylene (UHMWPE). Images were visualized by a phase contrast microscope (Olympus CKX41, Japan) and captured by a digital camera (Olympus PEN EPL1, Japan) mounted over the microscope.

3.2.3.2.2.3 Neutral red staining

The L929 mouse fibroblast cells were cultured in 24 well-cell culture plates and allowed to attain a monolayer. Hydrogel samples were UV-sterilized for 20 minutes as described in section 3.1.6.3.3 and a cut-into dimension of about 1/4th size of 24 well culture plates were placed in the cell monolayer and incubated for 48 hours. The media was removed and washed carefully with PBS. Then 200µl Neutral red stain was added and incubated for 10 minutes at 37^{o}C in a CO_2 incubator (Thermo Electron Corporation, Forma series II). After incubation, the dye was removed and washed with PBS to remove the background stain. Images were then captured in a digital camera (Olympus PEN EPL1, Japan) mounted on a phase contrast microscope (Olympus CKX41, Japan).

3.2.3.2.2.4 Live/Dead assay

Live/Dead assay was performed using Calcein-AM and Ethidium homodimer-1 stain Thermofisher (USA) to test the viability of L929 cells (Sanfilippo *et al.*, 2011) on hydrogel coated tissue culture plates. Briefly, the L929 fibroblast cells were seeded at a seeding density of 1×10^6 cells/ml on 30µl hydrogel-coated 24 well plates. Images at 10x magnification were taken at 24-hour time points in a fluorescent microscope (Olympus IX71) and basic adjustments in brightness and contrast were done uniformly using ImageJ (National Institutes of Health) software.

3.2.3.2.2.5 (3-(4,5-Dimethylthiazol-2-yl)-2,5- diphenyltetrazolium bromide assay

The (3-(4,5-Dimethylthiazol-2-yl)-2,5- diphenyltetrazolium bromide (MTT) assay was conducted by the classical ‘test on extract’ method based on ISO 10993 Part 5 and 12. The ISO 10993 Part 12 was followed for the extraction of hydrogels. Briefly, the hydrogel samples of 0.1gm in 1 ml DMEM medium containing 10% serum were placed in a 37^0C incubator (Thermo Electron Corporation, Forma series II) for 24 hours. The resultant extract was filtered using a syringe filter (Sartorius Minisart®, Germany). Then the extracted media was supplemented to L929 mouse fibroblast cells cultured in 24 well plates (Thermofisher) and incubated for 24 at 37^0C in a CO_2 incubator (Thermo Electron Corporation, Forma series II). Then MTT assay was performed based on ISO 10993 Part 5. Briefly, the culture media from the cell culture plates were removed and added 50µl MTT dye and incubated for two hours at 37^0C in a CO_2 incubator. After the incubation MTT solution was removed and 100µl isopropanol to each well and swirled well and absorption was detected at 570nm.

Simultaneously, an additional MTT assay was performed on a predicate device named Collogel, which is a commercially available formulation of porcine dermal collagen manufactured and marketed by Cologenesis Healthcare Pvt Ltd, India for wound healing applications.

3.3 Wound healing studies

3.3.1 *In vitro* scratch wound assay

In vitro, scratch wound assay was performed to evaluate the rate of migration of L929 cells after the creation of scratch wound (Ortega-Llamas *et al.*, 2022). The *In vitro* scratch assay was performed with HG00, HG60, and the predicate device Collogel. Briefly, a scratch wound was created using a 200µl pipette tip on a monolayer of mouse L929 cells in a 12-well culture plate. The scratch wound was carefully washed with PBS twice to remove the detached cells during the wounding. Then cell culture inserts were placed over each well and 10 mg samples of HG60, CG and HG00 were placed to allow the release of gel components. The control groups did not undergo any treatment. The Calcein-AM staining was performed to identify live cells (Sanfilippo *et al.*, 2011) at the time points 0th hour, 4th hour, and 8th hour. The Calcein-stained cells were fixed with 0.025% formaldehyde and stored at 4^0C for image capturing at a later stage. The images were then captured at 4x magnification using a fluorescent microscope (Leica DMIRB) and evaluated the rate of migration of fibroblast cells which resulted in the scratch wound closure

3.3.2 *In vivo* evaluation of wound healing potential of HG60

3.3.2.1 Materials

Ketamine hydrochloride (Indian Immunologicals Limited, India), xylazine (Neon Laboratories Limited, India), Povidine-iodine solution (Win-medicare, India), Collogel (ColoGenesis Healthcare Pvt.Ltd, India), Wooden ruler (Camlin, India), RNA*later* solution (Thermofisher, USA), Tissue cassettes (Leica, Germany), Surgical blade (Lister^{TM}(Germany), Tissue processor (Leica TP1020, Germany), Paraffin embedding center (SLEE MPS P1, Germany), Cooling module (SLEE MPS/C, Germany), semi-automated rotary microtome (Leica RM 2255, Germany), hot air oven (MRC DFO 240, Israel), Microscopy slides (StarFrost adhesive slides, Germany), Hematoxylin (Sigma, USA), Glacial acetic acid (Merck, USA), Ammonia (Molychem, India), Eosin yellow (Sigma, USA), Hydrochloric acid (Molychem, India), Picric acid (Merck, USA), Acid Fuchsin (S.D.Fine Chemicals, India), Ethanol (Himedia, India), Phosphomolybdic acid (Nice, India), Glycerol (Merck, USA), Lithium carbonate (Qualigens, India) aniline blue solution (S.D.Fine Chemicals, India), Ferric chloride(Molychem, India), Sodium citrate (Himedia, India), Hydrogen peroxide (Merck, USA), Super Sensitive^{TM} Polymer-HRP IHC Detection System (BioGenex, USA), primary antibodies against CD8+ for cytotoxic T lymphocytes cells (Abcam, Mouse monoclonal, Clone OX-8; Catalogue number, ab33786) CD4+ for helper T cells (Abcam, Rabbit polyclonal, Clone EPR19533; Catalogue number, ab183686), CD80+ for M1 macrophage (Abcam, Rabbit polyclonal; Catalogue number, ab215166), and CD163+ for M2 macrophages (Abcam, Rabit monoclonal, Clone EPR19518; Catalogue number ab182422). Olympus microscope (BX51) having DP71 camera mounted, DPX mounting medium (Leica CV Ultra, Germany), *Image-Pro* (version 3DS6.1, Media cybernetics, USA), ImageJ software (National Institutes of Health, USA).

3.3.2.2 Methods

3.3.2.2.1 Creation of full-thickness excision skin wound in rats

Animal experiments were conducted in compliance with the ARRIVE guidelines (du Sert *et al.,* 2020) by a randomized block design and the animal numbers were calculated by the Resource Equation Method (Arifin and Zahiruddin, 2017) requiring fewer number of animals, in view of ethics. Experiments were conducted with the permission of the Institutional Animal Ethics Committee (No: SCT/IAEC-340/NOVEMBER/2019/104) on Eighty young adult Sprague Dawley rats maintained at the Division of Laboratory Science (an ISO-17025 certified laboratory) of the host institution under the direct supervision of veterinarians. Specifically, a veterinarian performed the anesthesia and peri-surgery care of animals as described below. Every effort was made to comply with the ARRIVE guidelines.

Rats of 6-8 weeks of age weighing 220-280g were randomly anaesthetized by intramuscular injection of Ketamine (80mg/Kg body weight) and Xylazine (10mg/kg body weight) as per the approval of IAEC. The fur on the dorsum of rats was shaved and sterilized with povidone-iodine solution. Full-thickness excision wounds measuring 1.5 cm width × 2.5 cm length were created ensuring the removal of the panniculus carnosus muscle to avoid wound healing by contraction (Rittié, 2016). Then the rats were divided into four groups and wound size was measured by digital planimetry under anesthesia (will be explained in detail in section 3.2.2). The first three groups received gels of HG60, the predicate device Collogel (CG) or HG00 for treating the wounds. The fourth group with open wounds (OW) did not receive any assistance for healing except the routine veterinary care common to all groups. Animals were then placed in individually ventilated cages maintaining the optimum conditions (18°C to 26°C temperature with 30% to 70% humidity, *ad libitum* feed and water). The health of the rats was monitored every day under the supervision of a veterinarian and the wounds were cleaned daily with hypertonic saline. The designated hydrogels were applied to the wound bed continuously for the first five days and thereafter once in three days. At the predetermined time points namely 9, 12, 15, 18, and 21 days, four randomly selected animals were euthanized by CO_2 inhalation (followed as per the guidelines in the Compendium of CPCSEA 2018) from each group. Digital planimetry of the wound soon after the euthanasia and the wound along with normal skin was explanted and made into equal halves The anterior portion from all animals was incubated in 10% NBF for histomorphological evaluation and the posterior half from all animals was incubated in RNA*later* solution for molecular evaluations.

3.3.2.2.2 Digital planimetry using a custom-made photographic stand

Digital planimetry was performed to evaluate the percentage of wound area using a custom-made photographic stand (Figure 5). Wounds were photographed using a digital camera (Sony A6000) mounted on the stand at a constant focal distance of 30 cm from the wound surface to the camera sensor and the images were collected in RAW format (6024x4024 Resolution). The scale holder was repositioned to ensure the scale and wound surface was in the same plane of photography.

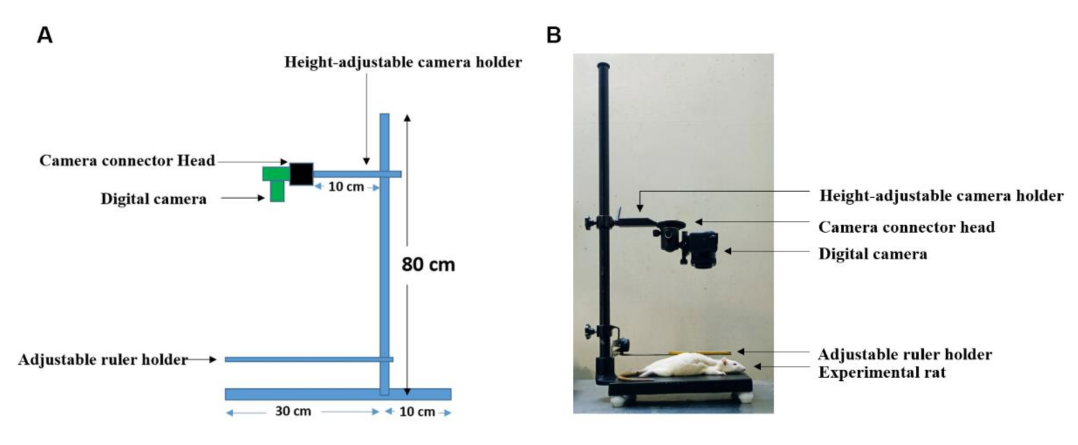

Figure 5. Illustration showing the design (A) and use (B) of the developed digital planimetry system made of a photographic stand mounted with a digital camera used for measuring wound size in experimental rats.

The images captured with the help of the photographic stand were then analyzed using ImageJ software (National Institutes of Health). First, the images were calibrated with the known distance in the ruler. Then the outline of the wound was drawn using the polygon tool from the software and measured the area. The percentage of wounds remaining was calculated using the formula.

Percentage of wound remaining = 100 (Final wound area at the time of euthanasia/ Initial wound area at the time of surgery)

3.3.2.2.3 Histomorphological evaluation

The tissue collected in 10% NBF was incubated for 48-96 hours to ensure adequate fixation. The tissues were then processed in a tissue processor (Leica TP1020) by dehydration in ascending grades of isopropyl alcohol, cleared in xylene, and impregnated with paraffin wax. The processed tissue was paraffin-embedded using a paraffin tissue embedder (SLEE MPS P1) connected with a cooling module (SLEE MPS/C). Then thin sections of 4μm thickness were cut using a semi-automated rotary microtome (Leica RM 2255) and spread on a water bath (make/ model) pre-programmed at 54^0C. The thin sections were then collected on charged microscopy slides (StarFrost) in a slanting position and labeled with a graphite pencil (Camlin). The tissue slides were then dried at 37^0C for at least 24 hours in a hot air oven (MRC DFO 240) and stored at ambient temperature until further use. They were stained with routine hematoxylin and eosin staining (H&E), Masson’s trichrome staining, Herovici’s staining or appropriate immunohistochemistry as required.

3.3.2.2.4 Hematoxylin and eosin staining

The staining was performed as per the protocol followed in the host laboratory. Briefly, the slides with tissue sections were deparaffinized in xylene and hydrated using ascending grades of isopropanol and water. It was stained with hematoxylin solution for 20 minutes, washed in running water for five minutes, differentiated in 1% acid alcohol with a dip, and washed in running tap water. The slides were then treated with ammonia water for bluing. After rinsing with water, sections were stained with eosin solution for 2.5 minutes. The slides were then dehydrated in isopropanol, cleared in xylene, and mounted using DPX mounting medium (Leica CV Ultra).

3.3.2.2.5 Histomorphology by hematoxylin and eosin staining

The slides were observed under a bright field microscope (Olympus BX51) at 4x, 10x, and 40x magnifications and histomorphology parameters like re-epithelialization, granulation tissue formation, infiltration of mononuclear cells, and nature of remodeling were considered for evaluation. The observations were made under the supervision of a qualified veterinary pathologist and the images were captured using a bright field microscope (Olympus BX51) mounted with camera DP71.

3.3.2.2.6 Immunofluorescence for cytokeratin and percentage re-epithelialization from hematoxylin and eosin-stained images

Briefly, the histology slides were deparaffinized and hydrated as described in section 3.2.4.1. The slides were then heated for 1 hour in citrate buffer for antigen retrieval and allowed to cool. Blocking was done using 1% bovine serum albumin for 30 minutes. The primary antibody was added and incubated overnight at 4ºC in a humidity chamber. Washed with PBS and added secondary fluorescent-conjugated antibody for cytokeratin-7 (CK7) and incubated for one hour at room temperature in a humidity chamber. Washed and counterstained with DAPI and mounted using fluorescent mounting media (Leica, Acrytol mounting media). Images were captured using a fluorescence microscope (Leica DMIRB).

The percentage-epithelialization was calculated from the H&E images using Image-Pro® software (Media Cybernetics). First, the images were calibrated and then with the pen tool, the length of the wound was determined by measuring the distance between the original epithelium was recorded. After that the length of the neo epithelium was measured from the original wound edges. The percentage re-epithelization was calculated by using the formula.

$$Percentage\ reepithelilization$$

$$= \frac{Total\ wound\ length(\mu m) - Remaining\ \ wound\ length(\mu m)}{Total\ wound\ length(\mu m)} X\ 100$$

3.3.2.2.7 Special staining for collagen and stereology

3.3.2.2.7.1 Masson’s trichrome staining

Masson's trichrome staining was performed as per the protocol followed in the host laboratory. Briefly, the slides with tissue sections were deparaffinized and hydrated as described in section 1.4.9.2. Then for secondary fixation the tissues were heated for 1 hour at 60^0C in a water bath (Julabo TW 20, Germany) with the mordant Bouin’s fixative and allowed to cool at room temperature. Then the slides were washed in running tap water until the yellow colour of the picric acid disappeared. It was then stained with Weigert’s Iron hematoxylin stain for 10 minutes, and washed in running water for five minutes. It was then differentiated in 1% acid alcohol and treated with 0.2% ammonia water for 3 minutes for bluing. The sections were then stained with acid fuchsin for 5 minutes, rinsed in distilled water two times, and differentiated in phosphomolybdic acid solution. Then this was stained with aniline blue solution for 20 seconds, rinsed with water, and differentiated in 1% acetic acid. The sections were then dehydrated, cleared, and mounted using a mounting media (Leica CV Ultra). The slides were allowed to dry and observed under a bright field microscope (Olympus BX51) and images were captured using a camera (DP71) attached to the microscope at 10x and 40x magnifications.

3.3.2.2.7.2 Herovici's staining

Herovici staining was performed as practiced in the host laboratory. Briefly, the slides with tissue sections were deparaffinized and hydrated as described in section 3.2.4.1. The sections were then stained with Weigert's iron hematoxylin solution for 20 minutes, washed in running water, and stained with Herovici's stain for 2 minutes. It was then rinsed with 1% acetic acid and washed in water for 2 minutes.The sections were then dehydrated, cleared, and mounted as described in section 1.4.9.2. The slides were dried and observed under a bright field microscope (Olympus BX51) and images were captured using a camera (DP71) attached to the microscope at different magnifications.

3.3.2.2.7.3 Stereology

Stereology for total collagen content was determined using sections stained with Masson's trichrome stain and collagen remodeling for type I and type III collagen was further determined using sections stained with Herovici's stain. For quantification of collagen remodeling, 40x magnification images were selected. First, the midpoint of the wound was marked by Image-Pro® software (Media

Cybernetics). From the midpoint, the maximum number of high magnification images (40x) were captured and evaluated using Image-Pro® software.

3.3.2.2.8 Immunohistochemistry

The presence of pro-inflammatory as well as anti-inflammatory cells was detected by immunohistochemistry (IHC) using Super Sensitive™ Polymer-HRP IHC Detection System (BioGenex, USA cat no: QD430-XAKE) and counterstained with Harris's hematoxylin. The antibodies (dilution 1:400) against the following antigens were used (Table 2): CD4+ for helper T cells, CD8+ for cytotoxic T lymphocyte, CD80+ for M1 macrophage, and CD163+ for M2 macrophages as practiced in the host laboratory. Briefly, the slides were deparaffinized and hydrated as described in section 3.2.4.1. The slides were then heated for 1 hour in citrate buffer for antigen retrieval and allowed to cool. Then primary antibody was added and incubated for one hour. After the incubation super enhancer in the kit was added and allowed to incubate for 30 minutes. The slides were then stained with Wiegerts hematoxylin and chromogen DAB was added and incubated for five minutes. The sections were then dehydrated, cleared, and mounted using a mounting media (Leica CV Ultra). The slides were allowed to dry and observed under a bright field microscope (Olympus BX51) and images were captured using a camera (DP71) attached to the microscope at 10x and 40x magnifications.

The slides were evaluated using a light microscope (Olympus BX51, Olympus, Japan), and images at 40x magnification were captured at the midpoint of the wound using a DP71 camera mounted onto the microscope. The number of positive cells was quantified manually and the CD4+/CD8+ ratio as well as the CD80+/CD163+ ratio was derived.

Table 2. List of antibodies used for immunohistochemistry

Sl.No.	**Target**	**Host**	**Dilution**	**Company**	**Cat. No.**	**Retrieval buffer**
1	$CD4^+$	Mouse	1:400	Abcam	ab183686	Citrate buffer, pH 6.8
2	$CD8^+$	Mouse	1:400	Abcam	ab33786	Citrate buffer, pH 6.8
3	$CD80^+$	Mouse	1:400	Abcam	ab215166	Citrate buffer, pH 6.8
4	$CD163^+$	Mouse	1:400	Abcam	ab182422	Citrate buffer, pH 6.8

3.3.2.2.9 Molecular studies

The tissue samples collected from the wounds of the experimental rats euthanized on day 18 and 21 post surgery which were preserved in RNA*later* solution and used for molecular studies. They were frozen with liquid nitrogen and crushed in a mortar and pestle. Liquid nitrogen was supplemented throughout the crushing process till a fine powder of the tissue was obtained. The RNA was then extracted by the Trizol reagent extraction method (Rio *et al.*, 2010) and constituted in RNAse-free water and stored at $^{-}80^{0}$C deep freezer. The concentration of RNA was checked using nanodrop. The RNA was reverse transcribed to cDNA using Superscript III™ Reverse Transcriptase (Thermo Fisher Scientific) kit. Quantitative Real-Time PCR (qPCR) was performed (Analytika gena 3G) with sybrgreen (Thermo Fisher Scientific, USA). The genes for Inducible Nitric Oxide Synthase (iNOS), Interleukin 10 (IL-10), Collagen type I (ColT1), Collagen type III (ColT3) was studied. For this, GAPDH was taken as the reference gene for the analysis (Table 3). Relative fold change was calculated by normalizing the control open wound using the 2^-ΔΔCt method. All the samples and reference genes were analyzed in triplicates.

Table 3. List of selected genes for RT-PCR studies

Sl. No.	**Gene**	**Forward Primer**	**Reverse Primer**
1	GAPDH	**5**`TGGCCTCCAAGGAGTAAGAAAC**3`**	**5**`GGCCTCTCTCTTGCTCTCAGTATC**3`**
2	*iNOS*	**5**`CACCACCCTCCTTGTTCAAC**3`**	**5**`CAATCCACAACTCGCTCCAA**3`**
3	*TNF-α*	**5**`AAATGGGCTCCCTCTCATCAGTTC**3**	**5**`TCTGCTTGGTGGTTTGCTACGAC**3`**
4	*IL10*	**5**`GCTCTTACTGGCTGGAGTGAG**3`**	**5**`CTCAGCTCTCGGAGCATGTG**3`**
5	*ColT1*	**5**`AGGGACCCTTAGGCCATTGTGTA**3`**	**5**`GACATGTTCAGCTTTGTGGACCTC**3’**
6	ColT3	**5**`GACAGATCCCGAGTCGCAGA**3`**	**5**`TTTGGCACAGCAGTCCAATGTA**3`**

CHAPTER 4

4 RESULTS

4.1 Gross features of CECM-CMC hydrogel

Thin sheets of CECM scaffolds prepared by the non-detergent/enzymatic method appeared greenish-yellow in color (Figure 6).

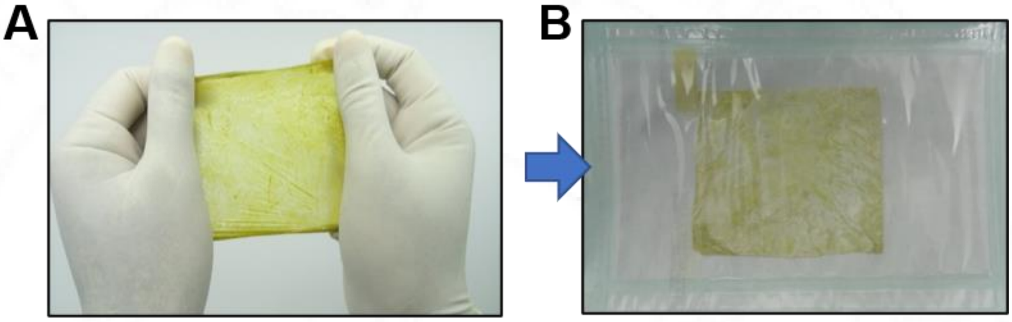

Figure 6. Gross photographs of sheet form of CECM (A) isolated by the non-enzymatic/detergent method and (B) the sterilized lyophilized form in a sachet.

Grossly the five formulations of the hydrogels, except the HG00 appeared greenish yellow probably because of the CECM content (Figure 7). The HG00 was a transparent gel and the opacity increased with the content of CECM. The proportions of CECM/CMC, and their gross features are presented in Table 4.

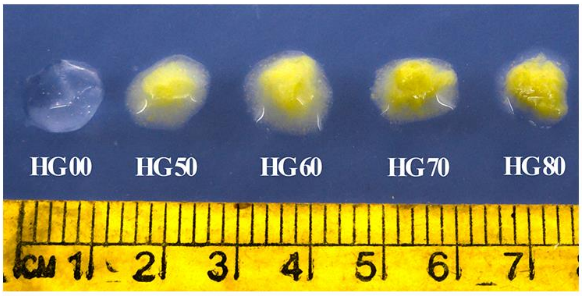

Figure 7. A photograph showing the gross physical appearances of the hydrogel formulations described in Table 4 *via* HG00, HG50, HG60, HG70, and HG80.

Table 4. The gross physical appearance and consistency of CECM-CMC hydrogels

Serial number	**Hydrogel Formulations**	**Gross appearance and consistency of the hydrogel preparations (please see the results of rheology experiments presented in section 4.2.1.4)**
1	HG00	• Relatively a stiffer gel compared to all other formulations • Transparent without any color
2	HG50	• Relatively a less stiff gel than HG00 • Partially transparent with a mild yellowish-green tinge
3	HG60	• Relatively a less stiff gel than HG50. • Partially transparent with a darker yellow color than HG50
4	HG70	• Relatively a less stiff gel than HG60 • Partially transparent with a darker yellow color than HG 60
5	HG80	• Relatively a less stiff gel than HG70 • Relatively opaque with a darker yellow colour than all other formulations

4.2 Biomaterial properties of the hydrogels

4.2.1 Physicochemical properties

The results of the physicochemical properties are detailed in the following sections

4.2.1.1 Gel fraction

The gel fraction was highest in HG00 (89.43%), which had the highest proportion of CMC. The gel fractions of the hydrogel preparations with CECM were 80.3%, 75.6%, 69% and 52% for HG50, HG60, HG70 and HG80 respectively (Figure 8)

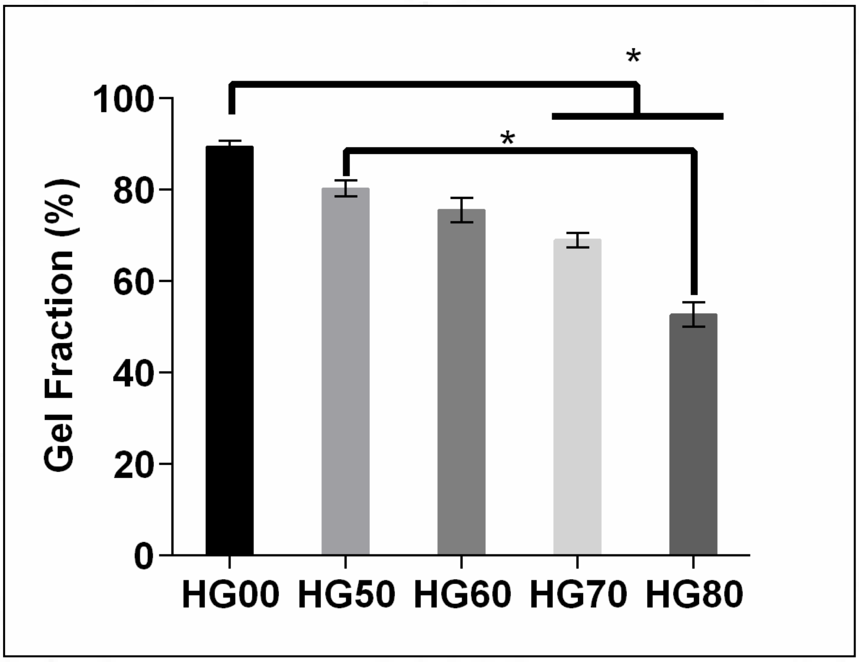

Figure 8. A bar diagram showing the percentage gel fraction of the hydrogels HG00, HG50, HG60, HG70 and HG80. Please note that the HG60 had a similar gel fraction as that of all other hydrogel formulations. (*P value ≤ 0.05, n=3).

4.2.1.2 Swelling rate

A rapid absorption of water was observed in all the hydrogel samples. All these hydrogel formulations showed a maximum volume within an hour representing their high-water absorption capability (Figure 9). The water uptake decreased with the proportion of CMC in the hydrogel and was significantly different each other.

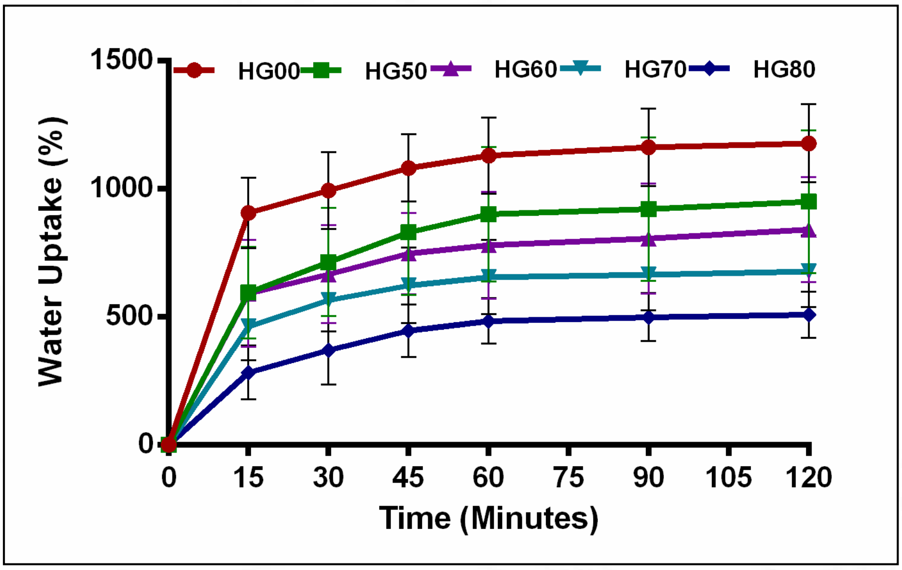

Figure 9. A line graph showing the percentage water uptake of the hydrogel formulations indicating that the swelling rate decreased with the higher content of the CECM (n=3).

4.2.1.3 Equilibrium water content

A higher percentage of equilibrium water content was observed in all hydrogel formulations (Figure 10). The equilibrium water content for HG00, HG50, HG60, HG70 and HG80 were 95.56% ± 0.06, 91.5%± 2.35, 90.48% ±7.23, 89.87% ± 0.73 and 89.61%± 0.89 respectively. Although the equilibrium water content appeared to decrease with increase in the proportion of CECM there was no significant differences between the preparations.

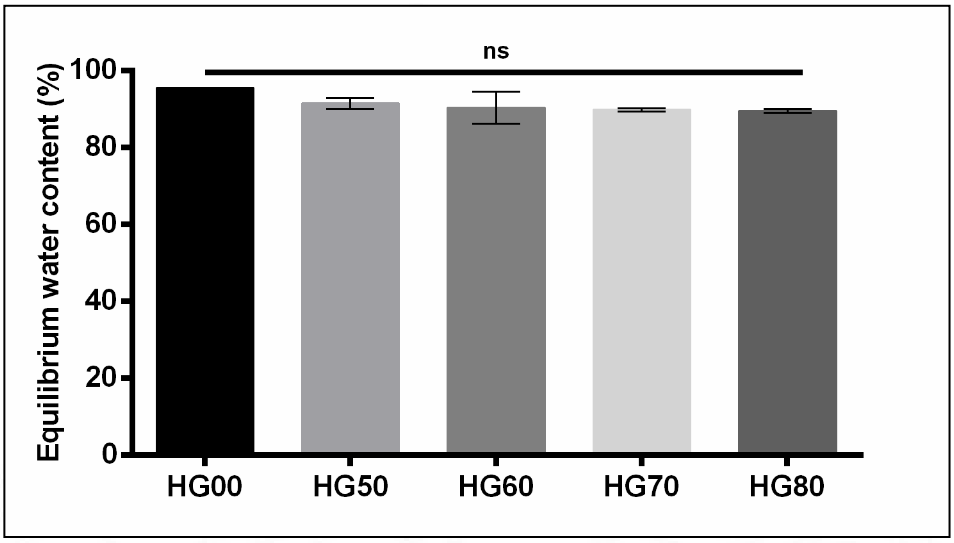

Figure 10. A bar diagram showing a higher percentage of equilibrium water content of the hydrogel formulations (n=3).

4.2.1.4 Rheology

The results of the amplitude sweep indicated that the LVER of the hydrogel occurred within the strain range of 0.1-5%. The ratio of G'/G" differentiated the relative stiffness of the hydrogels (Figure 11 A to E). Coupled with this, the results of frequency sweep indicated that the G'/G" ratios for all the hydrogel formulations were less than one, indicative of weaker gels (Figure 11 F to J). In fact, the storage modulus was found to be higher than the loss modulus in all the formulations indicative of their elastic solid nature. The HG00 and HG80 showed the higher LVER regions compared to the other formulations.

The estimated viscosity of all the hydrogels was observed to decrease at a higher shear rate. A lower rate of viscosity was observed in HG50 and HG60 compared to HG00. However, in HG70 and HG80, the viscosity was slightly higher than that of HG50 and HG60 and it was observed to be similar to HG00 (Figure 11K).

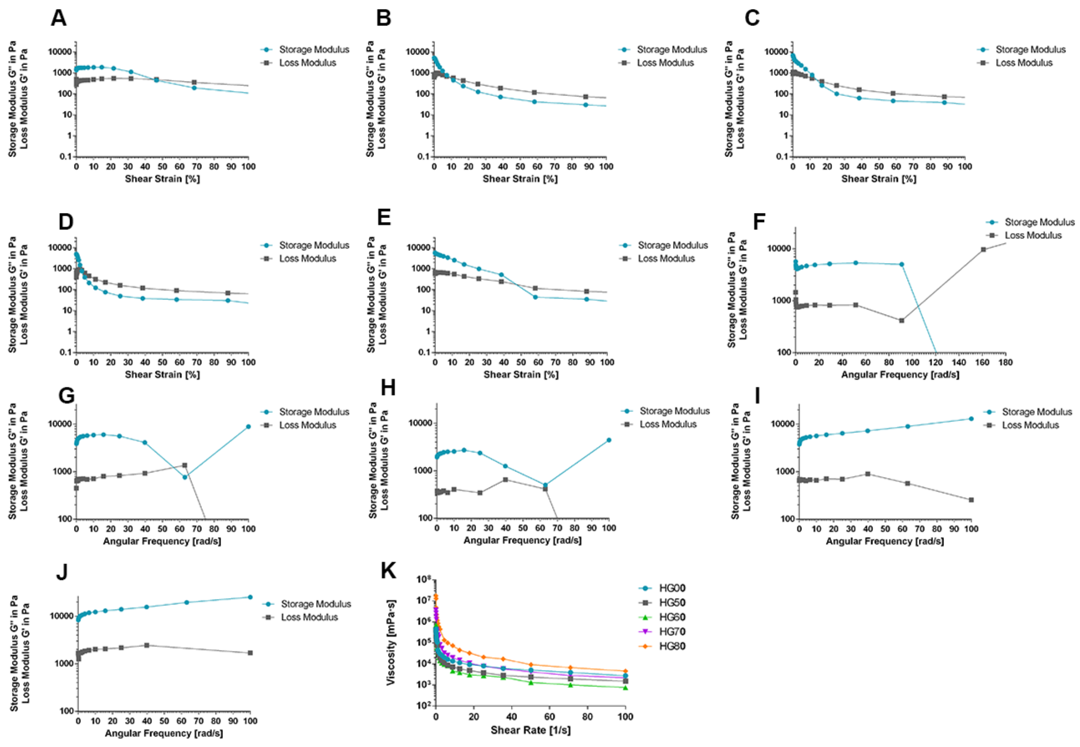

Figure 11. Rheology results representing the amplitude sweep of HG00 (A), HG50 (B), HG60 (C), HG70 (D) and HG80 (E) showing the linear viscoelastic region (LVER) at 0.1-5% strain range. The frequency sweep of hydrogel samples showed a higher storage modulus than loss modulus in HG00 (F), HG50 (G), HG60 (H), HG70 (I), HG80 (J). A line graph representing the viscosity of all the hydrogel samples (K).

4.2.1.5 Fourier transform infrared spectroscopy

Except for the HG00, the FTIR spectra of hydrogel formulations (Figure 12) showed the characteristic peaks of amide I at 1660 cm^{-1} (C=O stretching), amide II at 1540 cm^{-1} (NH deformation and C-N stretching), and amide-III at 1235 cm^{-1} (C-N stretching and N-H deformation) of CECM, as originally reported by Anilkumar *et al*., 2014. Furthermore, the spectral bands expected from the stretching vibrations of the carboxyl group of CMC were also observed in the HG00 at 1614 cm^{-1} and 1446 cm^{-1} (Yuwono *et al.*, 2021).

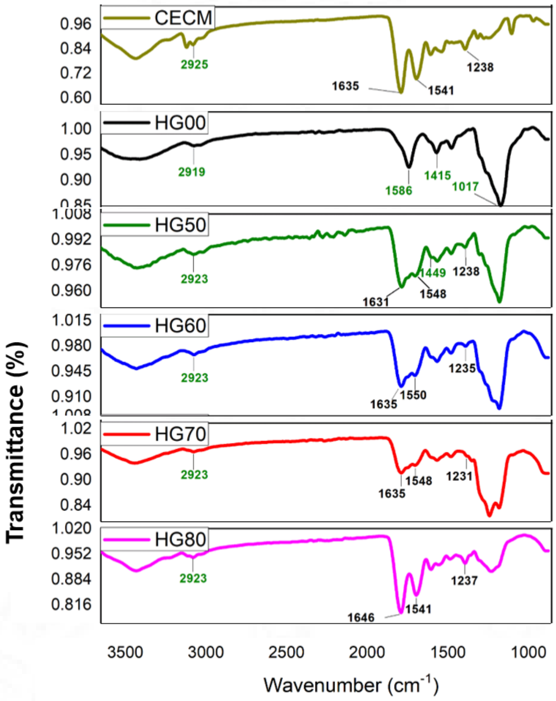

Figure 12. A stacked line graph of FTIR-spectra of CECM, HG00, HG50 HG60, HG70, and HG80 showing the various peaks at wavelengths of amide I at 1660 (C=O stretching), amide II at 1540 (NH deformation and C–N stretching) and amide-III at 1235 cm^{-1} (C–N stretching and N–H deformation) of porcine cholecyst extracellular matrix (CECM) and the symmetric and asymmetric modes of stretching vibrations of the carboxyl group 1614 cm^{-1} and 1446 cm^{-1} of carboxymethyl cellulose.

4.2.1.6 Scanning electron microscopy

The cut surface of the lyophilized hydrogel samples was found to be vastly porous with a higher content of CECM (Figure 13). The average pore size was 79µm ±3.8µm for HG00 and the porosity increased to 89µm (±3.8µm) for HG50, 106µm (±4.5µm) for HG60, 118µm (±9.8µm) for HG70, and 127µm (±4.6µm) for HG80 notably an increase with the content of CECM (Figure 14).

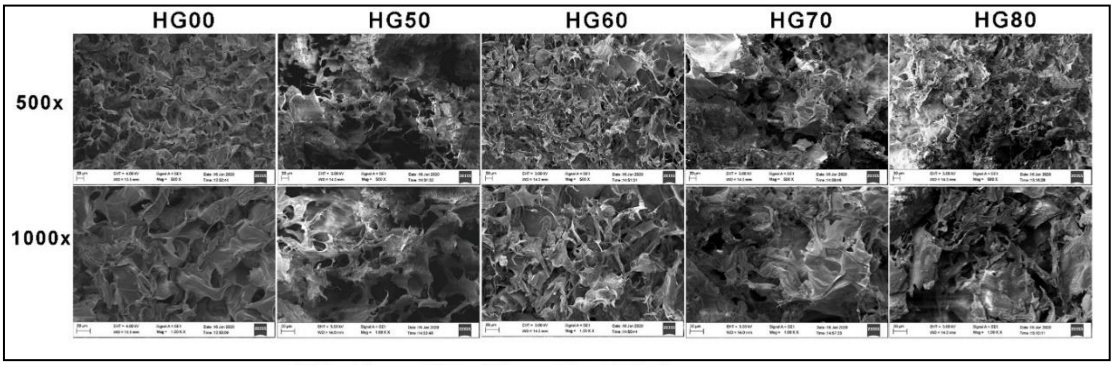

Figure 13. Scanning electron micrographs of the cut surface of the lyophilized samples of HG00, HG50, HG60, HG70 and HG80 (Magnification 500x, top panel; 1000x, bottom panel)

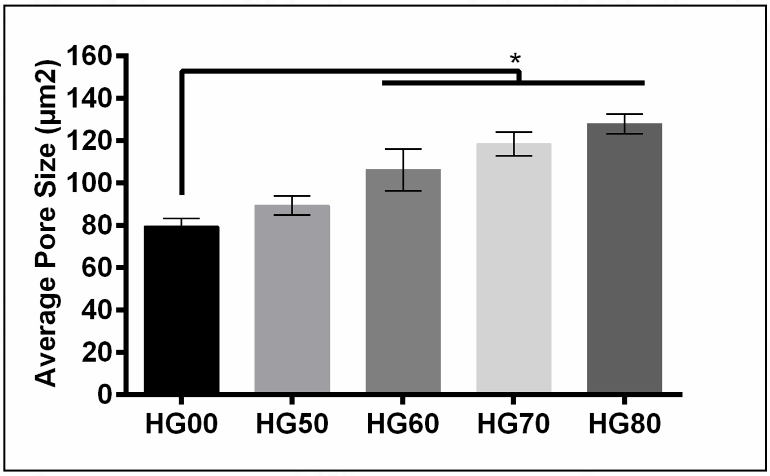

Figure 14. A bar diagram showing the average pore size of hydrogel formulations calculated from the images using ImageJ software.

4.2.1.7 Water contact angle

The water contact angle of HG00 was 92.4^0 which indicated its hydrophobic nature (Figures 15 and 16). The contact angles for HG50, HG60, HG70, and HG80 were 88.3^0, 80.6^0, 78.1^0, and 30.8^0 respectively which were considered relatively hydrophilic. A significant reduction in the water contact angle was observed in HG60, HG70, and HG80 compared to HG00. Obviously, the contact angle decreased with the increase in the CECM content.

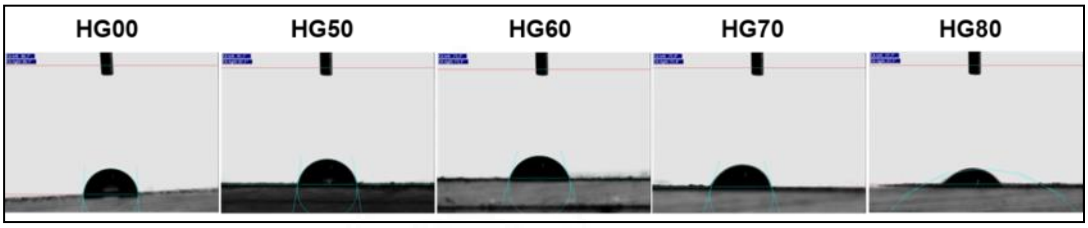

Figure 15. Water contact angle of the hydrogel formulations indicated an increase in the hydrophilicity when CECM concentration increased.

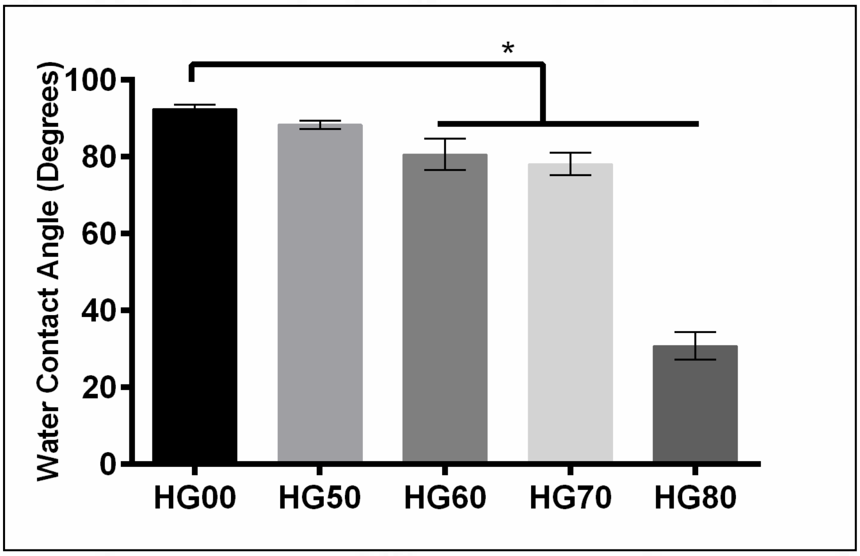

Figure 16. A bar diagram showing the water contact angle of the hydrogel formulations (n=3) (*P value ≤ 0.05)

4.2.1.8 *In vitro* degradation studies

The percentage degradation in terms of weight loss after treatment with water showed a high rate of degradation when the CECM concentration was increased. The percentage weight loss for HG00, HG50, HG60, HG70 and HG80 were 65.8%, 73.58%, 77.91%, 83.4% and 87.6% respectively (Figure 17 A).

The percentage degradation of collagen in the hydrogels by collagenase for HG50, HG60, HG70 and HG80 were 7.63%, 4.93%, 6.03% and 5.94% respectively. No significant difference was observed in the extent degradation among the various hydrogel preparations (Figure 17 B).

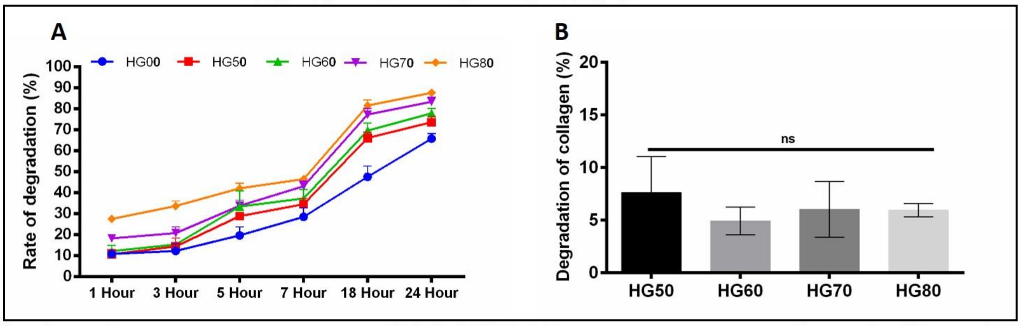

Figure 17. (A) A line graph showing the extent of nonenzymatic degradation profile of the hydrogels (B) A bar graph showing the enzymatic degradation rate of hydrogels.

4.2.1.9 Injectability

The stiction force, dynamic glide force, and end constraint force were below 20 Newton for all hydrogel formulations evaluated through 18, 19, 22 and 23 gauge needles except for HG00 which was injectable only through 18 and 19 gauge needles. Not surprisingly the maximum values were for HG00 and minimum for HG80 as presented in Figure 18.

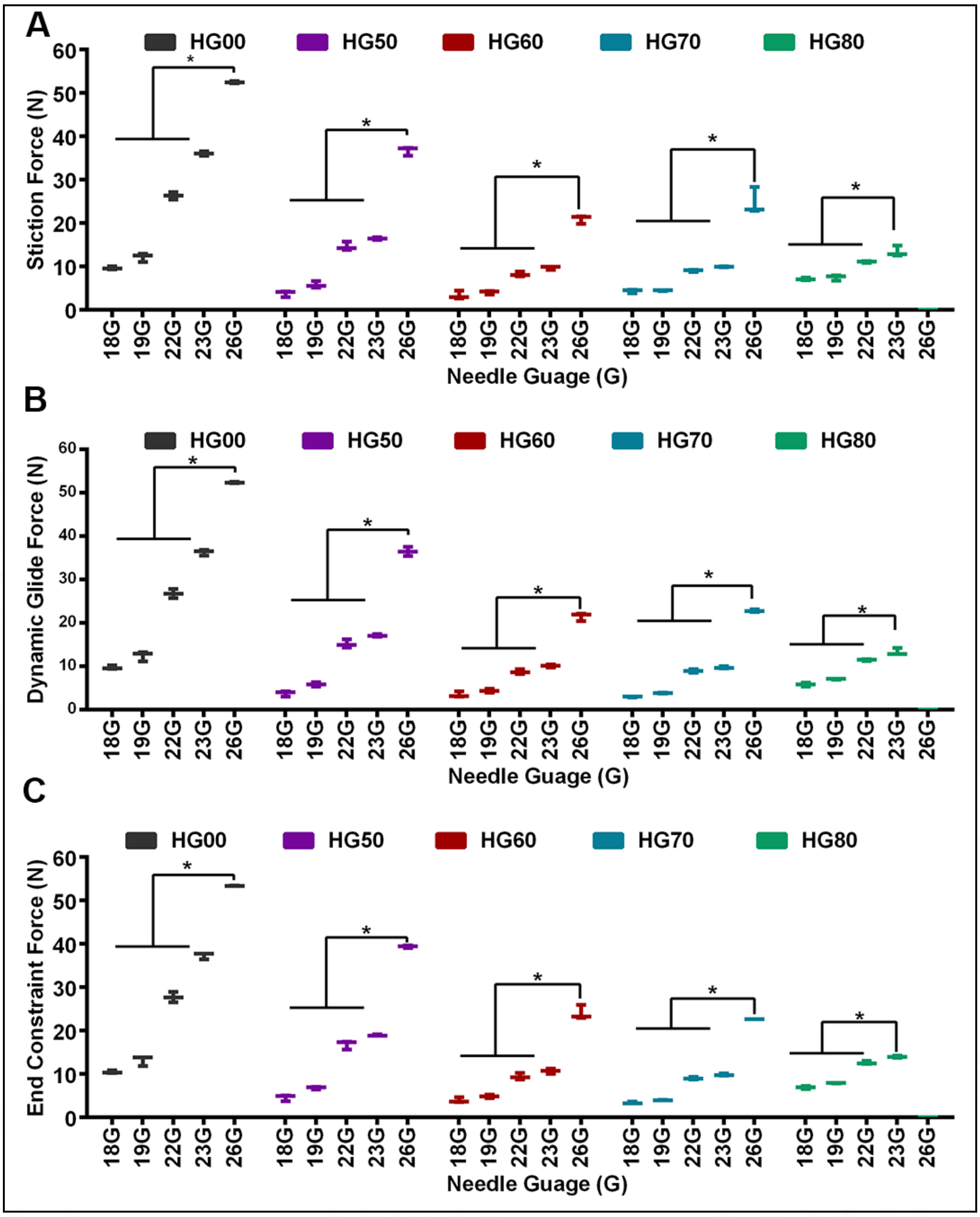

Figure 18. Box plots showing the injectability of HG formulations when injected through 18G, 19G, 22G, 23G, 26G needles (n=3): (A) stiction force, (B) dynamic glide force, and (C) end constraint force (*P value < 0.05)

4.2.2 Biological characterization

4.2.2.1 Live/Dead cell viability assay

The Live/Dead assay using Calcein AM (stained green) and Ethidium homodimer (stained red) showed a higher number of live cells than dead cells (Figure 19) in all experiments. The quantification of L929 fibroblast live cells using ImageJ revealed that all the five hydrogel formulations including the HG00 were non-toxic, with more than 90% of surviving cells. The percentages of live cells were 94.5% (+/-2.1), 93.75% (+/-2.4), 97.45 (+/-2.1) 95.65% (+/-1.6), 94.2% (+/-2.3) and 98% (+/-0.6) for HG00, HG50, HG60, HG70, HG80 and TCPS, respectively. The HG60 formulation had the highest percentage of live cells, at 97.45% (Figure 20).

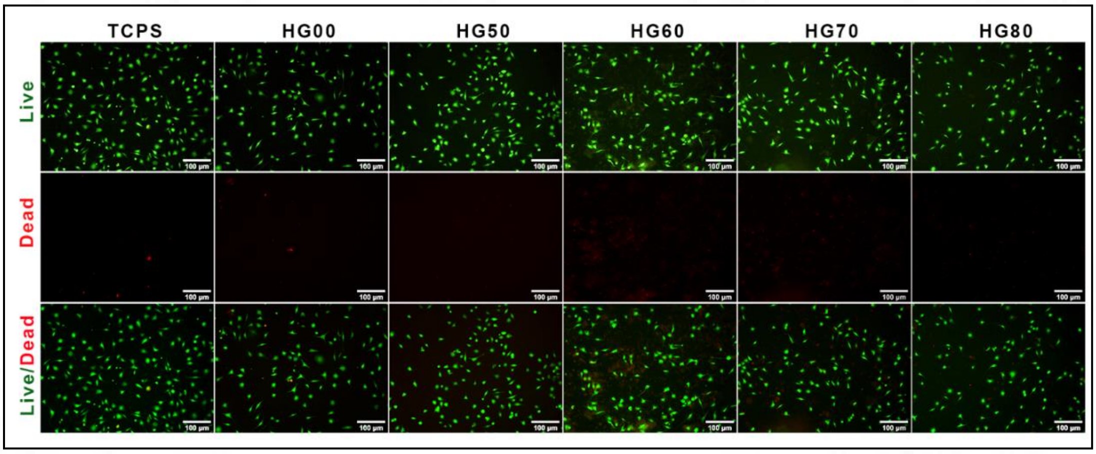

Figure 19. Fluorescent microscopic image of Live/Dead assay on L929 fibroblast cells treated with Calcein AM (green colored live cells) and Ethidium homodimer (red colored dead cells) conducted on hydrogel formulations and HG00-coated plates for 24-hour exposure. Uncoated tissue culture plates (TCPS) were used as the control (Scale bar 100µm).

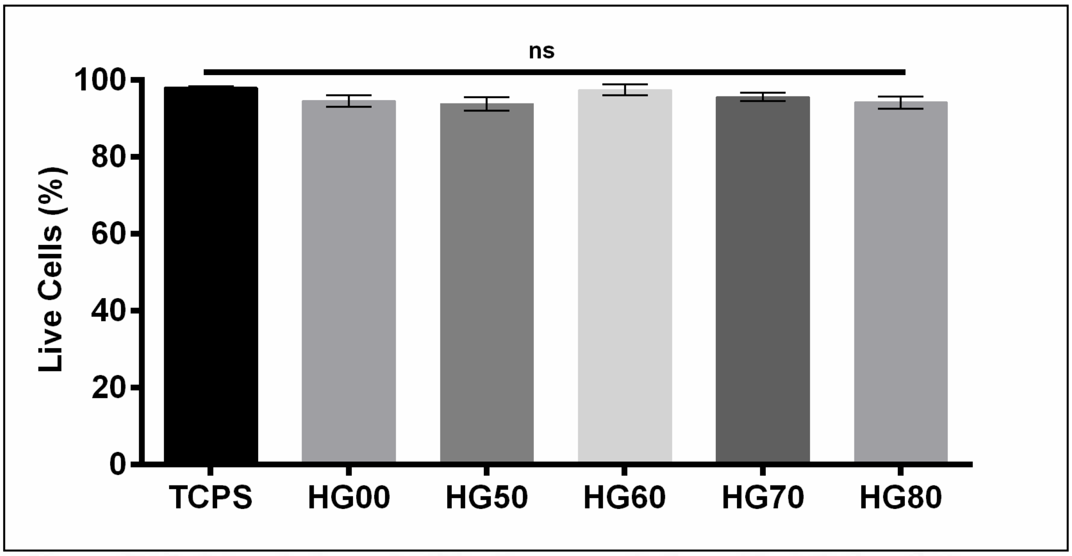

Figure 20. A bar diagram showing the percentage of live cells calculated based on photomicrographs using ImageJ software from Live/Dead-assay using L929 cells shown in Figure 19.

4.2.2.2 *In vitro* direct contact test

Direct contact of hydrogel samples with L929 fibroblast cell lines resulted in no cytotoxicity after 24 hours (Figure 21). Morphologically, there was no cell death or changes in size, shape, or growth pattern of cells in any test samples or the negative control UHMWPE. At the same time, as expected, the positive control PVC caused extensive cell death.

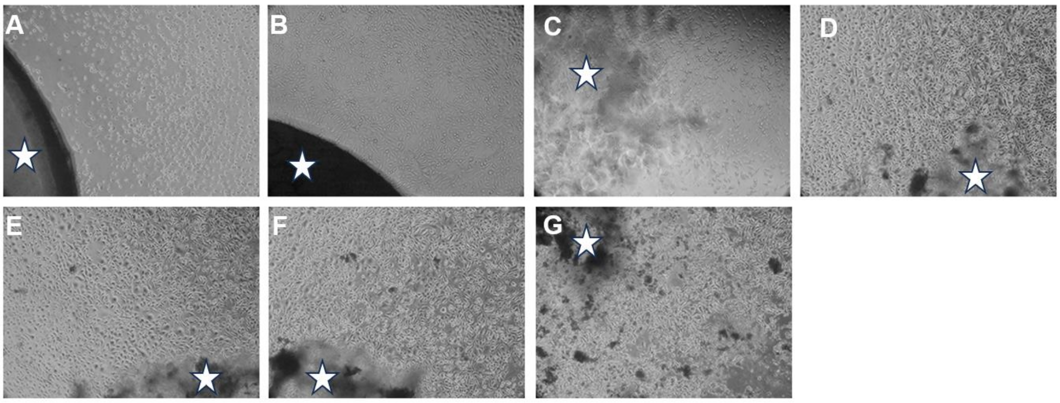

Figure 21. Light microscopic images of *in vitro* direct contact test of the hydrogel formulations *via* (A) Positive control Poly Vinyl Chloride (PVC) (B) Negative control Ultra High Molecular Weight Poly Ethylene (UHMWPE) (C) HG00, (D) HG50, (E) HG60, (F) HG70, and (G) HG80 after 24-hour direct contacts on L929 fibroblast cells. The materials are marked in asterisk (magnification, 10x).

4.2.2.3 Neutral red staining

The neutral red dye stained the lysosome of L929 cell and visible as red color at 48 hours. This indicated that the cells were metabolically active (Figure 22)

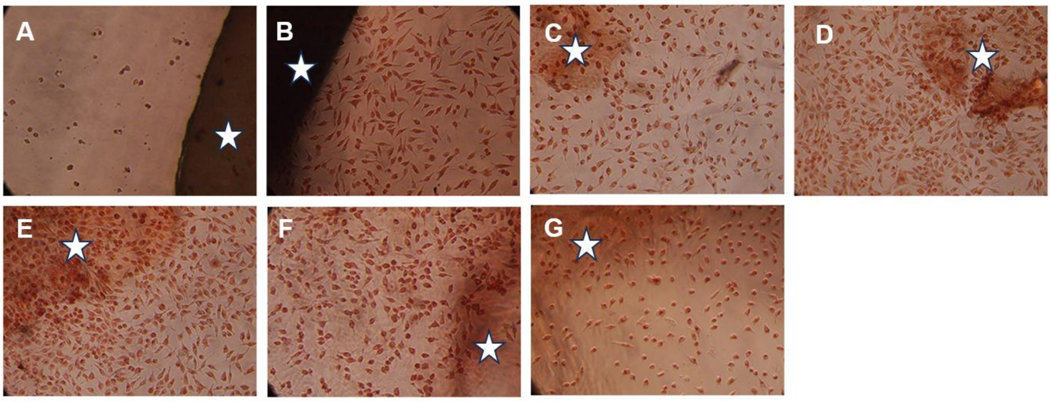

Figure 22. Light microscopic photographs of neutral red staining of L929 fibroblast cells after 48-hour direct contact *via* (A) Positive control Poly Vinyl Chloride (PVC) (B) Negative control Ultra High Molecular Weight Poly Ethylene (UHMWPE) (C) HG00, (D) HG50, (E) HG60, (F) HG70, and (G) HG80. The materials are marked in asterisk (magnification, 10x).

4.2.2.4 3-(4,5-Dimethylthiazol-2-yl)-2,5- diphenyltetrazolium bromide assay

As per the ISO 10993- Part 5, a minimum of 70 percent cells should be viable for a cytocompatible materials. The results indicated that all hydrogel formulations were cytocompatible (Figure 23), and the percentage viability for HG50, HG60, HG70, HG80, and HG00 were 94.7% ± 2.5, 95.6 % ± 3.1, 95.5 ± 3.5, 93.7 % ± 1.6, and 97.16% ± 1.1 respectively which exceeded the requirement of the standard.

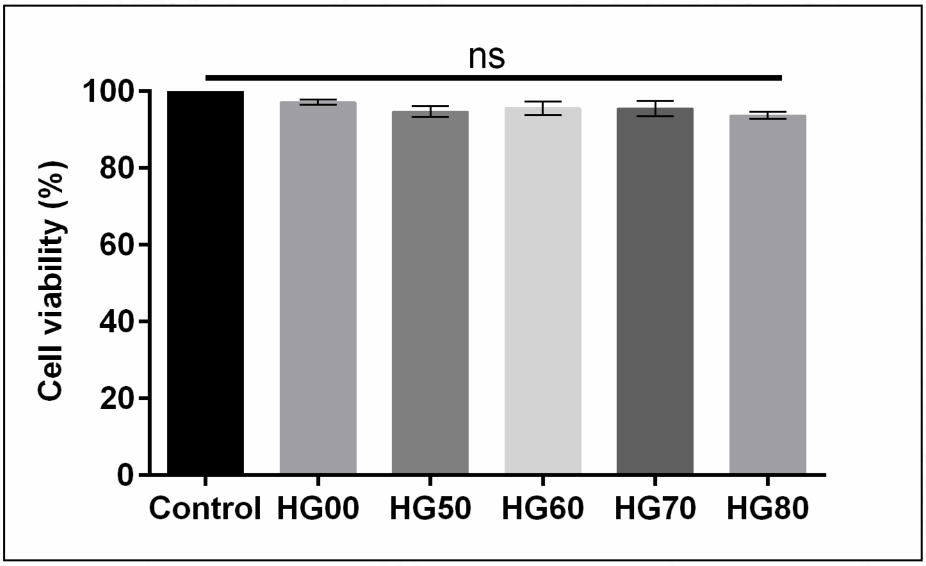

Figure 23. A bar diagram representing the percentage viability of L929 cells tested by MTT assay on extracts of the hydrogel formulations, indicating their non-cytotoxic nature.

4.3 Selection of biomaterial for wound healing studies

The hydrogel formulations were sequentially graded from 1+ to 4+ for all parameters evaluated. The results were tabulated (Table 5).

Table 5. Tabulated result of the ranking of the hydrogel formulations based on the results of the physicochemical and biological tests. Relative gradient scores from 1+ (lowest value) to 4+ (highest value) were given to the each of the four formulations for every biomaterial property evaluated in this study.

Serial. Number	**Tests/parameters**	**HG50**	**HG60**	**HG70**	**HG80**
1	Gel fraction	++++	+++	++	+
2	Swelling rate	++++	+++	++	+
3	Rheology	++++	+++	++	+
4	Average pore Size	++++	+++	++	+
5	Contact angle	+	++	+++	++++
6	Non-enzymatic degradation	+	++	+++	++++
7	Injectability	++	++++	+++	+
8	*In vitro* direct contact test	++++	+++	++	+
9	Live/Dead assay	+	++++	+++	++
10	MTT assay by test on extract	++	+++	++++	+
Total		27	30	26	17

4.4 *In vitro* experiments in comparison with a predicate device

4.4.1 3-(4,5-Dimethylthiazol-2-yl)-2,5- diphenyltetrazolium bromide assay

The results indicated that the HG60, CG and HG00 were cytocompatible (Figure 24), and the percentage viability for HG60, CG and HG00 were 97.4% ± 3.4, 89.4 % ± 3.9, 86.8 ± 6.2 respectively which exceeded the requirement of the standard.

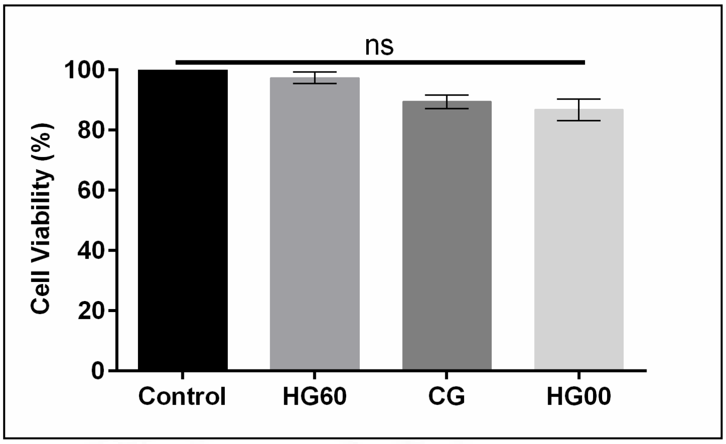

Figure 24. A bar diagram representing the percentage viability of L929 cells tested by MTT assay on extracts of the HG60, CG and HG00, indicating their non-cytotoxic nature.

4.4.2 *In vitro* scratch wound assay

A faster rate of migration was observed in the culture plate treated with the HG60 treated (79%) whereas the migration was much lower in plates treated with the non-treated TCPS (67.9%), predicate device (56.2%), and HG00 gel (31.8%) (Figures 25 and 26).

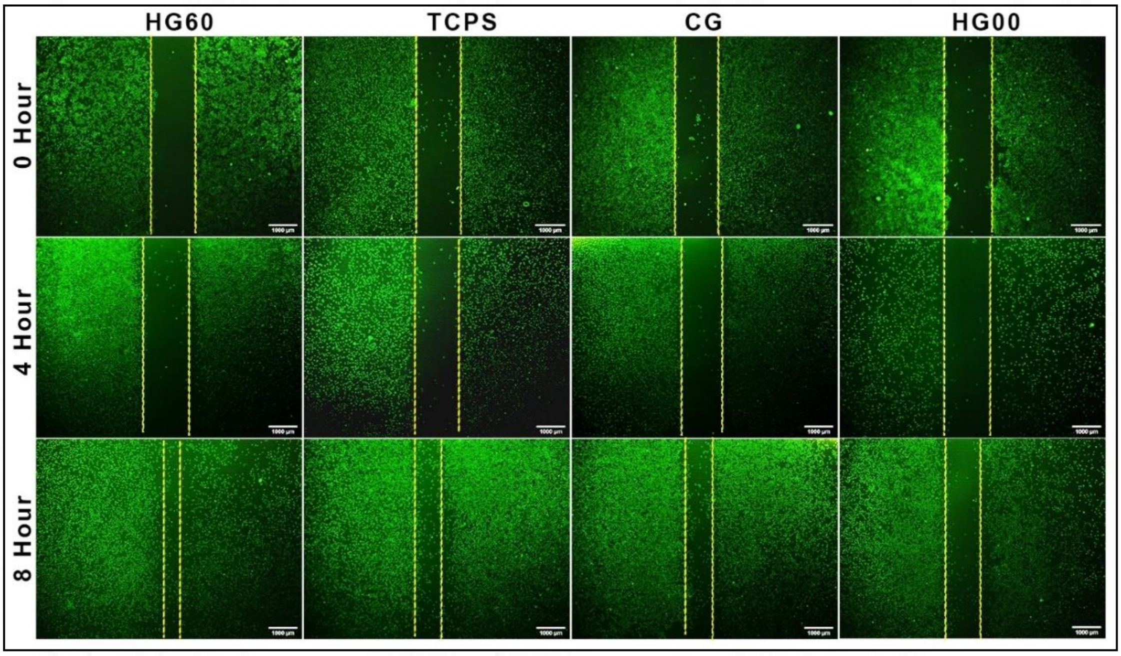

Figure 25. Results of *in vitro* scratch wound assay on treatment with HG60, CG, and HG00 and untreated tissue culture plates (TCPS) after 0, 4, and 8 hours of incubation on L929 fibroblast cells (magnification, 4x; scale bar 1000µm).

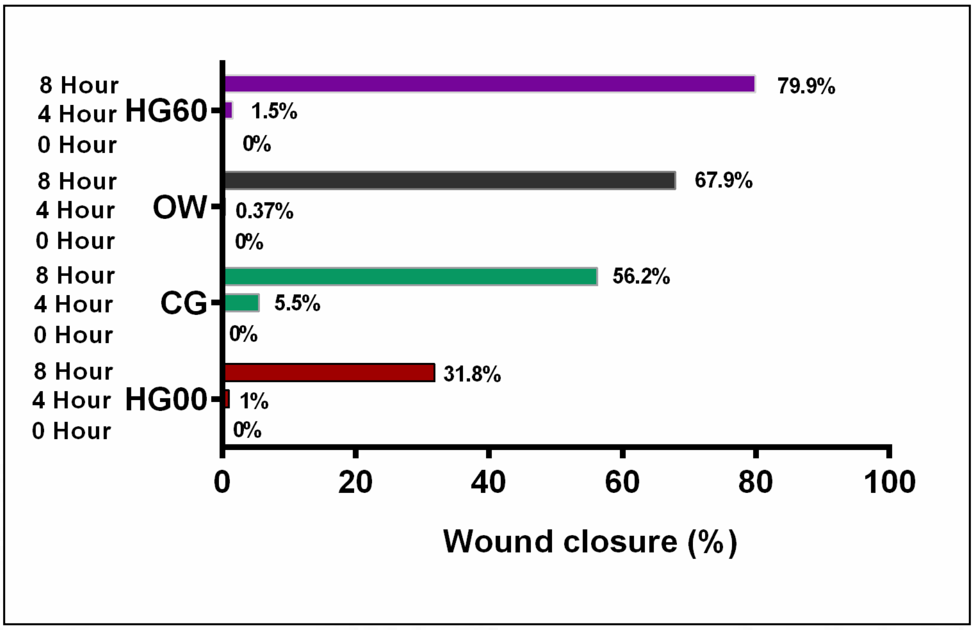

Figure 26. A bar diagram showing the percentage of wound closure calculated using ImageJ software (n=3).

4.5 *In vivo* wound healing study

4.5.1 Gross observations on wound closure

At the initial time points of the experiment, the wound area remained similar in all treatment groups (Figures 27 to 29). However, on the 15th day, a change in the healing rate was observed in HG60 hydrogel-treated animals which became more prominent on the 18th day. On the 18th day, the percentage of wound area was significantly reduced in the HG60 hydrogel (1.02% ± 1) treated animals compared to the OW (6.3% ± 1.8), the group treated with the predicate device (6.4% ± 1.6), and the HG00 group (4.2% ± 2.7). On the 21st day of the experiment, a complete wound closure was observed in animals treated with HG60 hydrogel compared to the incomplete healed wounds of the controls (Figures 28 and 29), The results prompted detailed histomorphology evaluation.

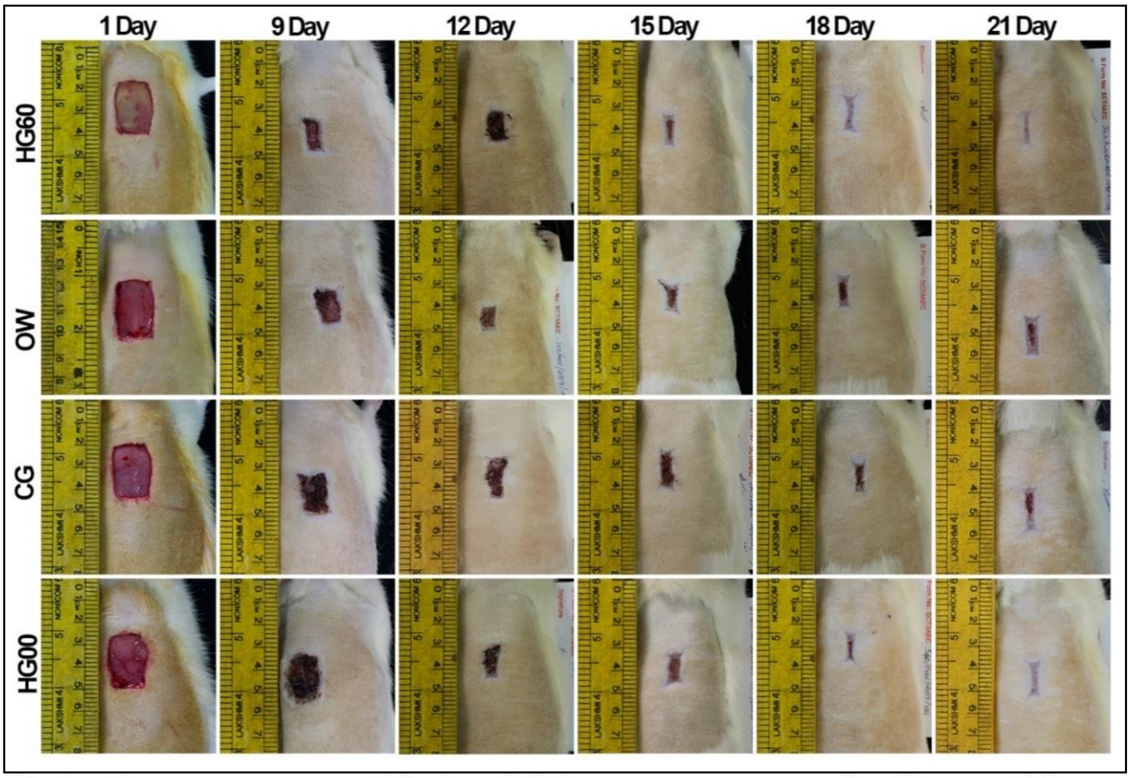

Figure 27. Gross photographs showing the morphology of wounds treated with the selected CECM hydrogel formulation (HG60) for *in vivo* studies, open wounds (OW) without any treatment, wounds treated with predicate device Collogel (CG), and wounds treated with carboxymethyl cellulose hydrogel (HG00) on the first, 9th, 12th, 15th,18th, and 21st day after the surgery(n=4). Please note, these abbreviations are used to explain the illustrations in Figures 28 to Figure 55.

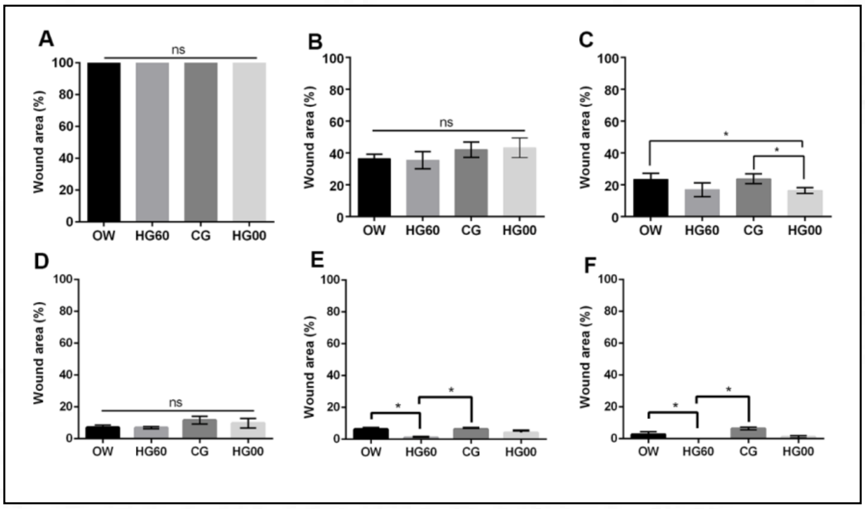

Figure 28. Bar graphs showing the extent of wound healing calculated by digital planimetry on the day of wound creation (A), the 9th day (B), 12th day (C), 15th day (D),18th day (E), and the 21st day (F) after the surgery of (n=4) (*P value < 0.05). Please see the legend the Figure 27 for an explanation of the abbreviations.

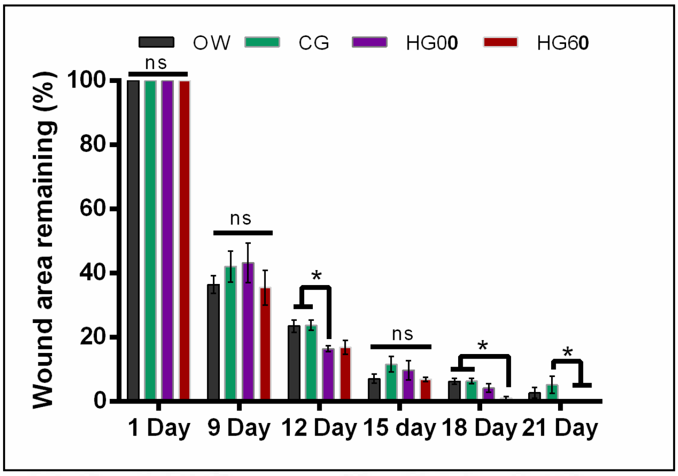

Figure 29. A bar graph showing the extent of wound healing calculated by digital planimetry on the day of wound creation and on the 9th, 12th, 15th,18th, and 21st days after the surgery, where the faster rate of healing was evident in HG60 treated animals compared to OW, CG, and HG00 (n=4; *P value < 0.05). Please see the legend the Figure 27 for an explanation of the abbreviations.

4.5.2 Re-epithelialization

Result of Immunofluorescence study of cytokeratin marker CK7 showed a complete re-epithelialization on the 18th day in the HG60 treated group (Figure 30).

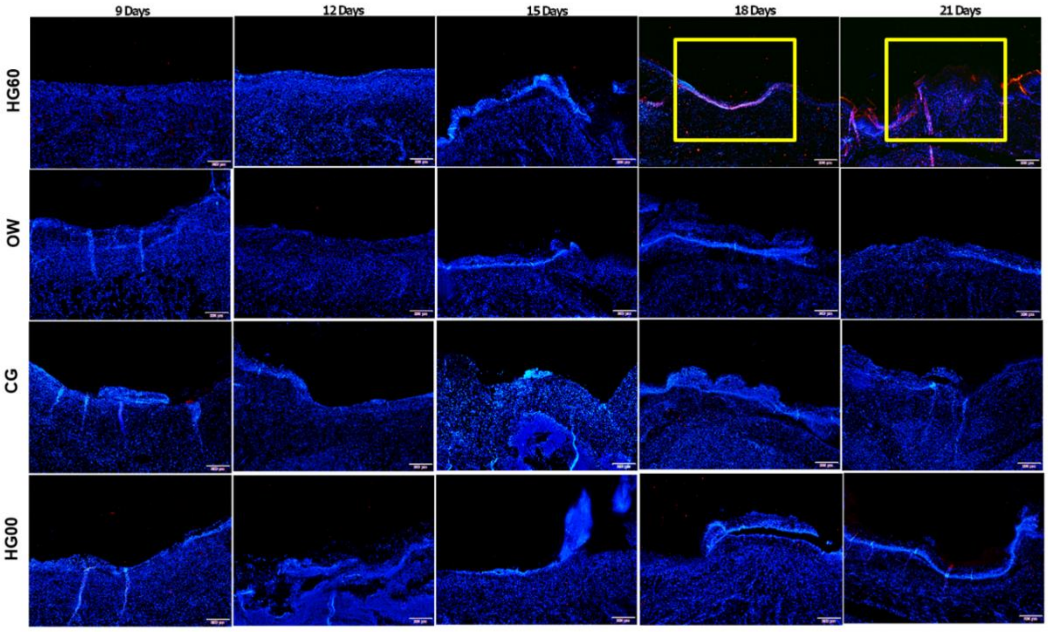

Figure 30. Immunofluorescence sections of CK7 antibody on wounds treated with HG60, OW, CG, and HG00 representing the nature of re-epithelialization, remarkably complete re-epithelialization happened in the HG60 treatment group by the 18th day (magnification, 4x; scale bar, 500µm). Please see the legend the Figure 27 for an explanation of the abbreviations.

From the H&E staining it was confirmed that as early as 15 days of wound healing, the HG60-treated animals (61.8% ± 8.8) showed a faster rate of re-epithelialization than the OW (48.5% ± 27.4), and the wound treated with the predicate device (41.8% ± 8.9) or HG00 (49.6% ± 16.8) (Figures 31 and 32). By the 18th day of the experiment, all HG60-treated rats had undergone complete re-epithelialization. Interestingly, even after 21 days, re-epithelialization was incomplete in all other groups, with only 81.6% ± 22.2, 88% ± 21.1), and 75.9% ±24.1 re-epithelialization in OW, CG, and HG00 respectively.

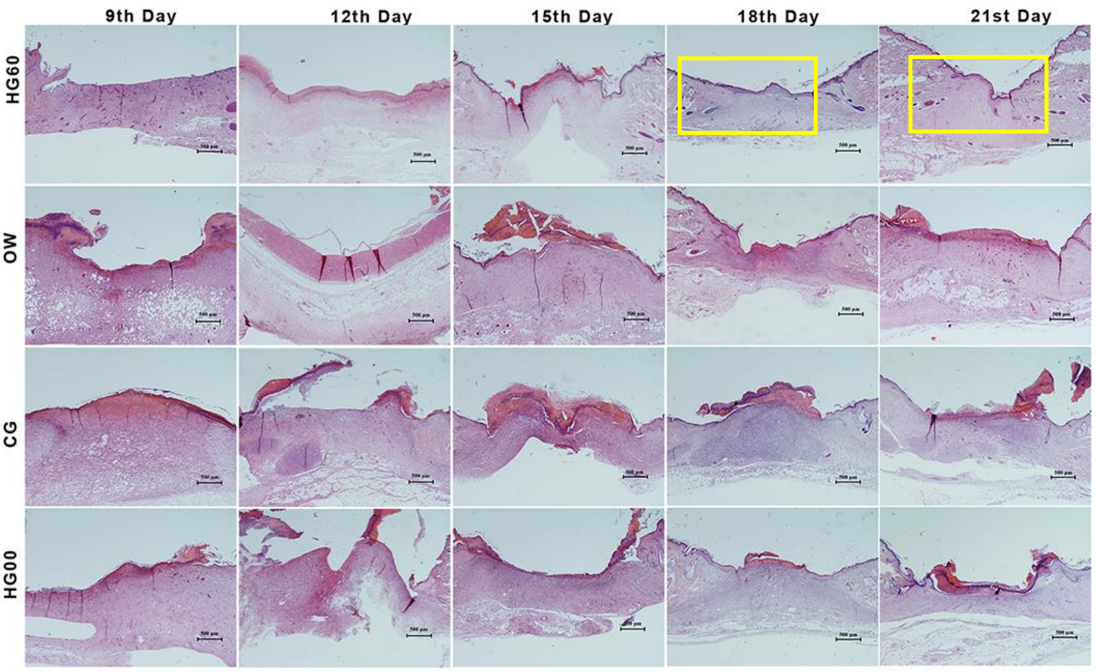

Figure 31. Photomicrographs of hematoxylin and eosin-stained sections of wounds treated with HG60, OW, CG, and HG00 representing the nature of re-epithelialization, remarkably complete re-epithelialization happened in the HG60 treatment group by the 18th day (the quantitative values shown in Figure 32 (n=4; magnification, 4x; Scale bar, 500µm). Please see the legend the Figure 27 for an explanation of the abbreviations.

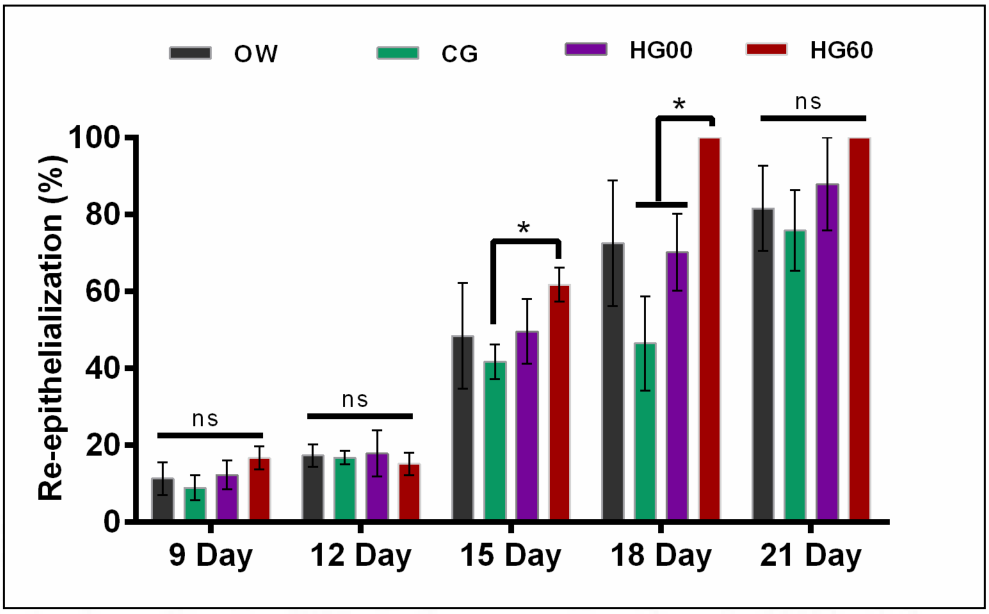

Figure 32. A bar diagram showing the percentage re-epithelization wherein complete epithelialization was observed by the 18th day in HG60 treatment groups, much earlier than all other groups (n=4; *P value < 0.05). Please see the legend the Figure 27 for an explanation of the abbreviations.

4.5.3 Histomorphology

Photomicrographs depicting representative lesions from H&E-stained sections are shown at low magnification (Figure 33) and higher magnifications Figure 34. Histomorphological evaluation and morphometric data by immunohistochemistry and its quantification (Figures 35 to 44), histochemistry for collagen by Masson' trichrome (Figures 45 to 47), and histochemistry for Type I/III collagen by Herovici's stain (Figures 48 to 51) elucidated the nature of the healing reaction in various treatment groups. The observations are detailed below.

4.5.4 Healing reaction in the dermis

All the histological slides evaluated after H&E stain showed varying levels of granulation tissue, mononuclear cell infiltration, and collagen deposition in the dermis (Figures 33 and 34). On the ninth day, most animals showed mild to moderate granulation tissue made up of sprouting blood vessels and fibroblasts. At this stage, several sections contained loosely packed fibrin strands and occasional neutrophils, both of which indicated remnants of acute inflammation. At later time points in the study (12-21 days), the granulation tissue was characterized by sprouting blood vessels and diffuse infiltration of mononuclear cells which gradually decreased, while pale staining of diffusely scattered neo-collagen increased and became more compact with a dense red staining pattern as healing progressed. Even on the 21st day of the recovery, there were occasional dense multifocal mononuclear cells present.

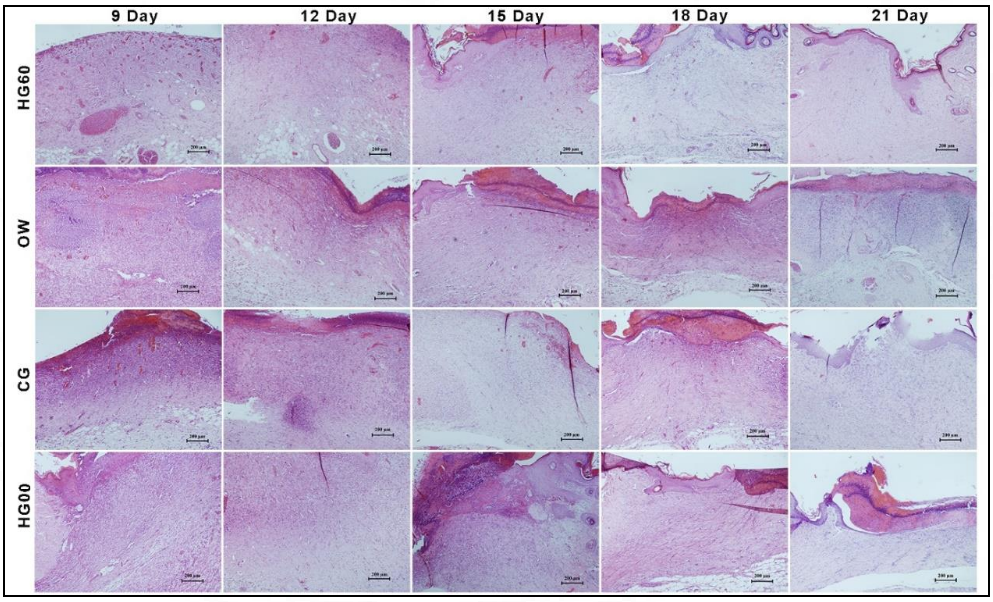

Figure 33. Light microscopic images of hematoxylin and eosin-stained sections of wounds treated with HG60, OW, CG, and HG00 (n=4; magnification, 10x; Scale bar, 500µm). Please see the legend the Figure 27 for an explanation of the abbreviations.

Overall, there was a slight variation in the severity of the reactions among groups at various time points. In general, animals treated with HG60 and HG00 had a milder reaction at all times than animals treated with unassisted healing (OW), while the reaction was intense in animals treated with the predicate device (CG).

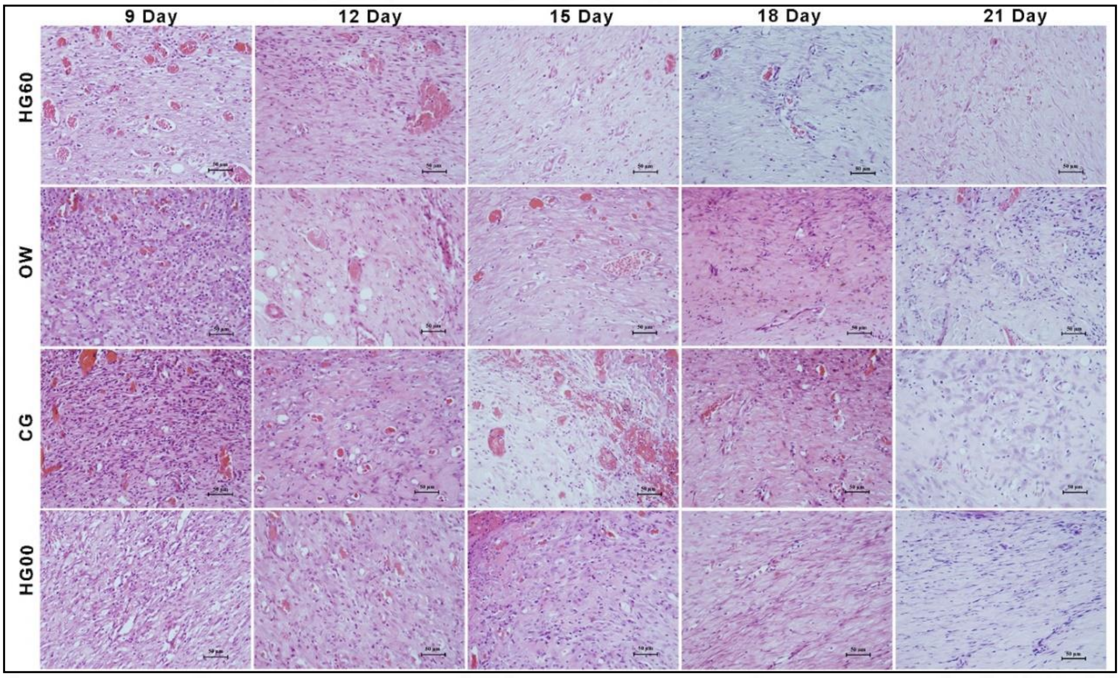

Figure 34. Light microscopic images of hematoxylin and eosin-stained sections of wounds treated with HG60, OW, CG, and HG00 (n=4, magnification, 40x; Scale bar, 50μm) Please see the legend the Figure 27 for an explanation of the abbreviations.

4.5.5 Immunohistochemistry

The cells positive for immunohistochemistry stains appeared brown and in each staining reactions, the number of positive cells were quantified (Figures 35 to 44). On the ninth day, CD4+ positive cells were very low and nearly identical in all groups, averaging only around 10 cells/HPF (Figures 35 and 36). Later, the numbers increased in all groups up to the 12th day, but this reaction was significantly higher in HG60-treated wounds, with an average of 88 ± 12 cells per HPF. The cell numbers decreased in all groups till the end of the study period.

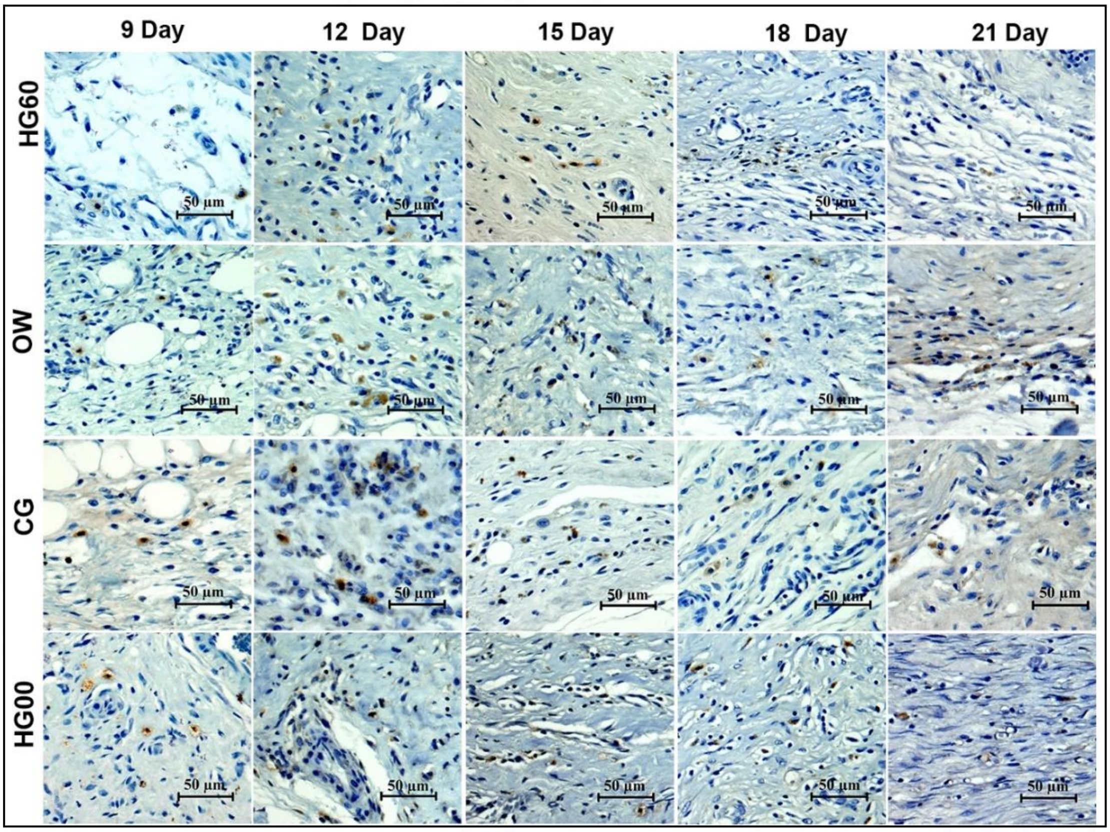

Figure 35. Light microscopic images were obtained after immunohistochemistry for CD4 T helper cells on the 9th, 12th, 15th, 18th, and 21st days treated with HG60, OW, CG, and HG00 (n=3; magnification, 40x; scale bar: 50µm). Please see the legend the Figure 27 for an explanation of the abbreviations.

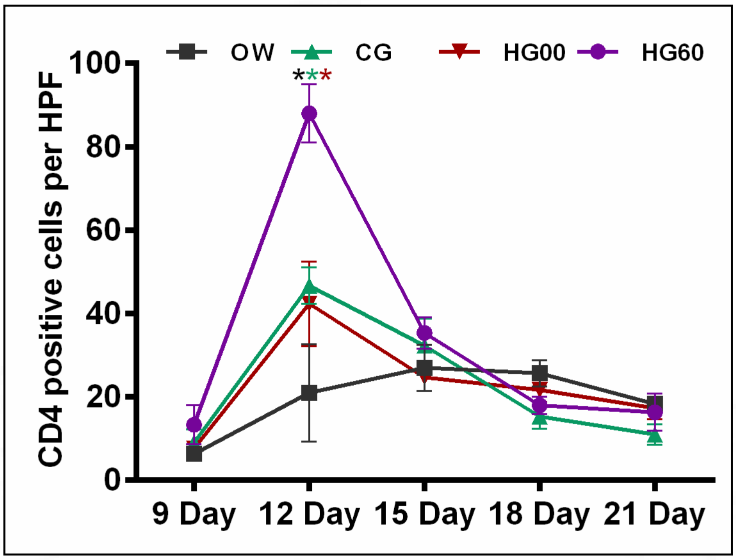

Figure 36. Line graph showing the results of quantification for CD4+ helper T cells on 9th, 12th, 15th, 18th and 21st day treated with HG60, OW, CG and HG00 (n=3; HPF, high power field). Please see the legend the Figure 27 for an explanation of the abbreviations.

The number of CD8+ cytotoxic T-lymphocytes in the open wound increased from the 9th to the 12th day, with an average of 101 ± 31 cells/HPF, and then declined (Figures 37 and 38). In the HG60 group, the number was quite high for 9-12 days, then dropped to 78 ± 22 cells/HPF on the 15th day and subsequently reduced further. For the animals treated with the predicate device, the number increased from the ninth to the fifteenth day, averaging 208 ± 61 cells/HPF and subsequently, the numbers decreased. The HG00-treated group had a trend comparable to OW with respect to these numbers.

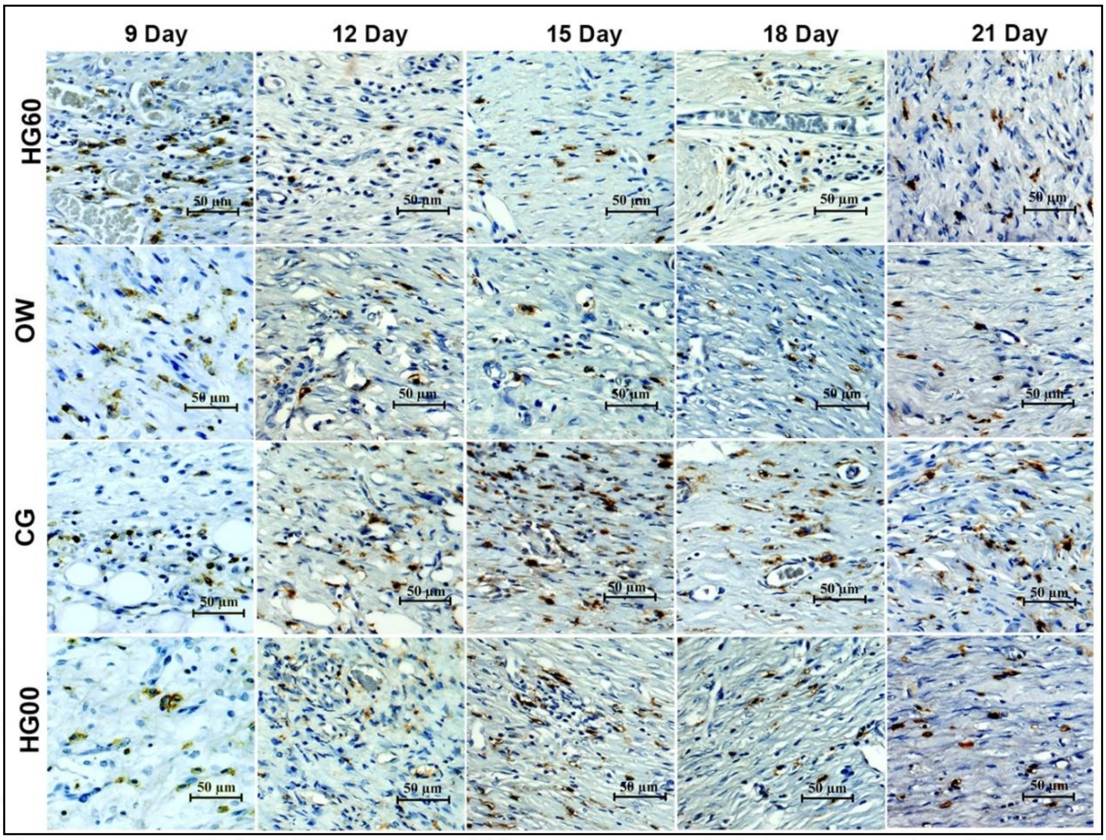

Figure 37. Light microscopic images of immunohistochemistry for CD8^{+} cytotoxic T cells on the 9th, 12th, 15th, 18th, and 21st day treated with HG60, OW, CG, and HG00 (n=3; magnification, 40x; scale bar: 50µm). Please see the legend the Figure 27 for an explanation of the abbreviations.

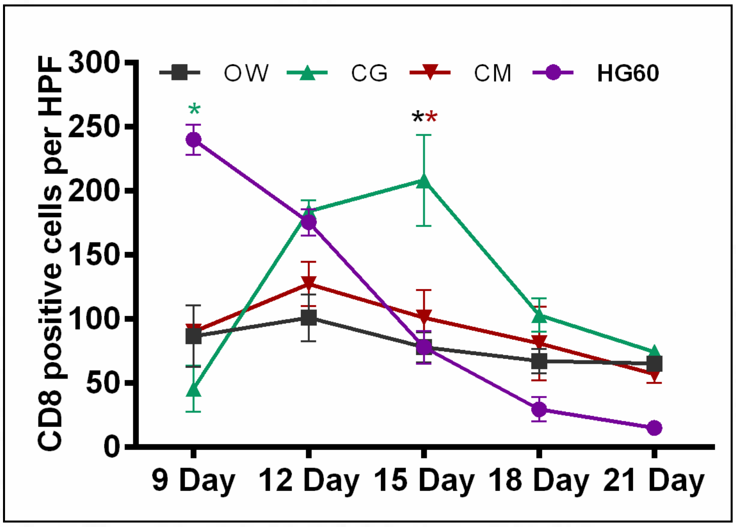

Figure 38. Line graph showing the quantification of CD8+ cytotoxic T cells on 9th, 12th, 15th, 18th and 21st day treated with HG60, OW, CG and HG00 (n=3) Please see the legend the Figure 27 for an explanation of the abbreviations.

Throughout the study, the HG60-treated wounds had a consistently lower number of CD 80+ M1 macrophages than the other groups (Figures 39 and 40).

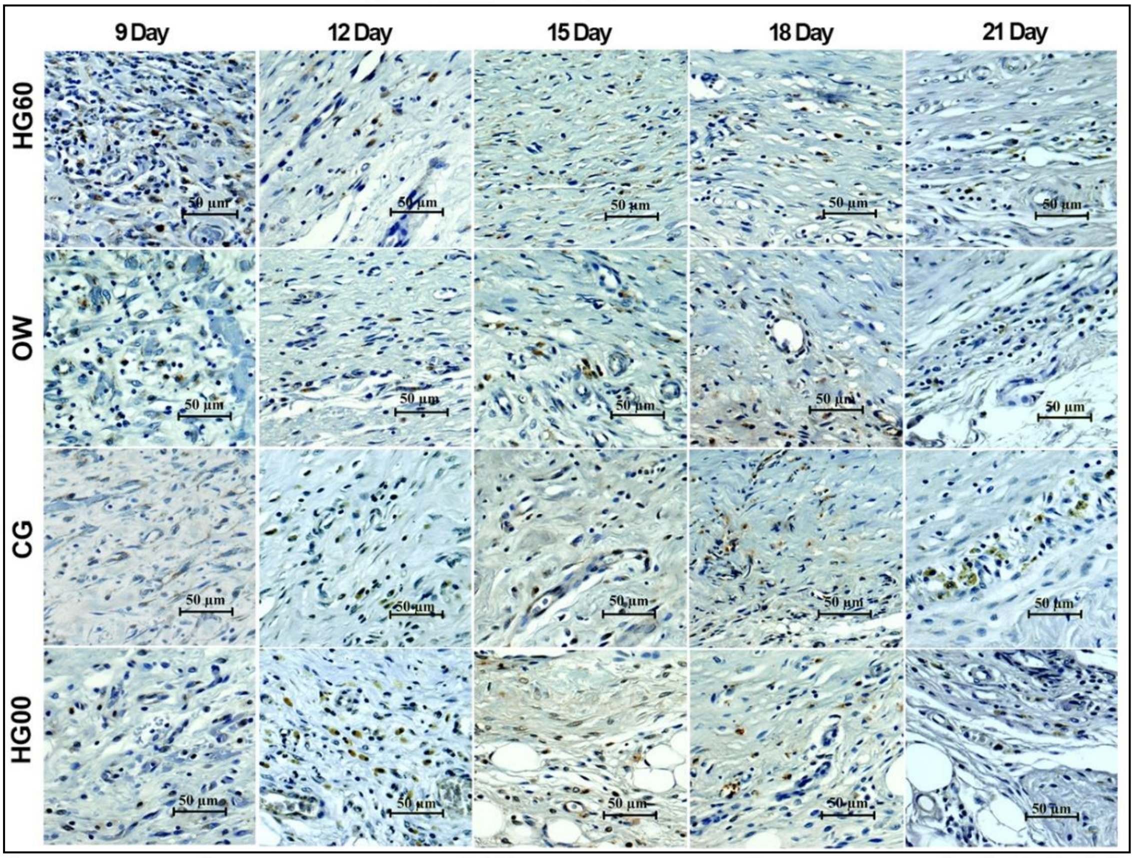

Figure 39. Light microscopic images after immunohistochemistry for CD80^{+} M1 Macrophages on the 9th, 12th, 15th, 18th, and 21st days treated with HG60, OW, CG, and HG00 (n=3; magnification, 40x; scale bar: 50μm). Please see the legend the Figure 27 for an explanation of the abbreviations.

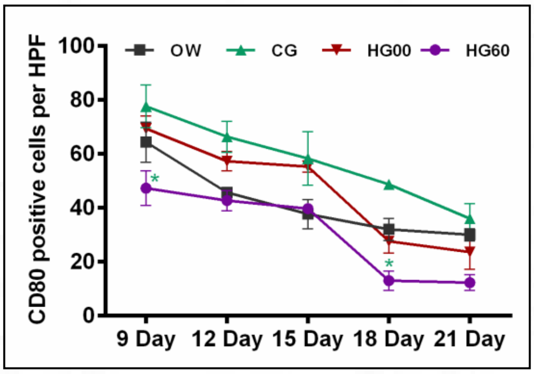

Figure 40. Line graph showing the quantification of CD80+ M1 macrophages on 9th, 12th, 15th, 18th and 21st day treated with HG60, OW, CG and HG00 (n=3; magnification, 40x; scale bar: 50μm). Please see the legend the Figure 27 for an explanation of the abbreviations.

In the HG60 treatment group, the number of CD163+ M2 macrophages was higher on the 9th day, averaging 146 ± 38 cells/HPF, but decreased significantly over time to 12 ± 8 cells/HPF on the 21st day (Figures 41 and 42). In other groups, the number on the ninth day was substantially lower, averaging 40 cells/HPF, and peaked later on day 12. On the 12th day, the number of M2 macrophages was 62 ± 7 cells/HPF, 51 ± 23 cells/HPF, and 94 ± 7 cells/HPF in OW, CG, and HG00, respectively, but by the 21st day, the numbers decreased to 42 ± 9 cells/HPF, 54 ± 20 cells/HPF, and 30 ± 15 cells/HPF.

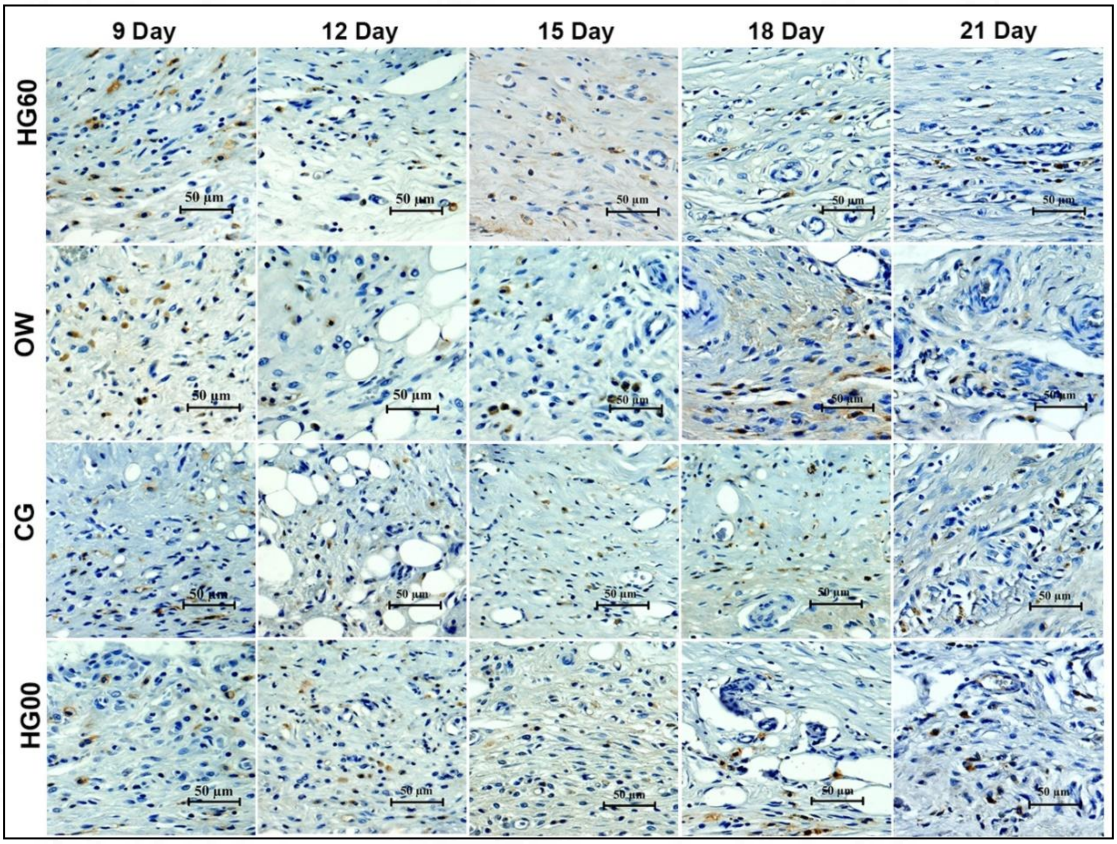

Figure 41. Light microscopic images were obtained after Immunohistochemistry of CD163^{+} M2 Macrophages on the 9th, 12th, 15th, 18^{th,} and 21st days treated with HG60, OW, CG, and HG00 (n=3; magnification, 40x; scale bar: 50µm). Please see the legend the Figure 27 for an explanation of the abbreviations.

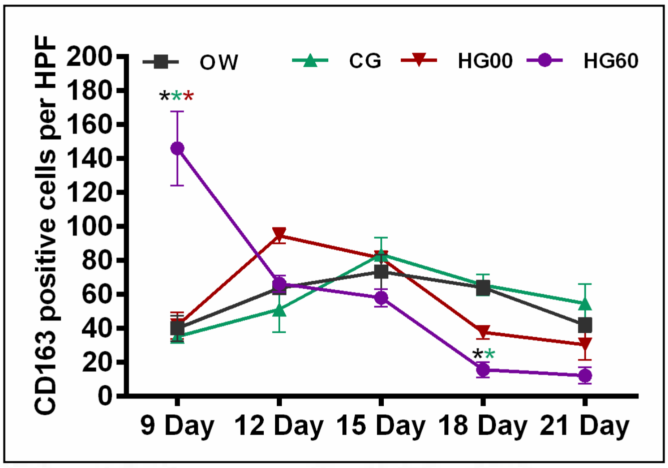

Figure 42. Line graph showing the quantification of CD163+ M2 Macrophages on 9th, 12th, 15th, 18th and 21st day treated with HG60, OW, CG and HG00 (n=3). Please see the legend the Figure 27 for an explanation of the abbreviations.

The CD4+/CD8+ ratio (Figure 43) and M1/M2 ratio (Figure 44) in HG60-treated wounds reached a balance closer to a ratio one: one by the 18th day. However, in the control groups, the ratio never did not get closer to ratio one: one, even on the 21st day. The CD4+/CD8+ ratio for OW, CG, and CM was 0.44, 0.15, and 0.37, respectively. The M1/M2 ratios for OW, CG, and CM were 0.72, 0.77, and 0.8, respectively.

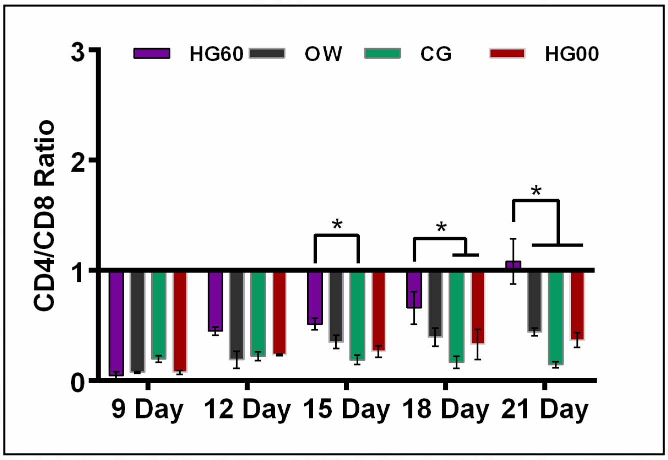

Figure 43. Bar diagram showing the CD4+/CD8+ ratio on 9th, 12th, 15th, 18th and 21st day treated with HG60, OW, CG and HG00 (n=3). Please see the legend the Figure 27 for an explanation of the abbreviations.

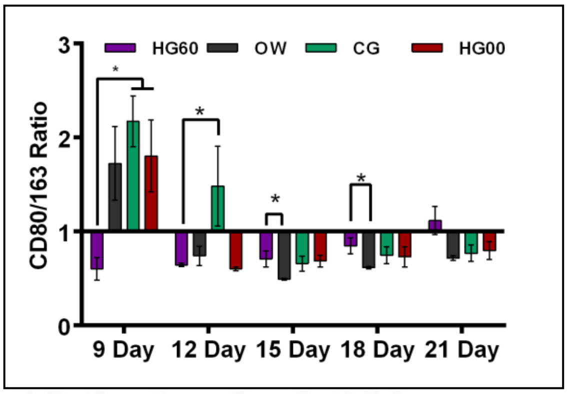

Figure 44. Bar diagram showing the CD80+/CD163+ ratio on 9th, 12th, 15th, 18th and 21st day treated with HG60, OW, CG and HG00(n=3). Please see the legend the Figure 27 for an explanation of the abbreviations.

4.5.6 Collagen remodeling

The collagen in histology sections stained with Masson's trichrome appeared as blue color (Figures 45 and 46). The results of the trichrome staining revealed a progressive rate of collagen deposition in all groups with no significant variations between any of the experimental groups at any study point of the investigation (Figure 47).

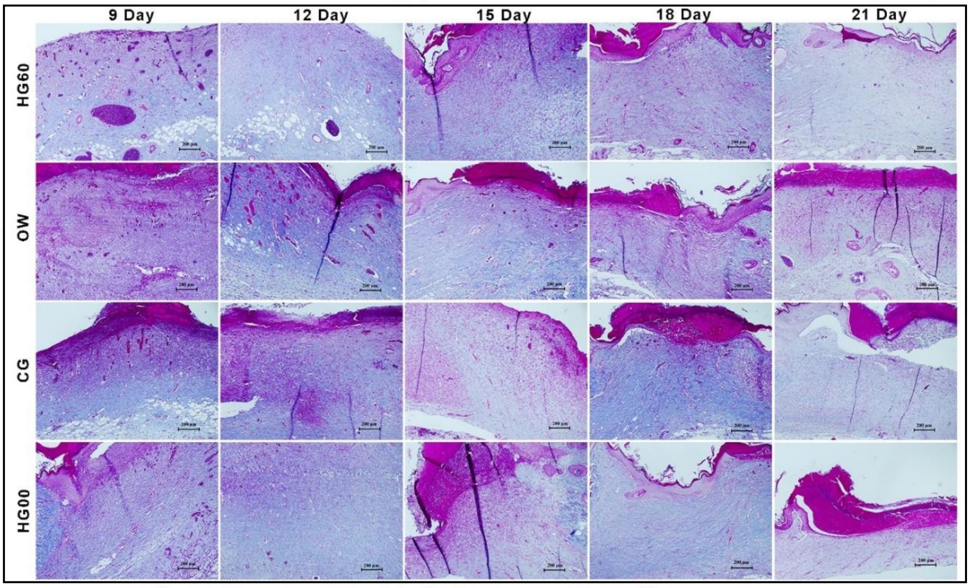

Figure 45. Light microscopic images of Masson’s trichrome-stained sections of wounds treated with HG60, OW, CG, and HG00 (n=4; magnification, 10x; scale bar, 500μm). Please see the legend the Figure 27 for an explanation of the abbreviations.

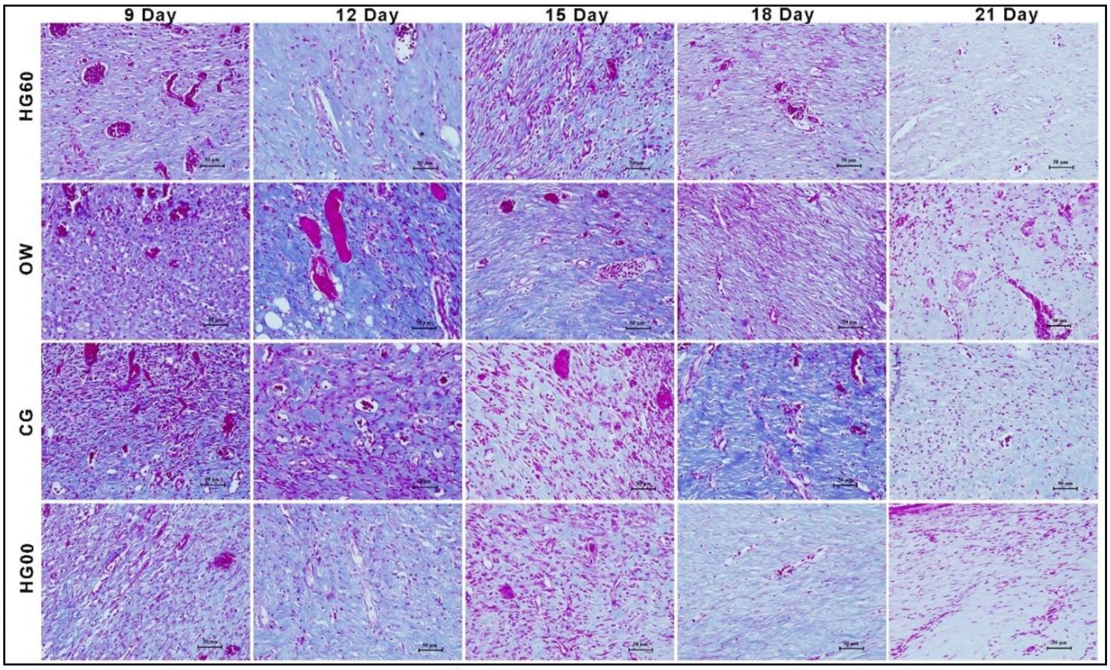

Figure 46. Light microscopic images of Masson’s trichrome-stained sections of wounds treated with HG60, OW, CG, and HG00 (n=4; magnification, 40x; scale bar: 50μm).

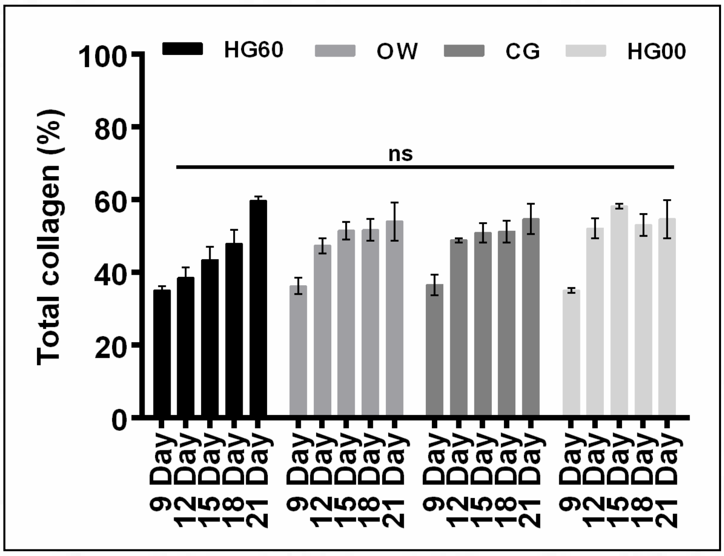

Figure 47. A bar diagram showing the quantification of the total collagen from Masson’s trichrome-stained sections (n=4). Please see the legend the Figure 27 for an explanation of the abbreviations.

After Herovici's staining of histology sections type I collagen was pink and type III collagen was blue in colour (Figure 48). It was observed that HG60 produced a high amount of Type I collagen on the 9th day and maintained the content throughout the study, except on the 21st day, which slightly reduced (Figure 49). In contrast, in all other groups, the amount of Type I collagen was lower on the ninth day and increased subsequently. Throughout the experiment, the HG60 had significantly lower collagen Type III levels than the other treatment groups (Figure 50). On the 21st day, the HG60, OW, CG, and HG00 groups had a Type I to Type III ratio of 3.3, 1.7, 2.2, and 2.7, respectively (Figure 51).

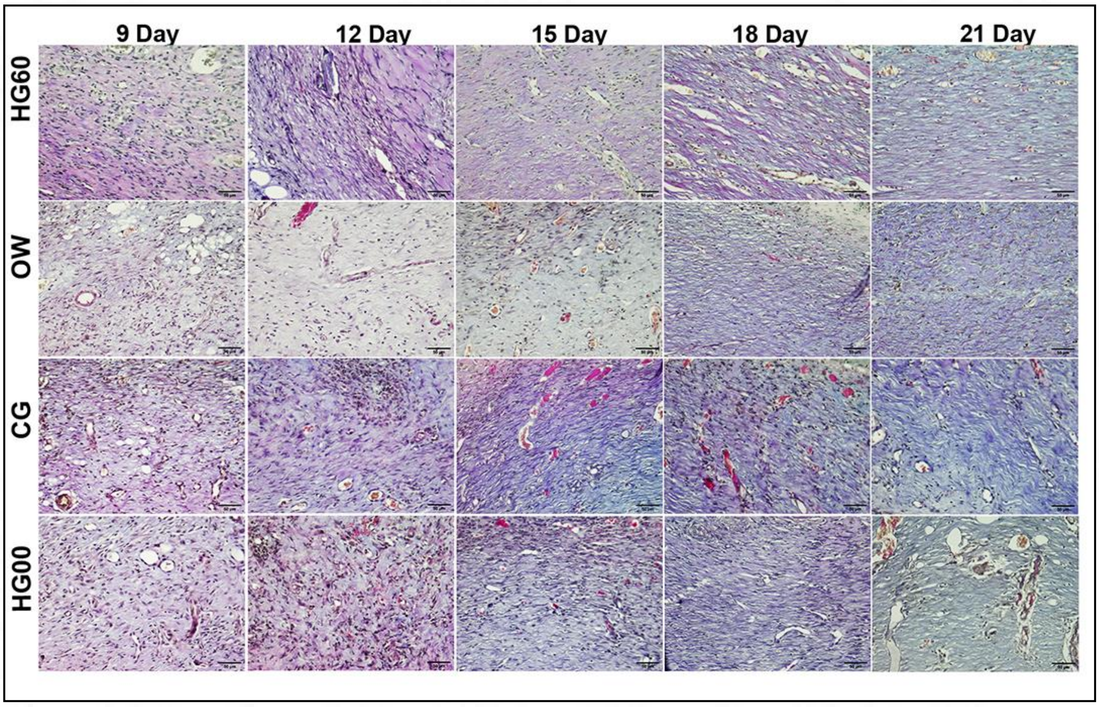

Figure 48. Light microscopic images of Herovici's stained sections of wounds treated with HG60, OW, CG, and HG00 (n=4; magnification, 40x; scale bar, 50µm). Please see the legend the Figure 27 for an explanation of the abbreviations.

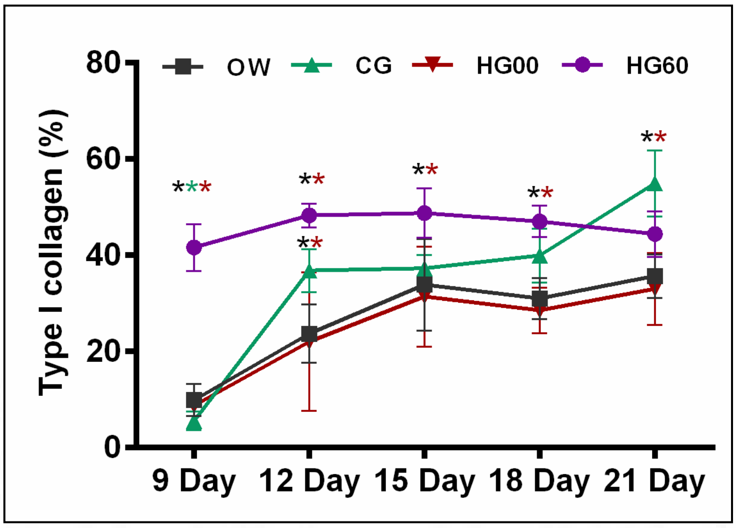

Figure 49. Line graphs showing the content of type I collagen (%) quantified using ImageJ from Herovici's stained sections on the 9th, 12th, 15th, 18th, and 21st days (n=4). Please see the legend the Figure 27 for an explanation of the abbreviations.

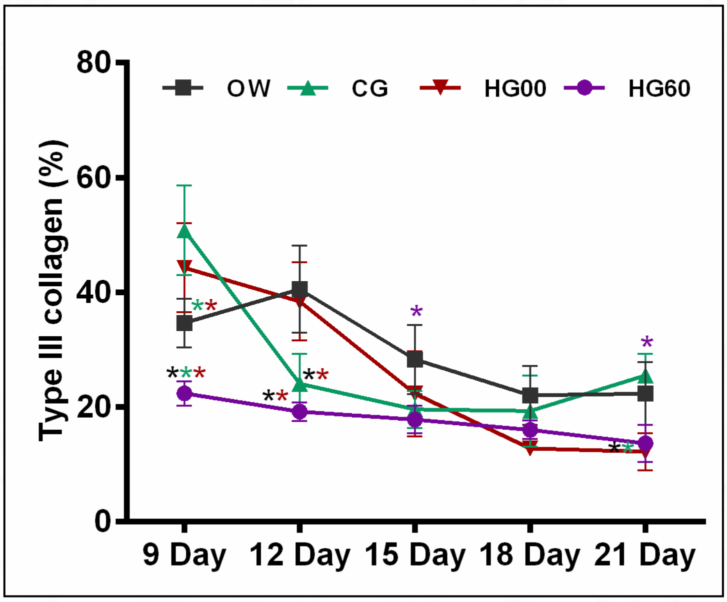

Figure 50. Line graphs showing the content of type III collagen (%) quantified using ImageJ from Herovici's stained sections on the 9th, 12th, 15th, 18th, and 21st days (n=4). Please see the legend the Figure 27 for an explanation of the abbreviations.

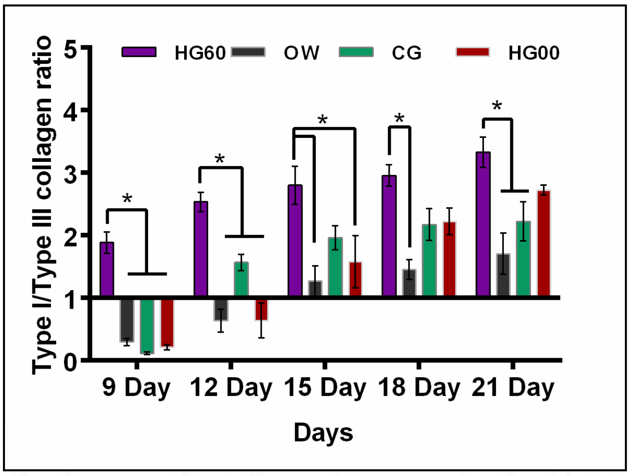

Figure 51. Bar graph representing the ratio of type I/type III collagen quantified using ImageJ from Herovici's stained sections on the 9th, 12th, 15th, 18th, and 21st days (n=4). Please see the legend the Figure 27 for an explanation of the abbreviations.

4.5.7 RT-PCR

The results of RT-PCR on the relative fold change of mRNA for the proinflammatory cytokine TNF α (Figure 52), was lower in HG60-treated wounds on the 18th day compared to other groups and was significantly different from the HG00. By the 21st day, the relative fold change decreased further.

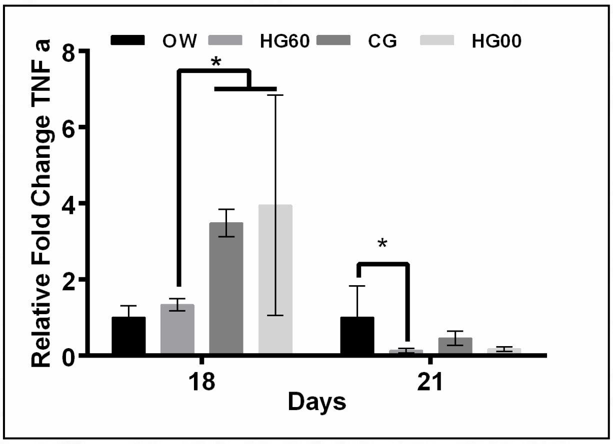

Figure 52. A bar graph showing the results of RT-PCR data of TNF α mRNA on the 18th and 21st day (n=3; *P value < 0.05). Please see the legend the Figure 27 for an explanation of the abbreviations.

A similar result was seen in the relative fold change of mRNA levels for iNOS on the 18th day and thereafter it reduced on the 21st day (Figure 53). The HG00 also induced a reduction in iNOS mRNA but the predicate device-treated groups consistently had higher relative fold change.

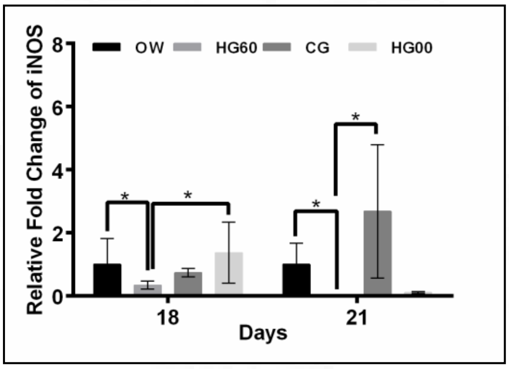

Figure 53. A bar graph representing the results of RT-PCR data of iNos mRNA on the 18th and 21st day (n=3; *P value < 0.05). Please see the legend the Figure 27 for an explanation of the abbreviations.

The relative fold change of anti-inflammatory effector molecule IL-10 mRNA levels showed no significant difference in HG60 treatment groups against the predicate device on the 18th day (Figure 54). However, a significant reduction was observed against the open wound and the predicate device groups on the 21st day.

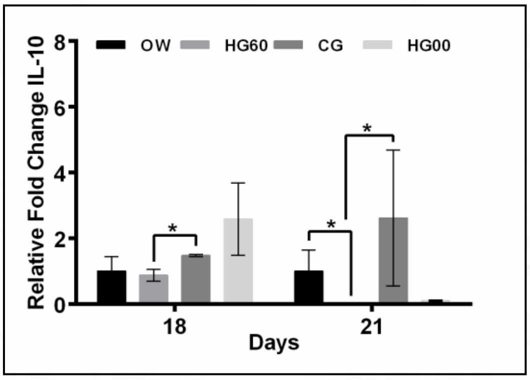

Figure 54. A bar graph representing RT-PCR of mRNA for IL-10 on the 18th and 21st day (n=3; *P value < 0.05). Please see the legend the Figure 27 for an explanation of the abbreviations.

The relative fold change of mRNA for collagen Type I of the HG60 on the 18th day had significant differences with the HG00-treated group (Figure 55). However, the relative fold change of mRNA for collagen Type III on the 18th day and 21st day did not show a significant difference in the HG60-treated groups (Figure 56).

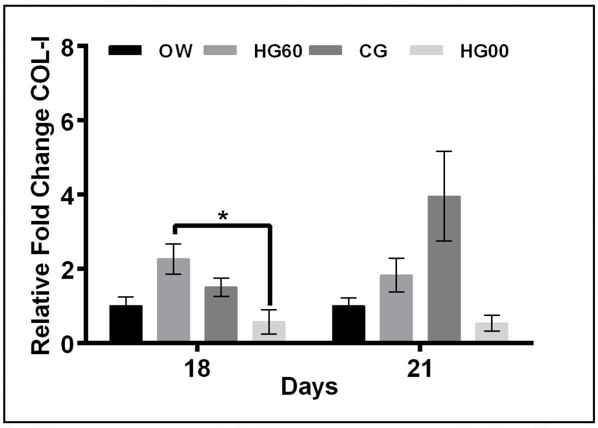

Figure 55. A bar graph representing the results of RT-PCR of COL-I mRNA on 18th and 21st day (n=3; *P value < 0.05). Please see the legend the Figure 27 for an explanation of the abbreviations.

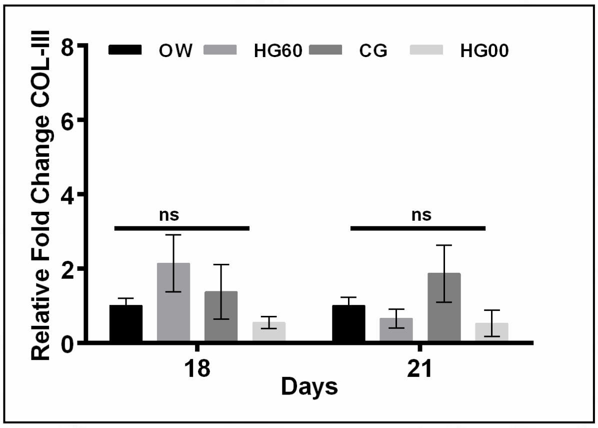

Figure 56. A bar graph representing the RT-PCR data of COL-III mRNA on 18th and 21st day (n=3; *P value < 0.05). Please see the legend the Figure 27 for an explanation of the abbreviations.

CHAPTER 5

5 DISCUSSION

Hydrogels intended for wound healing applications prepared by physical crosslinking methods are usually hydrogen bonding reactions, crystallization, ionic reactions, hydrophobic interactions, or protein interactions (Su *et al.*, 2021). The present study deployed an ionic crosslinking reaction using Potassium Aluminium Sulphate (Liu *et al.*, 2018) for preparing CECM hydrogels with CMC which is a natural polymer approved by the United States Food and Drug Administration for preparing tablets, capsules, injections, suspensions, paste, and gels (Zennifer *et al.*, 2021). The Aluminium ions (Al^{3+}) of the cross-linker $KAl\ (SO_4)_2$ could interact with the carboxymethyl group of the CMC to create a polymer network facilitating the formation of hydrogel. The reaction was expected to generate a thin reticular layer on the surface thereby preventing CMC from dissolving in water and trapping soluble contents inside (Liu *et al.*, 2018). However, the optimum proportion of CECM and CMC for a desirable hydrogel appropriate for medical application was not known. Therefore, five formulations of hydrogels were prepared empirically with variable proportions of CECM and CMC solutions. The hydrogel formulations were named as HG00, HG50, HG60, HG70 and HG80 based on the content of CECM in the final formulations (Table 1), the HG00 did not contain CECM. The biomaterial properties of these hydrogels were evaluated and detailed as follows.

5.1 Biomaterial properties of HG60

The yellowish color of the hydrogels was due to the CECM content and the consistency became less stiff with the increase in proportion of the CECM (Figure

7). It has been reported that the higher percentage of gel fraction represents a low concentration of unbound cross-linkers (McBath and Shipp, 2010). The percentage of the gel fraction appeared to decrease with the reduction in the content of the CMC (Figure 8) but there was no significant difference in the gel fractions. Grossly, the HG60 had a consistency of neither being too stiff nor too loose (Table 4). Wounds require a moist environment for optimum healing (Junker *et al.*, 2013) and a hydrogel can provide the same (Tavakoli and Klar, 2020; Firlar *et al.*, 2022). Therefore, the high-fluid absorption capability of CMC was considered an added advantage for the wound healing product because it is known to provide a moist environment in wound beds (Kanikireddy *et al.*, 2020). The prepared hydrogels had good fluid absorption swelling ability (Figure 9) and equilibrium water content (Figure 10) and attained maximum volume within an hour. As expected, the extent of swelling increased with a higher proportion of the CMC in the hydrogels.

The frequency sweep conducted in the LVER (Figure 11A to E), within the strain range of 0.1-5% demonstrated that the G' exceeded the G", which indicated the hydrogel's solid elastic nature (Zuidema *et al.*, 2014; Alam *et al.*, 2020; Sun and Purohit, 2022). The results showed that the HG00 was a stiffer viscoelastic solid gel than all other preparations and the stiffness decreased with higher proportions of CECM except HG80 (Figure 11 F to J). This observation correlated with the results of the gel fraction experiment (Figure 8). The percentage gel fraction is essentially the insoluble fraction of a polymer in a hydrogel which stands as an indicator of its stiffness and stability. It has been reported that a higher percentage gel fraction represented a higher crosslinking thereby forming a stiffer hydrogel (Kurniati and

Nuraini, 2021). However, the hydrogel with the highest CECM concentration had higher viscosity than the HG00 (Figure 11 K). This might be due to the contractile property of collagen present in the hydrogel (Hameed and Manivasagam, 2021). Despite the difference in proportions of CECM, all the hydrogels displayed a similar shear-thinning behavior (Figure 11 K), where the viscosity decreased with increase in the shear rate which is an ideal requirement for an injectable gel (Chen *et al.*, 2017; Bernhard and Tibbitt, 2021).

Lyophilized sheet forms of CECM had three major peaks of the amide bonds in the wavelength ranging between 500 cm^{-1} and 3500 cm^{-1} detectable through FTIR spectra (Anilkumar *et al.*, 2014) essentially that of amide I at 1660 (C=O stretching), amide II at 1540 (NH deformation and C–N stretching), and amide-III at 1235 cm^{-1} of C–N stretching and N–H deformation. The FTIR-spectra (Figure 12) of the hydrogel formulations except the HG00 had all these peaks confirming the presence of CECM and presumably no denaturation or alterations in the fundamental chemical composition of CECM proteins had happened even after the ionic crosslinking reaction. In addition, the spectral bands that are characteristics of CMC were also observed at 1614 cm^{-1} and 1446 cm^{-1} indicative of the symmetric and asymmetric modes of stretching vibrations of the carboxyl group (Yuwono *et al.*, 2021).

The SEM images of lyophilized hydrogel samples were performed to provide details on the surface topography of the cut surface of the hydrogels and a possible indication of their porosity (Martinez-Garcia *et al.*, 2022). It is known that the stiffness of the hydrogels is reduced with an increase in porosity (Annabi *et al.*, 2010). In this study, the cut surface of the lyophilized hydrogel samples was observed to be highly porous (Figure 13) and the porosity increased with the content of CECM (Figure 14).

A material with a water contact angle greater than 90^0 is considered hydrophobic and a lesser value indicates the extent of hydrophilicity (Wang *et al.*, 2023). Here, all the hydrogel samples were hydrophilic (Figure 15) and the hydrophilicity increased with higher content of the CECM whereas the HG00 was more hydrophobic than others (Figure 16).

Degradation of a biomaterial when it is in contact with the human body is a crucial parameter when identifying a probable biomedical application (Azevedo and Reis, 2004). The nonenzymatic degradation study in terms of weight loss showed a higher degradation rate in the hydrogel samples which increased with the content of CECM (Figure 17 A). Considering the rich content of collagen in CECM (Anilkumar *et al.*, 2014), the extent of *in vitro* degradation of the hydrogels was evaluated by treatment with collagenase enzyme. All the hydrogel samples had a low rate of degradation, similar to that of CECM (Figure 17 B). Treatment with 10 % neutral buffered formalin for controlled cross-linking (Mony and Anilkumar, 2020) during the preparation of the hydrogel might have been a reason for the diminished degradation profile.

The injectability of a hydrogel has a lot of implications in biomedical applications, especially while defining the site and nature of the biomaterial delivery (Alonso *et al.*, 2021; Hunter *et al.*, 2022). Injectable hydrogels assume importance when other forms like solid sheets, and powder cannot be applied as in deep wounds or when catheter-based deep tissue delivery is desired (Sun *et al.*, 2020; Karmakar *et al.*, 2023). Against this background, the injectability of the hydrogel formulations was studied with a series of needles with varying gauges ranging from 18G to 26G (Figure 18) and three commonly preferred parameters *via* stiction force, dynamic glide force and end constraint force (Zhang and Fassihi, 2018) were evaluated. A stiction force of 20 Newton (N) has been considered as the injection force required for the normal delivery of hydrogels (Chen *et al.*, 2017). All the hydrogel formulations containing CECM had a stiction force below 20 N through 18, 19, 22 and 23 gauge needles but HG00 was below only through 18 and 19 gauge needles (Figure 18).

A hydrogel for wound healing application will be in direct contact with body of patients during biomedical applications. Therefore, evaluation of its cytocompatibility is essential and robust standards are available for such evaluations (Li, Zhou and Xu, 2015). Here, three well-known cytotoxicity studies were conducted to define the cytocompatibility of the hydrogels using protocols suggested in ISO 10993 Part 5. The results of the Live/Dead assay using Calcein AM and ethidium homodimer-1 (Figures 19 and 20) direct contact test (Figure 21) and the neutral red staining (Figure 22) showed the hydrogels were cytocompatible. Moreover, the classical MTT assay by the ‘test on extract’ method which is considered as the gold standard in cytocompatibility evaluation also indicated that none of the hydrogel formulations caused any cytotoxicity to L929 cells (Figure 23). Notably, the maximum number of live cells were present in the culture plate seeded with the HG60 formulation (Figure 20) in the Live/Dead viability assay. Therefore, the HG60 formulation containing 60% CECM is probably a better preparation than the others for biomedical use.

5.2 Selection of biomaterial for wound healing studies

To identify the overall performance of hydrogel formulations, a scoring method was adopted through a ranking system from 1+ to 4+ for comparing the biomaterial properties for the four formulations containing CECM based on the physio-chemical and biological tests (Table 5). The HG60 had a maximum score and hence it was selected for *in vivo* experiment. A commercially available wound healing gel namely Collogel was included in subsequent studies to facilitate comparison of the healing property of HG60 with a predicate device.

5.3 Wound healing studies

In view of animal welfare an *in vitro* wound closure assay was conducted before *in vivo* experiments. Here, an in vitro wound healing assay (Liang and Park, 2007) that indicates the ability of a biomaterial to facilitate cell migration was conducted. Progressive wound closure was evident as early as four hours after the creation of the wound in the cell culture plate with HG60 and the healing improved with time (Figures 25 and 26).

The animal experiments were subsequently conducted to demonstrate the suitability of the HG60 for a potential clinical application. In order to achieve this objective, a commonly used animal model of full-thickness excision skin wound healing using Sprague Dawley rats was selected (Grada and Mervis, 2018). Considering that this study was interested only in evaluating the nature of the late inflammatory responses (Hench, 2005) and collagen remodeling (Madden and Peacock, 1971) rather than the early phases of wound healing like hemorrhage, hemostasis and acute inflammation, a window period of 9-21 days was selected with a wound size of 2 x1.5cm.

Wound planimetry is a commonly adopted procedure for evaluating healing of wounds in experimental animals (Jorgensen *et al*., 2016). Generally, two methods of planimetry were followed to record the rate of wound healing, including the standard ruler measurement method and digital planimetry (Rogers *et al*., 2010). In this study digital planimetry was performed instead of the standard ruler measurement method using a custom-made photographic stand (Figure 5). Although the custom-developed procedure was not validated against any standard method, it certainly minimized the contamination of the wounds *via* contact with the tracing sheet during wound tracing (Rogers *et al.*, 2010). A higher rate of wound closure was observed in wounds treated with HG60, as early as 15 days, (Figures 27 to 29) in comparison with the group treated with the predicate device, the gel base and the untreated open wounds. The differences became more prominent by the 18th day. By the 21st day of the experiment, a complete wound closure was observed in all animals treated with HG60 giving a clear indication of its potential to heal wounds faster than the other treatments. Notably, complete wound closure did occur in in all animals of any other group. The results prompted a detailed histomorphological evaluation to elucidate the probable mechanism of the accelerated wound healing.

5.3.1 HG60 induced faster re-epithelialization

Complete reepithelization was observed in all animals of HG60 treated groups by 18 days (Figures 30, 31 and 32). This observation was highly in favor of the developed hydrogel, considering that complete reepithelization did not happen in all animals in no other group even after the completion of the experimental period of 21 days. The results corroborated the gross observations made by the digital planimetry (Figure 28 and 29).

Histomorphology of the major components of wound healing in the dermis modulated by mononuclear cells (Rodrigues *et al.*, 2019) and collagen remodeling (Mathew-steiner and Roy, 1969; Madden and Peacock, 1971) was studied in detail. All these components of the tissue reaction were present in all the healing wounds (Figures 33 and 34). However, the intensity of the reaction varied among the different treatment groups. The reaction was relatively milder at all-time points in animals treated with HG60 and HG00 compared to the animals with unassisted healing. The reaction was intense in animals treated with the predicate device. Hence, further evidence was required to elucidate the nature of the healing reaction in the dermis.

5.3.2 HG60 favored a tissue regeneration reaction

When a biomaterial is in contact, a living animal body recognizes it as a foreign body and uses the defense mechanism to eliminate it by triggering native immune response. In a wound environment, this contributes a lot in defining the subsequent healing response (Tan *et al.*, 2019). With this in view, the present study evaluated the nature of some of the key cells like T-helper lymphocytes, cytotoxic T-lymphocytes, M1 macrophages and M2 macrophages participating the tissue immune reaction but the focus was on wound healing responses.

The number of CD4$^+$ positive T-lymphocytes is considered an important predictor of skewed immune response towards a graft acceptance reaction (Adusei and Ngo, 2021) because they play a key role in adaptive immunity especially in dampening immune responses by acting as helper cells for various immune responses (Chesko and Wilgus, 2022). In the present study, the pattern of CD4$^+$ lymphocytes reactivity was similar in all wounds with maximum reaction on day 12 (Figures 35 and 36) but the number of these cells in the HG60-treated animals was much higher than in the other groups. Therefore, the HG60 had certainly induced a favorable regenerative response compared to other treatments.

Another important mononuclear cell participating in immune response is cytotoxic T lymphocytes which are expected to be very aggressive during early phases of inflammation to mitigate immunogens (Adusei and Ngo, 2021). Therefore, an assessment of the nature of cytotoxic T cells (CD8$^+$) response was evaluated to clarify the nature of the tissue reaction induced by the HG60. The nature of the CD8$^+$ cell reaction (Figures 37 and 38) was maximum in the HG60-treated animal, on the 9th day and decreased drastically thereafter. Moreover, the number of CD8$^+$ cells were much less in this group compared to all other group on 18th and 21st day. In all other groups the peak reaction occurred either on 12th or 15th day. The observation suggested that the essential pro-inflammatory reaction in the HG60 treated wound happened much earlier than the other groups. Unfortunately, the experimental design did not permit to evaluate the nature of CD8+ cells in six or three days of healing reactions. Despite this limitation, the author believes that the HG60 stimulated a faster healing response than in other groups of rats.

The next pro-inflammatory mononuclear cell studied was the M1 macrophages. The presence of M1 macrophages over an extended period is considered an indication of delayed wound healing (Uygun *et al.*, 2018). Therefore, a consistently lower number of CD 80^+ M1 macrophages (Figures 39 and 40) present in the HG60 treated groups during the entire study period also suggested a diminished pro-inflammatory reaction. This observation strongly supports the earlier deduction that the HG60 created a congenial environment for a favored healing response.

It is known that biological scaffold materials promote pro-regenerative reactions by triggering CD163-positive M2 macrophages and encouraging beneficial tissue remodeling (Brown *et al.*, 2012). The numbers of M2 macrophages were maximum on day 12th day and 15th day (Figures 41 and 42) except in the HG60 treatment group. In HG60-treated animals the maximum number of M2 macrophages occurred on the 9th day, notably much earlier than in other groups. Therefore, it is plausible to believe that the peak beneficial pro-regenerative reactions occurred much earlier in the HG60 treated group than in other groups. These cumulative evidences placed the healing reaction stimulated by HG60 much faster than the base HG00 or the predicate device, needless to comment about the reaction in rats with OW.

The increased numbers of CD4$^+$ (Figure 36) and M2 macrophages (Figure 42) as well as the reduced numbers of both CD8$^+$ cells (Figure 38) and M1 macrophages (Figure 40) in HG60, treated animals were adequate evidence for reduced inflammation and a favorable regenerative environment prevailing in the wound. It has been generally agreed that the proportion of each type of different subpopulation of certain T-cells or macrophages is more important than the actual numbers. Specifically, the ratio of CD4$^+$ and CD8$^+$ (Amadori *et al.*, 1995; Hautz *et al.*, 2012), as well as M1 and M2 (Uygun *et al.*, 2018) macrophages, are very important in defining the nature of a healing response. It is known that in a progressively healing wound, their numbers are approximately equal so that the healing reaction will take place without complications (Chesko and Wilgus, 2022; Hassanshahi *et al.*, 2022). It is known that lyophilized sheets of CDS induce a balanced proportion of these cells in subcutaneous tissue (Muhamed *et al.*, 2015) and skeletal muscle (Balakrishnan-nair *et al.*, 2018). Here, both the ratios of lymphocytes and macrophages in HG60 treated wounds have attained a ratio closer to ‘one’ from the 18th day onwards (Figures 43 and 44) compared to other groups. In other groups, the ratios did not reach the desirable value even on the 21st day.

All these above-mentioned observations were further substantiated by molecular studies for the expression of TNF α (Figure 52) and iNOS (Figure 53) which are the key functional molecules of CD8+ lymphocytes and M1 macrophages. The data provided insight into the nature of healing reactions happening at the biochemical level. Firstly, the pro-inflammatory molecule iNOS could cause oxidative stress and damage cells and tissues (Abd El-Aleem *et al.*, 2019). The level of this molecule was much lower in the HG60-treated wounds on the 18th day and 21st days (Figure 53). The HG00 also caused a substantial reduction in iNOS compared to other groups. In fact, the predicate device-treated groups consistently had higher relative fold change in the levels of mRNA indicating persistent inflammation in those wounds. Secondly, the TNF α is a pro-inflammatory effector molecule (Goldberg *et al.*, 2007), which also contributes to the oxidative stress in sites of inflammation. It is mainly secreted by naive CD8+ T cells (Ye *et al.*, 2018) for attracting circulating white blood cells, especially monocytes, which eventually develop into macrophages (Kotwal and Chien, 2017). The wounds treated with HG60 had a lower level of TNF α on the 18th day compared to all the others (Figure 52). The relative fold changes in the expression of mRNA for TNF α and iNOS on the 18th and 21st days in conjunction with the results of the immunohistochemistry for the cytotoxic T lymphocytes (Figure 38) and the M1 macrophages (Figure 40) indicated that the healing reaction in the wound progressed much faster in the HG60 treated groups and the reaction was associated with diminished inflammation.

The discussion made in sections largely confirms that the HG60 promoted a favorable pro-regenerative reaction stimulating faster healing rather than a pro-inflammatory graft rejection reaction.

5.3.3 HG60 modulated collagen remodeling

The nature of collagen remodeling in the wound-healing reaction was evaluated in detail. The histology sections when studied by trichrome staining and stereology (Figures 45 and 46), a progressive rate of collagen deposition was observed in all groups without any significant differences (Figure 47). Therefore, a deeper investigation was performed to unravel the differential nature of collagen remodeling happening in HG60 treated wounds, if any consequent to the pro-regenerative reaction discussed in section 4.9.

At least 28 different types of collagens have been identified in mammalian tissues but only collagen Type I and collagen Type III are critical in wound healing reactions (Rittié, 2016). During the healing process, the most prominent type of collagen in the early phases of the reaction is a relatively soluble collagen Type III, which gets removed by matrix metalloproteinases. Simultaneously less degradable Type I fibrillar collagen that contributes to scarring also accumulates (Mathew-steiner and Roy, 1969; Singh and K Agrawal, 2023). In reality, the deposition of adequate quantity of type I collagen is considered a desirable feature of a good wound healing reaction (Mathew Steiner and Roy, 1969), but the excess can lead to keloid (Ekstein *et al*., 2022).

The results of Herovici's staining pattern elucidated the nature of collagen remodeling in the healing wounds by providing the differential staining of collagen Type I and III (Figure 48). It was observed that as early as the 9th day, the HG60 induced a lot of Type I collagen, which was maintained at the same level throughout the study (Figure 49). In all other groups the amount of Type I collagen was lower on the 9th day which increased gradually with the advancement of time. Surely, the HG60 treated wound had adequate type I collagen much earlier than the other groups. On the other hand, the collagen Type III in the HG60 was very low throughout the study compared to other treatment groups (Figure 50) indicating that either the Type III collagen was minimally produced in the HG60-treated wounds or it got quickly removed from the healing wound. In other words, it can be inferred that effective collagen remodeling was happening in this group than in any other group.

The above contention was further substantiated by the ratio of collagen Type I to Type III. In normal human skin, the ratio of collagen Type I to Type III is identified to be closer to 3.5:1 (Widgerow *et al.*, 2000). In this study of rat skin wound healing, it was observed that only the HG60-treated wounds reached a value of 3.3 at least by the 21st day (Figure 51), indicating that the texture of the skin was nearly restored by this time. It was noted that the HG60-treated group showed a higher ratio from the 9th day and attained a value near the desired on the 15th day of wound healing. On the other hand, the maximum ratios in the other groups indicative of higher type I collagen indicative of scarring were observed to be much lower level to 2.7 in the HG00 group, 2.2 in the predicate device treated group, and 1.7 in the open wound on the 21st day (Figure 51). From these results, it is clear that the collagen remodeling in the HG60-treated groups happened effectively quicker than in the other groups with minimal scarring.

Moreover, the results of biochemical analysis with RT-PCR for mRNA translating Collagen Type I and Type III on the 18th and 21st days corroborated the above stereology observations on collagen remodeling. There was a noticeable change in the relative fold change of mRNA for collagen Types I and III among various treatment groups. The relative fold change of collagen Type I mRNA on the 18th day was significantly higher than the HG00 (Figure 55). The relative fold change in mRNA for collagen Type III on the 18th day and 21st day did not show a significant difference between the groups (Figure 56). These findings substantiated the ability of the HG60 containing CECM for more effective collagen remodeling than in other groups.

5.4 Significance of the study

Considering the ionic crosslinking strategy employed in the CECM hydrogel preparations, here the base CMC and the cross-linker Potassium Aluminum Sulphate used were pharmaceutical grade chemicals. Therefore, the CECM-CMC hydrogel is a potential Class D biomedical device similar to *CholeDerm*^{TM}. This study prepared five formulations of injectable hydrogels based on the content of CECM and investigated the physicochemical, and biological characteristics as satisfactory for an injectable hydrogel for wound healing applications.

Evidence collected from the *in vivo* studies provided insights into the faster wound-healing potential of the HG60 formulation. The HG60 formulation accelerated wound healing through an anti-inflammatory response. It was well evidenced that the hydrogel enhanced re-epithelialization, modulated CD4+/CD8+ T lymphocytes, M1/M2 macrophages, and an effective collagen remodeling much earlier in comparison to the control groups consisting of a predicate device, untreated open wound and the hydrogel base.

A summary of the findings in this thesis is graphically represented in the Figure 57.

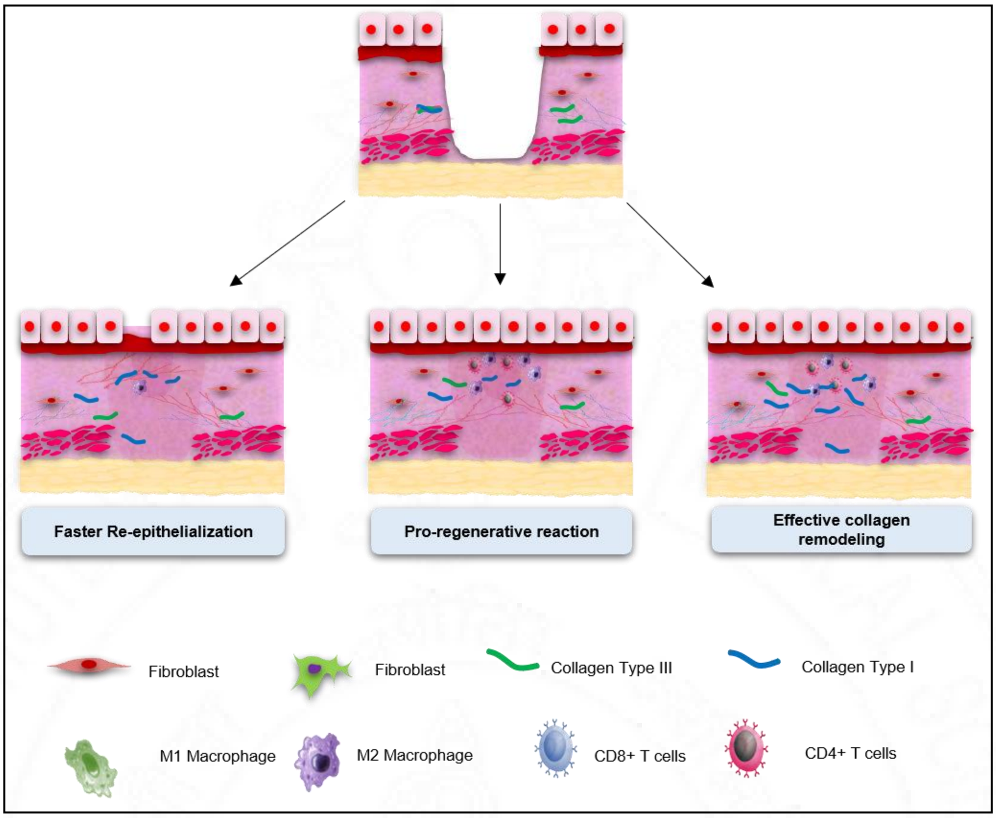

Figure 57. A graphical representation of the mechanism of healing modulated by the HG60 accounting for faster re-epithelialization, pro-regenerative reaction favored by CD4+ lymphocytes and M2 macrophages and effective collagen remodeling.

CHAPTER 6

6 SUMMARY AND CONCLUSION

6.1 Summary

- Porcine cholecyst extracellular matrix was formulated into an injectable hydrogel formulation by ionic crosslinking reaction with carboxymethyl cellulose
- The hydrogel formulations showed excellent physicochemical characteristics required for a wound-healing gel formulation
- The hydrogels had very good cytocompatibility confirmed by *in vitro* biological characterization
- The hydrogel formulations proved to be injectable when monitored in a texture analyzer
- An animal model of full-thickness excision skin wound in Sprague Dawley rats was used as the *in vivo* model
- Gross photographs of wounds were captured using a custom-made photographic stand to ensure uniformity in all the images
- The wound healing rate evaluated by digital planimetry indicated a faster rate of wound healing in HG60-treated animals
- The nature of the *in vivo* healing response induced by the HG60 formulation was evaluated by histomorphology

- A faster rate of re-epithelialization was observed in the HG60-treated animals as early as the 18th day
- The histomorphological evaluation showed that on the 9th day, most animals had mild to moderate granulation tissue made of sprouting blood vessels and fibroblast which gradually decreased with an increase in more compact and diffusely scattered neo-collagen
- At 21 days, occasional dense multifocal mononuclear cells were observed in experimental groups but the intensity was lower in HG60-treated groups compared to the control groups
- Compared to control groups a significantly higher number of CD4+ cells were observed in the HG60 group at the initial time points and decreased gradually
- A higher number of CD8+ cells was observed in HG60 groups during the initial time points and reduced which showed the reaction happened much earlier than the control groups
- A lower number of M1 macrophages was observed in HG60 groups throughout the experiment indicative of a low inflammatory response
- A higher number of M2 macrophage reactions was observed in the HG60 groups in the initial time points and reduced gradually
- The CD4+/CD8+ ratio in the HG60-treated group reached a balanced ratio on the 21st day whereas the control group did not reach a balanced state
- The M1/M2 ratio showed a ratio closer to one from the 18th day in the HG60 group, whereas the control groups didn’t reach even on the 21st day

- A progressive rate of total collagen deposition was observed in all experimental groups throughout the study
- Stereology by Herovici staining showed that Type 1 collagen maintained a stable amount throughout the study in HG60 groups
- Stereology by Herovici staining showed that the Type 3 collagen was very low in HG60 groups throughout the study compared to control groups
- The collagen Type 1 to Type 3 ratio attained a value near the normal range of "three" as reported for normal rat skin in HG60 groups from the 15th day of treatment
- The relative fold change of TNF α mRNA, a marker for proinflammatory cytokine was lower in HG60 groups on the 18th day and decreased further compared to control groups
- The relative fold change of iNOS mRNA, a marker for proinflammatory cytokine was lower in HG60 groups on the 18th day and decreased further compared to control groups
- The relative fold change of IL-10 mRNA, a marker for anti-inflammatory cytokine was significantly lower than the predicate device on the 18th day and thereafter decreased which represented the immune reaction has subsided
- The relative fold change of COL-I mRNA in HG60 groups was higher on 18th day and reduced by 21st day
- The relative fold change of COL-III mRNA in HG60 groups was higher on 18th day and a reduction was observed in the 21st day

6.2 Conclusion

- CECM hydrogels prepared by ionic crosslinking reaction with Carboxymethyl showed excellent biomaterial properties as required for a wound-healing gel
- The formulation named HG60 containing 60% of CECM and 40 % CMC satisfied the properties of an injectable hydrogel
- Faster wound closure and re-epithelization were evident in the HG60 treatment group
- The HG60 hydrogel promoted a pro-regenerative reaction predominated by helper T cells and M2 macrophages
- The HG60 injectable hydrogel was probably a promising candidate to be used as an advanced skin wound care product for accelerated healing of skin wounds

6.3 Limitations of the study

- *In vivo,* injectability has not been performed to study the efficacy of the hydrogel
- Molecular studies on the initial time points have not been performed

6.4 Future perspectives of the study

- *In vivo* injectability study has to be performed to study the efficacy of the hydrogel

- *In vivo* injectability study for catheter-based delivery models like myocardial infarction has to be performed
- Comparative study on the mechanism of healing needs to be studied in multiple animal species
- Comparative study on the mechanism of healing needs to be studied in multiple wound models

REFERENCE

- Adden R, Hubner B, Fortsch S, Knarr M (2021). Cellulosics. *Handb hydrocoll* 3 ed: 481-508.
- Adusei KM, Ngo TB, Sadtler K (2021). T lymphocytes as critical mediators in tissue regeneration, fibrosis, and the foreign body response. *Acta Biomater* 133**:** 17-33.
- Alam K, Iqbal M, Hasan A, Al-Maskari N (2020). Rheological characterization of biological hydrogels in aqueous state. *J Appl Biotechnol Reports* 7**:** 172-176.
- Almadani YH, Vorstenbosch J, Davison PG, Murphy AM (2021). Healing, Inflammation, and Fibrosis: Wound Healing: A Comprehensive Review. *Semi in Plast Surg* 3**:** 141-144.
- Alonso JM, Del JA, Gonzalez RP, Saez-martinez V (2021). Injectable hydrogels: From laboratory to industrialization. *Polym* 13**:** 650-672.
- Amadori A, Zamarchi R, De Silvestro G (1995). Genetic control of the CD4/CD8 T-cell ratio in humans. *Nat Med* 1**:** 1279-1283.
- Anderson K, and Hamm RL (2012). Factors That Impair Wound Healing. *J Am Coll Clin Wound Spec* 4**:** 84–91.
- Anilkumar TV, Vineetha VP, Revi D, Muhamed J, Rajan A (2014). Biomaterial properties of cholecyst-derived scaffold recovered by a non-detergent/enzymatic method. *J Biomed Mater Res - Part B Appl Biomater* 102**:**1506-1516.
- Annabi N, Nichol JW, Zhong X (2010). Controlling the porosity and

microarchitecture of hydrogels for tissue engineering. *Tissue Eng - Part B Rev* 16**:** 371-383.

- Arifin WN, Zahiruddin WM (2017). Sample size calculation in animal studies using resource equation approach. *Malaysian J Med Sci* 5**:** 101–105.
- Aswathy SH, Narendrakumar U, Manjubala I (2020). Commercial hydrogels for biomedical applications. *Heliyon* 6**:** 3719-3732.
- Avishai E, Yeghiazaryan K and Golubnitschaja O (2017). Impaired wound healing: Facts and hypotheses for multi-professional considerations in predictive, preventive and personalised medicine. *EPMA Journal* 8**:** 23–33.
- Azevedo HS, Reis RL (2004). Understanding the enzymatic degradation of biodegradable polymers and strategies to control their degradation rate. *Biodegrad Syst Tissue Eng Regen Med* 1 ed**:** 177-202.
- Balakrishnan DK, Nair ND, Venugopal SK, Das VN, George S, John MA, Eassow S, Alison MR, Sainulabdeen A, Anilkumar TV (2018). An immunopathological evaluation of the porcine cholecyst matrix as a muscle repair graft in a male rat abdominal wall defect model. *Toxicol Pathol* 46**:** 169-183.
- Baldwin G, Colbourne M (1999). Puncture Wounds. *Pediatr Rev* 35**:** 141–144.
- Bernhard S, Tibbitt MW (2021). Supramolecular engineering of hydrogels for drug delivery. *Adv Drug Deliv Rev* 171**:** 240–256.
- Borbolla FV, Pena SI, Farah SJ (2023). Films for wound healing fabricated using a solvent casting technique. *Pharmaceutics* 15**:** 1914-1941.

- Boyce DE, Jones WD, Ruge F, Harding KG, Moore K (2000). The role of lymphocytes in human dermal wound healing. *Br J Dermatol* 143**:** 59–65.
- Brown BN, Ratner BD, Goodman SB, Amar S, Badylak SF (2012). Macrophage polarization: an opportunity for improved outcomes in biomaterials and regenerative medicine. *Biomaterials* 33**:** 3792-3802.
- Buttaravoli P (2007). Contusion: (Bruise). *Min Emer* 557–560.
- Cao X, Lin X, Li N, Zhao X, Zhou M, Zhao Y (2023). Animal tissue-derived biomaterials for promoting wound healing. *Mater Horizons* 10**:** 3237-3256.
- Cao J, Wu B, Yuan P, Liu Y, Hu C (2023). Rational design of multifunctional hydrogels for wound repair. *J. Funct. Biomater* 11**:** 553-575.
- Capanema SV, Mansur AP, Jesus AC, Carvalho SM, Oliveira LC, Mansur H (2018). Superabsorbent crosslinked carboxymethyl cellulose-PEG hydrogels for potential wound dressing applications. *Int J Biol Macromol* 106**:** 1218-1234.
- Carmeliet P (2005). Angiogenesis in life, disease and medicine. *Nature* 438**:** 932-936.
- Chen MH, Wang LL, Chung JJ, Kim YH, Atluri P, Burdick JA (2017). Methods to assess shear-thinning hydrogels for application as injectable biomaterials. *ACS Biomater Sci Eng* 12**:** 3146–3160.
- Chesko DM, Wilgus TA (2022). Immune cells in cutaneous wound healing: a review of functional data from animal models. *Int J Mol Sci* 23**:** 2444-2462.
- Deng X, Gould M, Ali MA (2022). A review of current advancements for wound healing: Biomaterial applications and medical devices. *J Biomed*

Mater Res - Part B Appl Biomater 11**:** 2542-2573.

- Diller RB and Tabor AJ (2022). The Role of the Extracellular Matrix (ECM) in Wound Healing: A Review. *Biomimetics* 3**:** 87-93.
- Du Sert NP, Hurst V, Ahluwalia A, Alam S, Avey MT, Baker M (2020). The arrive guidelines 2.0: Updated guidelines for reporting animal research. *PLoS Biol* 7**:** e3000410.
- Ekstein SF, Wyles S, Moran S, Clinic (2022). Keloids: A Review of Therapeutic Management Samuel. *Int J Dermatol* 6**:** 661–671.
- Eming SA, Martin P, Tomic M (2014). Wound repair and regeneration: Mechanisms, signaling, and translation. *Sci. Transl. Med* 6**:** 265-270.
- Farahani M, Shafiee A (2021). Wound Healing: From Passive to Smart Dressings. *Adv. Healthc. Mater* 16**:** 210-217.
- Firlar I, Altunbek M, McCarthy C, Ramalingam M, Camci G (2022). Functional Hydrogels for Treatment of Chronic Wounds. *Gels* 8**:** 127-150.
- Gefen A, Alves P, Beeckman D (2023). Mechanical and contact characteristics of foam materials within wound dressings: Theoretical and practical considerations in treatment. *Int Wound J* 20**:** 1960-1978.
- Giraudo MV, Di Francesco D, Catoira MC, Cotella D, Fusaro L, Boccafoschi F (2020). Angiogenic potential in biological hydrogels. *Biomedicines* 10**:** 436–451.
- Gonzalez A, Andrade Z, Costa TF, Medrado A (2016). Wound healing - A literature review. *An Bras Dermatol* 91**:** 614-620.
- Grada A, Mervis J, Falanga V (2018). Research Techniques Made Simple:

Animal Models of Wound Healing. *J Invest Dermatol* 138**:** 2095-2105.

- Grover GN, Rao N, Christman PKL (2015). Myocardial matrix-polyethylene glycol hybrid hydrogels for tissue engineering. *NIH Public Access* 25**:** 14011-14034.
- Guo S, DiPietro LA (2010a). Critical review in oral biology & medicine: Factors affecting wound healing. *J. Dent. Res* 3**:** 219–229.
- Guo S, DiPietro LA (2010b). Factors Affecting Wound Healing. *J. Dent. Res* 3**:** 219–229.
- Hameed P, Manivasagam G (2021). An overview of bio-actuation in collagen hydrogels: a mechanobiological phenomenon. *Biophys Rev* 13**:** 387-403.
- Han F, Wang J, Ding L, Hu Y, Li W, Yuan Z, Guo Q, Zhu C, Yu L, Wang H, Zhao Z, Jia L, Li J, Yu Y, Zhang W, Chu G, Chen S, Li B (2020). Tissue engineering and regenerative medicine: achievements, future, and sustainability in asia. *Front. bioeng. biotechnol* 8**:** 495-504.
- Hassanshahi A, Moradzad M, Ghalamkari S, Fadaei M, Cowin AJ, Hassanshahi M, (2022). Macrophage-Mediated Inflammation in Skin Wound Healing. *Cells* 11**:** 2953-2967.
- Hautz T, Zelger B, Brandacher G (2012). Histopathologic characterization of mild rejection (grade I) in skin biopsies of human hand allografts. *Transpl In* 25**:** 56-63.
- Hench JW (2005). Inflammation and wound healing. *Biomater Artif Organs Tissue Eng* 71-76.
- Herman TF, Bordoni B (2023). Wound Classification. *Principles of Surgery*

Vivas for the MRCS 323–328.

- Howard D, Buttery LD, Shakesheff KM, Roberts SJ (2008). Tissue engineering: Strategies, stem cells and scaffolds. *J. Anat* 213**:** 66–72.
- Hunter JD, Johnson TD, Braden RL, Christman KL (2022). Injectable ECM Scaffolds for Cardiac Repair. *Methods Mol Biol* 1181**:** 109-121.
- Jarbrink K, Ni G, Sonnergren H, Schmidtchen A, Pang C, Bajpai R (2017). The humanistic and economic burden of chronic wounds: A protocol for a systematic review. *Syst. Rev* 6**:** 15–22.
- Jeschke MG, Van Baar ME, Choudhry MA, Chung KK, Gibran NS, Logsetty S (2020). Burn injury. *Nat. Rev. Dis. Primers* 6**:** 11-29.
- Jorgensen LB, Sorensen JA, Jemec GB, Yderstrade KB (2016). Methods to assess area and volume of wounds – a systematic review. *Int Wound J* 4**:** 540–553.
- Junker JP, Kamel RA, Caterson EJ, Eriksson E (2013). Clinical Impact Upon Wound Healing and Inflammation in Moist, Wet, and Dry Environments. *Adv Wound Care* 2**:** 348-356.
- Kanikireddy V, Varaprasad K, Jayaramudu T, Karthikeyan C, Sadiku R (2020). Carboxymethyl cellulose-based materials for infection control and wound healing: A review. *Int J Biol Macromol* 164**:** 963-975.
- Karmakar PD, Velu K, Vineeth Kumar CM, Pal A (2023). Advances in injectable hydrogel: Design, functional regulation, and biomedical applications. *Polym Adv Technol* 13**:** 1345-1355.
- Koh TJ, DiPietro LA (2011). Inflammation and wound healing: the role of

the macrophage. *Expert Rev. Mol.Med* 13**:** 23–35.

- Kotwal GJ, Chien S (2017). Macrophage differentiation in normal and accelerated wound healing. *Macrophages* 62**:** 353–364.
- Krzyszczyk P, Schloss R, Palmer A, Berthiaume F (2018). The role of macrophages in acute and chronic wound healing and interventions to promote pro-wound healing phenotypes. *Front. Physiol* 9**:** 419-445.
- Kumar V, Abbas A, Aster CJ (2020). Robbins and Cotran Pathologic Basis of Diseases. *Elsevier* 10 ed.
- Kurniati M, Nuraini I, Winarti C (2021). Investigation of swelling ratio and textures analysis of acrylamide-nanocellulose corncobs hydrogel. *J Phys Conf Ser* 1805**:** 1742-1749.
- Li W, Zhou J, Xu Y (2015). Study of the in vitro cytotoxicity testing of medical devices. *Biomed. Rep* 3**:** 617-620.
- Liang CC, Park AY, Guan JL (2007). In vitro scratch assay: A convenient and inexpensive method for analysis of cell migration *in vitro*. *Nat Protoc* 2**:** 329-333.
- Liu J, Zhang C, Miao D (2018). Preparation and characterization of carboxymethyl cellulose hydrogel fibers. *J Eng Fiber Fabr* 13**:** 6-13.
- Madden JW, Peacock EE (1971). Studies on the biology of collagen during wound healing, dynamic metabolism of scar collagen and remodeling of dermal wounds. *Ann Surg* 174**:** 511-520.
- Mandal BB, Kapoor S, Kundu SC (2009). Biomaterials Silk fibroin/polyacrylamide semi-interpenetrating network hydrogels for

controlled drug release. *Biomaterials* 14**:** 2826–2836.

- Martinez FD, Fischer T, Hayn A, Mierke CT, Burgess JK, Harmsen MC (2022). A beginner’s guide to the characterization of hydrogel microarchitecture for cellular applications. *Gels* 8**:** 535-555.
- Mathew SS, Roy S, Sen CK (1969). Collagen in wound healing. *Injury* 8**:** 76-84.
- McBath RA, Shipp DA (2010). Swelling and degradation of hydrogels synthesized with degradable poly(β-amino ester) crosslinkers. *Polym Chem* 1**:** 860-865.
- Mony MP, Anilkumar TV (2020). Controlled cross-linking of porcine cholecyst extracellular matrix for preparing tissue engineering scaffold. *J Biomed Mater Res - Part B Appl Biomater* 108**:** 1057-1067.
- Moon H (2021). Wound management. *Annals of Hepato-Biliary-Pancreatic Surgery* 25**:** 2508-2511.
- Morwood AJ, El-Karim IA, Clarke SA, Lundy FT (2023). The Role of Extracellular Matrix (ECM) Adhesion Motifs in Functionalised Hydrogels. *Molecules* 12**:** 4616-4643.
- Muhamed J, Revi D, Rajan A, Anilkumar TV (2015). Comparative local immunogenic potential of scaffolds prepared from porcine cholecyst, jejunum, and urinary bladder in rat subcutaneous model. *J Biomed Mater Res - Part B Appl Biomater* 6**:** 1302–1311.
- Muhamed J, Revi D, Rajan A, Geetha S, Anilkumar TV (2015). Biocompatibility and Immunophenotypic Characterization of a Porcine

Cholecyst–derived Scaffold Implanted in Rats. *Toxicol Pathol* 43**:** 536-545.

- Murphy PS, Evans, GR (2012). Advances in wound healing: a review of current wound healing products. *Plast. Surg. Int* 2012**:** 190–198.
- Murray RZ, West ZE, Cowin AJ, Farrugia BL (2019). Development and use of biomaterials as wound healing therapies. *Burn Trauma* 7**:** 1-9.
- Murray PJ, Wynn TA (2011). Protective and pathogenic functions of macrophage subsets. *Nat. Rev. Immunol* 11**:** 723–737.
- Nair RS, Sobhan PK, Shenoy SJ, Prabhu MA, Kumar V, Ramachandran S (2023). Mitigation of fibrosis after myocardial infarction in rats by using a porcine cholecyst extracellular matrix. *Comp. Med* 4**:** 311-322.
- Natsui M (2003). Therapeutic management of problematic superficial wounds: a patient-centred approach. *Wound Care* 2**:** 63–66.
- Newman RK, Mahdy H (2022). Laceration. *Hand Plast Sur* 91–96.
- Nuutila K, Eriksson E (2021). Moist Wound Healing with Commonly Available Dressings. *Adv Wound Care* 10**:** 685-698.
- Ortega L, Quinones M, García M (2022). Cytotoxicity and wound closure evaluation in skin cell lines after treatment with common antiseptics for clinical use. *Cells* 11**:** 1395-2013.
- Raziyeva K, Kim Y, Zharkinbekov Z, Kassymbek K, Jimi S, Saparov (2021). Immunology of acute and chronic wound healing. *Biomolecules* 5**:** 700-725.
- Revi D, Geetha C, Thekkuveettil A, Anilkumar TV (2016). Fibroblast-loaded cholecyst-derived scaffold induces faster healing of full thickness burn

wound in rabbit. *J Biomater Appl* 7**:** 1036–1048.

- Revi D, Vineetha VP, Muhamed J, Rajan A, Anilkumar TV (2013). Porcine cholecyst–derived scaffold promotes full-thickness wound healing in rabbit. *J Tissue Eng* 4**:** 2041731413518060.
- Ribeiro M. Simoes M, Vitorino C, Mascarenhas F (2024). Hydrogels in cutaneous wound healing: insights into characterization, properties, formulation and therapeutic potential. *Gels* 10**:** 188-234.
- Richter DM, Ku JC, Keckler KE, Burke LR, Abd GM, Li Y (2023). Autologous blood clots: a natural biomaterial for wound healing, *Front. Mater. Sci* 10**:** 125-132.
- Rittie L (2016). Cellular mechanisms of skin repair in humans and other mammals. *J Cell Commun Signal* 10**:** 103-120.
- Robbins C (2015). Robbins & Cotran. *Robbins & Cotran Pathologic Basis of Disease, 8th edition* 1035–1040.
- Rodrigues M, Kosaric N, Bonham CA, Gurtner GC (2019). Wound healing: A cellular perspective. *Physiol Rev* 99**:** 665-706.
- Rogers LC, Bevilacqua NJ, Armstrong DG, Andros G (2010). Digital planimetry results in more accurate wound measurements: A comparison to standard ruler measurements. *J Diabetes Sci Technol* 4**:** 799-802.
- Rosique RG, Rosique MJ, Farina Junior JA (2015). Curbing Inflammation in Skin Wound Healing: A Review. *Int J. Inflamm* 2015**:** 316- 325.
- Saldin LT, Cramer MC, Velankar SS, White LJ, Badylak SF (2017). Extracellular matrix hydrogels from decellularized tissues: Structure and

function. *Acta Biomater* 49**:** 1-15.

- Sanfilippo S, Canis M, Ouchchane L (2011). Viability assessment of fresh and frozen/thawed isolated human follicles: Reliability of two methods (Trypan blue and Calcein AM/ethidium homodimer-1). *J Assist Reprod Genet* 28**:** 1151-1156.
- Schaefer TJ, Tannan SC (2023). Thermal Burns. *Environmental Emerg and Injur in Nat* 41–47.
- Sen CK (2021). Human wounds and its burden: Updated 2020 compendium of estimates. *Adv wound care* 10**:** 281-292.
- Shivani Gupta SS (2021). A global public health concern: perspectives from developed countries. *Wounds Asia* 4**:** 8–21.
- Singh D, Rai VK Agrawal D (2023). Regulation of Collagen I and Collagen III in Tissue Injury and Regeneration. *Cardiol Cardiovasc Med* 7**:** 5-16.
- Sivaraj D, Chen K, Chattopadhyay A, Henn D, Wu W, Noishiki C (2021). Hydrogel scaffolds to deliver cell therapies for wound healing, *Front. bioeng. Biotechnol* 9**:** 660-670.
- Smart H (2013). Deep tissue injury: What is it really? *Adv Wound Care* 2**:** 56–58.
- Stan D, Tanase C, Avram M (2021). Wound healing applications of creams and “smart” hydrogels. *Exp Dermatol* 30**:**1218-1232.
- Su J, Li J, Liang J, Zhang K, Li J (2021). Hydrogel preparation methods and biomaterials for wound dressing. *Life* 11**:** 1016-1038.
- Sun C, Purohit PK (2022). Rheology of fibrous gels under compression.

Extrem Mech Lett 54**:** 101757-101777.

- Sun Y, Nan D, Jin H, Qu X (2020). Recent advances of injectable hydrogels for drug delivery and tissue engineering applications. *Polym Test* 81**:** 106283.
- Tan RP, Chan HP, Wei S (2019). Bioactive Materials Facilitating Targeted Local Modulation of Inflammation. *JACC Basic to Transl Sci* 4**:** 56-71.
- Tavakoli S, Klar AS (2020). Advanced hydrogels as wound dressings. *Biomolecules* 10**:** 1169-1189.
- Tejiram, Kavalukas SL, Shupp JW, Barbul AS (2016). Wound healing, *Wound Healing Biomaterials: Therapies and Regeneration* 1**:** 3–39.
- Theoret CL, Stashak TS (2014). Integumentary System: Wound Healing, Management, and Reconstruction, *Equine Emergencies: Treatment and Procedures* 3 ed**:** 238–267.
- Thomas DC, Tsu CL, Nain RA, Arsat N, Fun SS, Sahid Nik Lah NA (2021). The role of debridement in wound bed preparation in chronic wound: A narrative review. *Ann med surg* 71**:** 102876.
- Tian J, Wong KY, Ho CM, Lok CN, Yu WY, Che CM (2007). Topical delivery of silver nanoparticles promotes wound healing. *ChemMedChem* 1**:** 129–136.
- Tonnesen MG, Feng X, Clark AF (2000). Angiogenesis in wound healing. *J Invest Dermatol* 5**:** 40–46.
- Toriseva MJ, Ala-Aho R, Karvinen J, Baker AH, Marjomaki VS, Heino J, Kahari VM (2007). Collagenase-3 (MMP-13) enhances remodeling of three-dimensional collagen and promotes survival of human skin fibroblasts. *J*

Invest Dermatol 127**:** 49–59.

- Tracy LE, Minasian RA, Caterson EJ (2016). Extracellular Matrix and Dermal Fibroblast Function in the Healing Wound. *Adv Wound Care* 3**:** 119–136.
- Uygun BE, Christophe HB, Berthiaume F, Krzyszczyk P, Schloss R, Palmer A, (2018). The Role of Macrophages in Acute and Chronic Wound Healing and Interventions to Promote Pro-wound Healing Phenotypes. *Front Physiol* 1**:** 419-441.
- Velnar T, Bailey T, Smrkolj V (2009). The wound healing process: an review of the cellular and molecular mechanisms. *Int. J. Med. Res* 5**:** 1528–1542.
- Vriend L, Sinkunas V, Camargo CP, Van Der Lei B, Harmsen MC, Van Dongen JA . (2022). Extracellular Matrix-Derived Hydrogels to Augment Dermal Wound Healing: A Systematic Review. *Tissue Eng. Part B Rev* 5**:** 1093–1108.
- Wang S, Yu P, Li X, Zhao Z, Dong Y, Li X (2023). Design and fabrication of functional hydrogels with specific surface wettability. *Colloids Interface Sci Commun* 52**:** 100697.
- Widgerow AD, Chait LA, Stals R, Stals PJ (2000). New innovations in scar management. *Aesthetic Plast Surg* 24**:** 227-234.
- Wilgus TA, Roy S, McDaniel JC (2013). Neutrophils and wound repair: positive actions and negative reactions. *Adv Wound Care.* 2**:** 379-389.
- Wilkinson HN, Hardman MJ (2020). Wound healing: cellular mechanisms

and pathological outcomes: Cellular Mechanisms of Wound Repair. *Open Biol* 10**:** 200223.

- Xiao H, Chen X, Liu X, Wen G, Yu Y (2023). Recent advances in decellularized biomaterials for wound healing. *Materials Today Bio* 19**:** 104-112.
- Yi DF, Gong L, Gu X (2017). Extracellular matrix scaffolds for Tissue engineering and regenerative medicine. *Curr Stem Cell Res Ther* 3**:** 233–246.
- Yu R, Zhang H, Guo B (2022). Conductive biomaterials as bioactive wound dressing for wound healing and skin tissue engineering. *Nano-Micro Lett* 14**:** 1-46.
- Yuwono SD, Wahyuningsih E, Noviany, Kiswandono AA, Simanjuntak W, Hadi S. (2021). Characterization of carboxymethyl cellulose (CMC) synthesized from microcellulose of cassava peel. *Mater Plast* 57**:** 225-235.
- Zennifer A, Senthilvelan P, Sethuraman S, Sundaramurthi D (2021). Key advances of carboxymethyl cellulose in tissue engineering & 3D bioprinting applications. *Carbohydr Polym* 256**:** 117561.
- Zhang Q, Fassihi MA, Fassihi R (2018). Delivery Considerations of Highly Viscous Polymeric Fluids Mimicking Concentrated Biopharmaceuticals: Assessment of Injectability via Measurement of Total Work Done "WT". *AAPS PharmSciTech* 19**:** 1520-1528.
- Zhou S Salisbury J, Preedy VR, Emery PW (2013). Increased collagen synthesis rate during wound healing in muscle. P*los one* 3**:** 583- 596.
- Zuidema JM, Rivet CJ, Gilbert RJ, Morrison FA (2014). A protocol for

rheological characterization of hydrogels for tissue engineering strategies. *J Biomed Mater Res - Part B Appl Biomater* 102**:** 1063-1073.

APPENDIX

LIST OF PUBLICATIONS

- **Pratheesh KV**, Nair RS, Purnima C, Raj R, Mony PM, Geetha CS, Praveen KS, Rekha MR, Nair PD, Anilkumar TV (2024), An injectable hydrogel of porcine cholecyst extracellular matrix for accelerated wound healing, *Journal of Biomedical Materials Research Part A*, DOI: 10.1002/jbm.a.37795
- Nair RS, Praveen KS, Shenoy SJ, Prabhu M, Surya R, Geetha CS, **Pratheesh KV**, Mony PM, Raj R, Anilkumar TV (2022), A porcine cholecystic extracellular matrix conductive scaffold for cardiac tissue repair, *Journal of Biomedical Materials Research Part B: Applied Biomaterials*, 110 (9):2039-2049
- Mony P M, Shenoy J S, Raj R, Geetha CS, **Pratheesh KV**, Nair RS, Purnima C, Anilkumar TV (2021), Gelatin-modified cholecyst derived Scaffold promotes angiogenesis and faster healing of diabetic wounds, *ACS Applied Bio Materials* 4 (4): 3320-3331
- Raj R, Shenoy JS, Mony PM, **Pratheesh K V**, Nair RS, Geetha CS, Praveen KS, Purnima C, Anilkumar TV (2021), Surface modification of polypropylene mesh with a porcine cholecystic extracellular matrix hydrogel for mitigating host tissue reaction, *ACS Applied Bio Materials* 4 (4), 3304-3319
- Raj R, Praveen KS, **Pratheesh KV**, Anilkumar TV (2020), A cholecystic

extracellular matrix-based hybrid hydrogel for skeletal muscle tissue engineering, *Journal of Biomedical Materials Research Part A* 108 (9), 1922-1933

LIST OF PATENTS

Indian Patent awarded

Pratheesh KV, Praveen KS, Anilkumar TV (Patent No. 427997 dated 31 March, 2021): Process of preparation of an injectable hydrogel formulation.

Australian Innovation Patents awarded

- **Pratheesh KV,** Anilkumar TV, Praveen KS, Nair RS, Raj R, Mony PM (Patent No. 2021105496 dated 27 October, 2021): A method for preparing an injectable hydrogel of porcine cholecystic extracellular matrix.
- **Pratheesh KV,** Anilkumar TV, Praveen KS, Nair RS, Raj R, Mony PM (Patent No. 2021106267 dated 1 December, 2021): A method for treating full thickness skin wound using a porcine cholecystic extracellular matrix hydrogel.
- Raj R, Purnima C, Anilkumar TV, Shenoy SJ, Mony MP, Nair RS, **Pratheesh KV**, Praveen KS (Patent No. 2021104933 dated 20 April, 2022): Tissue engineering applications of a tunable hydrogel of mammalian extracellular matrix.
- Raj R, Purnima C, Anilkumar TV, Mony MP, Nair RS, **Pratheesh KV**, Praveen KS (Patent No. 2021104930 dated 20 April, 2022): A method for preparation of hydrogel of mammalian cholecystic extracellular matrix.

- Nair RS, Anilkumar TV, Ameer, JM, Praveen KS, Mony PM, Raj R, **Pratheesh KV** (Patent No. 2021105411 dated 10 November, 2022): A method for modifying porcine cholecystic extracellular matrix for cardiac tissue engineering by conjugating amine functionalised gold nanoparticles.
- Nair RS, Anilkumar TV, Ameer, JM, Praveen KS, Mony PM, Raj R, **Pratheesh KV** (Patent No. 2021105731 dated 1 December, 2021): A method for mitigating a post-myocardial infarction fibrosis in mammals by using a porcine cholecyst derived extracellular matrix scaffold.
- Mony PM, Anilkumar TV, Nair RS, Raj R **Pratheesh KV**, Praveen KS (Patent No. 2021106067 dated 1 December, 2021): A method for modifying a porcine cholecyst derived scaffold by coupling with fibronectin for skin tissue engineering application.
- Mony PM, Anilkumar TV, Shenoy SJ, Nair RS, Raj R, **Pratheesh KV**, Purnima C, Praveen KS (Patent No. 2021104953 dated 20 April, 2022): A method for fabrication of a gelatin conjugated porcine cholecystic extracellular matrix scaffold for treating a diabetic wound.

Indian Patent Filed

Anilkumar TV, Nebu GT, **Pratheesh KV**, Dalvi YB, Praveen KS, Varghese N, Naga Lekshmi UN, Thomas B (Patent application No. 202341003820): A process for the fabrication of multi-layered porcine cholecystic extracellular matrix for tissue engineering applications.

CONFERENCE PRESENTATIONS

- **Pratheesh KV**, Praveen KS, Anilkumar TV. A Hydrogel Formulation of Porcine Cholecystic Extracellular Matrix for Accelerated Wound Healing at International Conference on Biomaterials, Regenerative Medicine and Devices, organized by society for tissue engineering and regenerative medicine India (STERMI) and Society for Biomaterials & Artificial Organs India (SBAOI) on 15th -18th December 2022 at IIT Guwahati, India (Paper presentation)
- **Pratheesh KV**, Anilkumar TV. “Preparation and characterization of an injectable hydrogel of porcine cholecystic extracellular matrix” at 32nd Kerala Science Congress in Yuvakshetra Institute of Management Studies on 25th-27th January 2020 at Mundoor, Palakkad, India (Poster presentation)
- **Pratheesh KV**, Anilkumar TV. “Preparation and characterisation of an injectable hydrogel from porcine cholecyst extracellular matrix” at Global congress and expo on biomaterials (Biomaterials 2019) on 13th-14th March, 2019 at Kuala Lumpur, Malaysia (Poster presentation)

WORKSHOPS ATTENDED

- “Image Analysis in Biomedical Research” organized by Sree Chitra Tirunal Institute for Science and Technology, Thiruvananthapuram on 12th September 2018
- “Laboratory animal handling” organized by the Department of Biochemistry, Kerala University, Kariyavattom campus, Thiruvananthapuram on 25th - 27th

September 2018

- "International Workshop on Electrospinning/Spraying–2021" organized by IWESS 2021 Organizing Team on 23-24th, April 2021
- "Intellectual Property Rights" organized by the Ministry of Education Government of India and University Grants Commission on 17th January 2022
- Hands-on training program on "Real time imaging for Biologists" organized by Rajiv Gandhi Centre for Biotechnology (RGCB), Thiruvananthapuram on 13th August 2022

ACHIEVEMENTS AND HONORS

- Shared the reputation of developing India's First, Class D Medical device of animal origin (Cholederm) as per the Medical Device Rules 2017 (Government of India).
- Student Representative of Society for Biomaterials & Artificial Organs (India)-SBAOI, 2021 – Present (2024).